REDUCTION OF VOID CONTENT IN LAMINATED COMPOSITES BY MECHANICAL VIBRATIONS

Jelena Muric-Nesic

A thesis submitted for the degree of Doctor of Philosophy

School of Engineering, College of Engineering and Computer Science
The Australian National University

August 2010.

STATEMENT

This thesis contains no material that has been previously accepted for the award of any other degree or diploma in any university, institute or college. To the best of author's knowledge and belief, it contains no material previously published or written by another person, except where due reference is made in the text.

Signed

Jelena Muric-Nesic

August 2010

ACKNOWLEDGMENTS

I would like to sincerely thank my supervisor Dr. Zbigniew Stachurski for his outstanding supervision, excellent guidance and friendly association throughout my PhD studies. I would also like to thank Dr. Paul Compston of the ANU, and Nick Noble from Quickstep for assistance in supervision, and many other members in the Department of Engineering of the ANU for loads of helpful suggestions, support and assistance. My special thanks go to Mr Rob Gresham, Dr Tony Flynn and Mr David Tychen-Smith. My gratitude is extended to the staff of Electron Microscopy Unit of the ANU, and especially to Dr John Terlet from Adelaide Microscopy, the University of Adelaide.

Quickstep Technologies Pty Ltd, Perth, financially supported the project and provided my scholarship and that is gratefully appreciated. Their excellent assistance and professional services have been of huge importance in the success of the project. I wish to thank especially Mr Deryck Graham Sr.

The receipt of ANU money awards kindly sponsored by the Department of Engineering, College of Engineering and Computer Science, and ANU Vice-Chancellor, as well as ARNAM (Australian Research Network for Advanced Materials), are also gratefully acknowledged.

My deepest appreciation goes to my parents and brother for providing me the means, support and love to come this far.

Finally, my affectionate thanks goes to my husband Sinisa for his understanding, patience, encouragement and endless love throughout the last four years, and for the sacrifice he made by following me.

ABSTRACT

Defects, such as voids and bubbles, are detrimental to mechanical properties of composite materials. Theory predicts and experiments show that mechanical properties deteriorate in the presence of voids, hence void management is critical to high quality composite parts.

Eliminating common defects such as voids, bubbles, and poor adhesion at interfaces will increase the quality of laminated sandwich composite structure. There is evidence from previous research that mechanical vibrations applied during curing of a laminated composite can reduce the number of bubbles. Previous experiments provide guidelines for the exploration of vibrations as void eliminator in composites.

This thesis reports experimental research results and analysis of the effect of mechanical vibrations applied to the curing system of composite materials production, particularly for minimizing void content. Range of frequency of vibrations covered was from 0 Hz to 40 kHz, for different period of vibrations (10-30 min), at different operating temperatures (20-55°C), along with vacuum assistance. The composite laminates were made by hand lay-up using glass fibers and either vinyl-ester or epoxy resin, and examined under microscope to determine types and quantity of defects. The results showed remarkable reduction in void content when low frequency vibrations were applied (5-50 Hz). Void content was determined by optical microscopy. Details of internal structure were examined by scanning electron microscopy and computed tomography. Mechanical testing (flexural, tensile and shear) also supported these observations.

After initial stage where electromagnetic shaker was introduced to the curing system, special apparatus (based on the Quickstep method) was built to explore suitable frequency range of vibrations for curing at elevated temperatures, supported with vacuum pump. Numerous tests were performed and conclusions are leading towards better mechanical properties of laminates cured with vibration assistance.

Theoretical background is described taking into account various factors, such as temperature and viscosity, pressure variations, mass diffusion, and vibration itself as a complex process. Although there are still some unknown areas in the understanding of the process, some hypotheses made are supported and corroborated with experimental results.

NOMENCLATURE

The following is the list of most commonly used acronyms and symbols in this work.

ANUQSM	Australian National University QuickStep Machine
ASTM	American Society for Testing and Materials
CFRP	Carbon Fibre Reinforced Polymers
CSIRO	Commonwealth Scientific and Industrial Research Organisation
CT	Computed Tomography
GFRP	Glass Fibre Reinforced Plastics
EM	Electromagnetic
HTF	Heat Transfer Fluid
ILSS	InterLaminar Shear Strength
RTM	Resin Transfer Moulding
SBC	Stokes Bubble Cell
SEM	Scanning Electron Microscope
StDev	Standard Deviation
VAVCP	Vibration Assisted Vacuum Composite Processing
VIARTM	Vibration Assisted Resin Transfer Moulding

a	Dimension of a plate
a_c	Critical crack size
b	Damping coefficient
C_e	Equilibrium concentration
C_{rB}	Concentration of the gas dissolved in the liquid adjacent to a bubble
Cp	Heat capacity of a fluid
c_s	Saturation concentration
D	Diffusion coefficient
D_f	Flexural rigidity
E	Modulus of elasticity
E_A	Activation energy
f	Frequency
f_0	Resonance frequency of a bubble
f_{11}	Resonance frequency of simple supported plate
f_d	Damped resonance frequency
F	Bjerkness force
F_b	Buoyancy force
F_d	Drag force
FE	Flexural modulus
FS	Flexural strength
g	Gravitational acceleration, 9.81 m/s^2
G	Weight gain
h	Liquid depth
h_p	Thickness of a plate

k	Boltzmann constant, 1.38×10^{-23} J/ K
k_e	Elastic rigidity
k_H	Henry's constant
K	Bulk modulus
K_{Ic}	Fracture toughness
K(T)	Temperature dependant constant
m	Mass
N	Number of moles
p_0	Atmospheric pressure
p_A	Pressure amplitude
p_B	Pressure inside the bubble
p_h	Hydrostatic pressure
p_L	Pressure in the liquid at depth h
p_p	Partial pressure
Q	Damping
r_B	Radius of a bubble
R	Gas constant, 8.314 J/mol.K
ShS	Shear strength
t	Time
T	Temperature
TE	Tensile modulus
TS	Tensile strength
v	Velocity of the bubble
V	Volume

V_m	Molar volume
W_d	Dissipated work
γ	Surface tension
γ_{int}	Interfacial surface tension
δ	Phase lag
$\sin\delta$	Internal friction
Δp	Pressure difference
ΔP	Pressure gradient
Δr	Change in radius
ΔS_B	Difference in surface area between the expansion and contraction intervals
η	Dynamic viscosity
ν	Poisson's ratio
ρ_f	Density of a liquid
σ	Stress
σ_c	Applied stress
ω	Angular frequency

TABLE OF CONTENTS

LIST OF FIGURES

LIST OF TABLES

Chapter 1 INTRODUCTION

Composite materials, considered the materials of the future, are widely used by industries all around the world and have significant effects on our everyday lives. Life without airplanes, high-performance cars, sporting goods, even replaceable human parts, for all are or incorporate composites, would not be the same. Improving the quality of composite materials will improve our everyday lives.

The most common of the man-made composites can be divided into three groups: Metal Matrix Composites (MMC), Ceramic Matrix Composites (CMC), and Polymer Matrix Composites (PMC), of which the latter is the focus of this thesis. The most common type of Polymer Matrix Composites is usually known as Glass Fibre Reinforced Plastics (GFRP).

A polymer-based resin can be used as a matrix and a variety of fibres, such as glass, carbon and aramid, as reinforcement. When resin systems are combined with reinforcing fibres exceptional properties can be obtained, with those properties depending not only on the properties of each constituent and their ratios - the fibre-volume fraction, but also on the manufacturing process.

The aspect common to all composite processes is the use of heat and pressure to shape and cure the mixture of resin and fibres. The processes used by the composite industry vary

widely in the type of equipment used and can be either automated or manual. The Quickstep process is the foundation of research in this thesis.

The Quickstep process is a method for the fast curing of composites that was invented by an Australian company, Quickstep Technology Pty Ltd, which involves rapid heat transfer and balanced pressure, combined with vibration, to remove entrapped air and compact laminates. This thesis investigates and reports on the use of vibrations to improve the quality of composite laminates, particularly in void-content reduction.

1.1. Background and Motivation

Manufacturing processes used in composite-materials production have a critical part to play in determining the performance of the resultant structure.

Composites can display up to approximately ten times the strength-to-weight ratio of most metals, but have been traditionally out of reach of most manufacturers because of the cost of their production where conventional autoclave processes and lengthy production times are necessary. While there is an abundance of fibres, resins, sandwich-core materials and manufacturing processes, not all produce excellent results.

The Quickstep process is an inexpensive, out-of-autoclave manufacturing system for the production of advanced composite materials. It is a unique fluid-filled, balanced-pressure, heated floating-mould technology for the curing, partial curing and joining of composite materials. Its technology delivers top-quality performance on larger parts with significantly

quicker cycle times at significantly lower pressures and lower labor costs than those associated with alternative autoclave-based production systems. The Quickstep process can produce cheaper, lightweight products that have both high strength and improved appearance as well as reduced cure times.

It is well known and reported that the properties of composite materials can be adversely affected by entrapped air, fibre distortion, and poor fibre wetting, and that these either alone or in combination will cause premature failure of products in which they are found.

I propose that the inclusion of vibrations at appropriate points during the composite-material production cycle may affect composite porosity levels with the effects of vibrations being governed by its parameters, i.e., frequency, amplitude and vibrational energy input. There is compelling evidence in the literature that void content in composite laminates can be reduced with the use of low frequency vibrations applied to the curing system.

1.2. Aims and Methods

The aim of this project was to investigate the effect of mechanical (acoustic) vibrations on void reduction in laminated fibre reinforced composite materials. The vibrations were applied during the curing stage of laminated composite materials, prior to the gelation of the resin.

Voids are defined as gas bubbles in the resin resulting mainly from two processes:

- Coalescence of gases dissolved in the resin,
- Introduction of gas bubbles into the laminated system during the lay-up stage.

The main focus of this work was to physical pressure and sinusoidal pressure variations, and the effect that these may had on the behaviour of the gas bubbles in the system.

In view of the composition of the studied materials, namely layers of woven glass fibres impregnated with resin in the weight ratio of approximately 50:50, it was only the behaviour of the gas bubbles in the liquid phase that was considered. The solid fibre phase was assumed to present a hindrance to bubble flow, but not to affect the mechanism of bubble flow and its escape to the surface.

It was assumed that the reduction of voids is achieved mainly through the flow of the gas bubbles to the surface of the liquid (surface of the laminate). The dissolution of gas in the liquid, and thus reduction of gas bubbles by these means, was assumed to have a small effect in comparison of the removal of bubbles by the process of flow and exit.

Experiments on and analyses of the effect of vibrations on composite-materials production conducted within this PhD study, were particularly targeting the minimisation of void content. Each stage of the experiments produced information relating to the process as a whole, such as frequency ranges and duration time of vibration, the position of different vibrations means, temperature dependence and vacuum assistance. All laminates were subjected to micrograph analysis for void-content determination, as well as to mechanical testing.

Special attention has been paid to theoretical development of the entire process. Hypotheses were proposed, and agreement between theory and experimental results was established. This thesis brings insight into many physical phenomenon, such as temperature-viscosity relationships, buoyancy and Stokes law, cavitation dynamics, mass diffusion, pressure variations, resonance frequency, energy-amplitude relationships, dissipated work, the chemistry of fibre-resin systems, and the influence of porosity on the properties of composite laminates.

Results presented in this thesis give insight into a range of parameters during vibration-assisted curing, with the frequency range 0 Hz - 40 kHz, different resin systems, and differing time duration of vibrations and operating temperatures as the most important shifting parameters. They reveal that composite laminates cured at elevated temperatures, along with vacuum assistance and low-frequency vibrations in the range 5 Hz to 50 Hz, produced the best laminates in terms of low void content and mechanical properties.

Results were achieved using specially designed and manufactured testing apparatus which incorporates vibration sources, based on the Quickstep process, the Australian National University Quickstep Machine, ANUQSM. The design parameters of this apparatus conform to the requirements of the basic principles of the Quickstep process.

A special low curing temperature epoxy resin was chosen to reduce the curing cycle time and thus to facilitate experimentation. A vinyl-ester resin was also studied to represent a system with a different curing mechanism and also being of industrial significance.

Void-content calculation was performed through optical micrograph analysis, while mechanical testing included flexural, tensile and shear tests. Water absorption by samples was also part of the investigation, with laminates being mechanically tested after being submerged in tap water for 7 days. Computed tomography provided insight into composite materials internal structure.

Other researchers in this field have proposed the use of vibration as a means by which composites' properties might be improved. Here it was hypothesized that introducing vibrations to the Quickstep curing system could help reduce defects in laminates and therefore produce better mechanical properties.

Four areas were chosen for investigation:

- The determination of frequencies suitable for the generation of vibrations necessary to minimize void content in a composite lay-up using the Quickstep process.
- The investigation of the mode of vibration to achieve maximum benefit (for example, whether the up-stroke should be faster than the down-stroke).
- Selection of the means by which vibration is transmitted to composite materials during curing in the achievement of maximum impact on the system.
- The determination of the position of vibration source on the apparatus most appropriate for the delivery of vibrations to the system.

1.3. The Quickstep Technologies and Process

The Quickstep Process enables the high-speed production of composite materials in volumes and cost structures not previously achievable using conventional autoclave processes. Quickstep Technologies Pty Ltd has a proprietary process based on fluid-based curing that significantly cuts the cost and time involved in producing composite components, compared with conventional processes. The plant consists of three tanks, a control unit and a curing chamber, as shown in Figure 1.1.

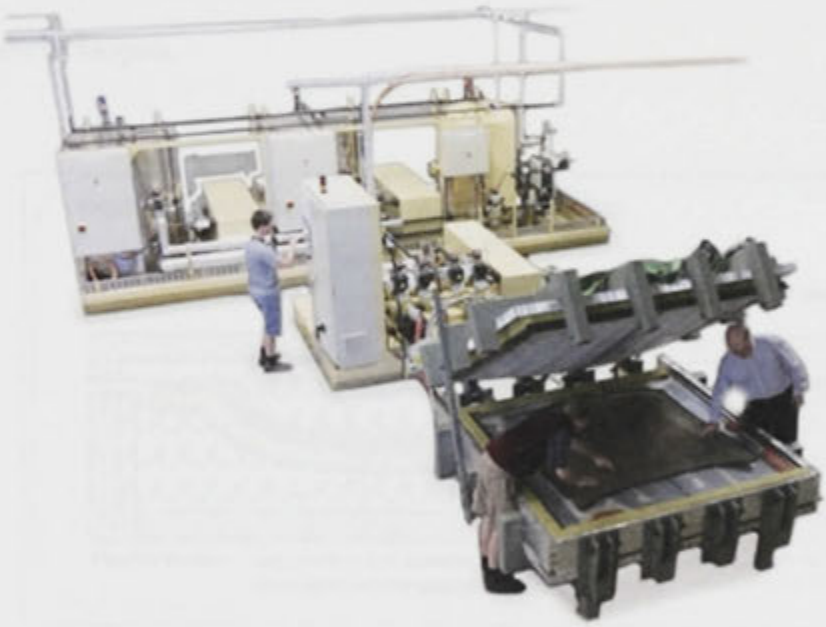

Figure 1.1: Quickstep plant with three fluid tanks (rear), control unit (mid) and curing chamber (front).

The initial process was developed by Quickstep Technologies Pty Ltd in conjunction with CSIRO. The Quickstep Holdings Company was founded in 2001 to commercialize the Quickstep Process. It has six pilot plants around the world and global alliances with major

international advanced-materials suppliers, with research and development and Applications Development Agreements with groups such as VCAMM (Victorian Centre for Advanced Materials Manufacturing) and the Australian National University.

Using balanced pressure and liquid heating and cooling, the Quickstep Process has applications in the aerospace and automotive industries where strength and weight are critical, as well as in many other industries seeking to replace metals with composites.
With reduced cure-cycle times and product weight, as well as increased strength and improved appearance, the process provides product properties comparable to conventional atmospheric-cure techniques and which are generally equal to or better than high-pressure autoclave techniques.

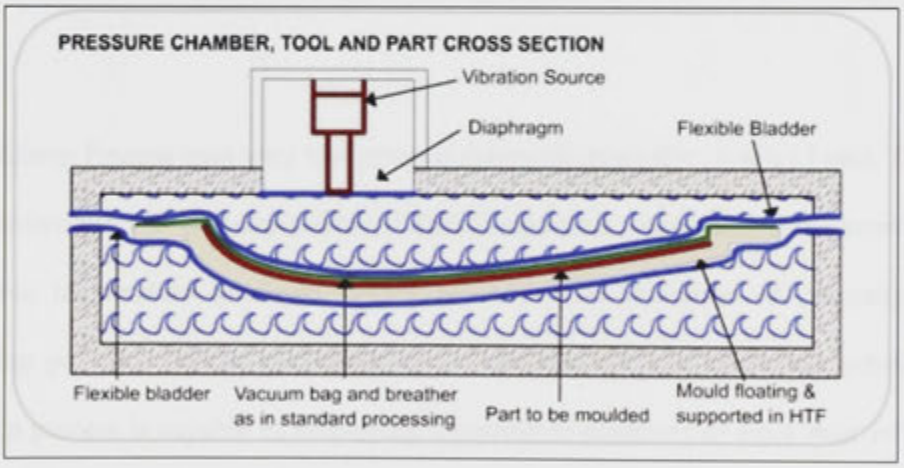

Figure 1.2: Quickstep Universal.

Quickstep Universal, depicted in Figure 1.2, works by rapidly applying heat to the laminate which is contained between a free floating rigid or semi-rigid mould that itself floats in a Heat Transfer Fluid (HTF). The mould and laminate are separated from the circulating HTF

by a flexible membrane or bladder. The Quickstep process uses balanced pressure, combined with vibration within the HTF, and vacuum applied to the laminate, to remove entrained air and then compact and heat the laminate to cure.

The HTF is stored in three separate tanks, a hot tank, medium tank and cold tank. The heat transfer liquid, stored in three vessels of user-defined temperature, are typically one each at ambient, dwell and full temperature. During processing, the fluid is continuously pumped behind two flexible bladders that enclose the part in a clamshell arrangement. The HTF has a significantly higher coefficient of heat transfer than any form of gas, having up to twenty-five times the heat transfer rate, and which is an efficient means of transmitting heat to the part to cure the polymer matrix. Simultaneously, the continuous flow eliminates the possible effects of exothermic reactions caused by a build-up of heat in the curing resin.

The Quickstep Process uses very low external pressures, typically 10 kPa (2 psi). The good consolidation and low porosity (<2%) of Quickstep-cured composites is achieved via the remarkable temperature gradients, which provide rapid reduction of viscosity in the reinforcing polymer matrix, permitting easy extraction of void-producing bubbles. The Quickstep process is capable of employing temperature gradients of more than 10° C/min, depending upon the latent heat of the tool or mould in use. This process enables very accurate temperature control in the curing process and significantly reduces cure-cycle times, as well as delivering important environmental benefits in the form of reduced emissions and energy use during the manufacture, of more energy-efficient end products.

The Quickstep process can easily be compared to Autoclave which is one of the most used traditional manufacturing processes. Significantly higher ramp rates can be achieved using the Quickstep method instead of the conventional autoclave cycle, as illustrated in Figure 1.3 [Campbell et al. 2005].

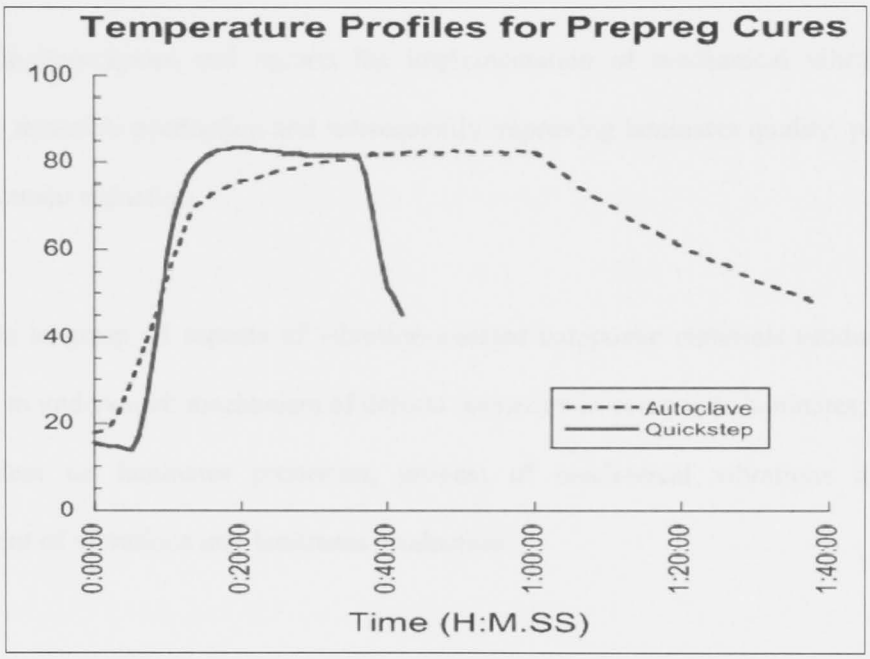

Figure 1.3: Comparison of autoclave and Quickstep processes.

More details can be found on the internet [Quickstep].

Chapter 2 LITERATURE REVIEW

This thesis investigates and reports the implementation of mechanical vibrations into composite materials production and subsequently improving laminates quality, particularly by void-content reduction.

To be able to grasp all aspects of vibration-assisted composite materials production it is important to understand: mechanism of defects formation in composite laminates; effects of void content on laminates properties; process of mechanical vibrations itself; and employment of vibrations into laminates production.

This chapter provides a general background on these issues individually, as well as an insight on behavior and interaction of laminates constituents. It presents an overview of mechanical properties affected by voids; vibrations application in various types of materials manufacturing; and physical chemistry of laminates themselves.

The results of various mechanical characterization studies of composite materials are explored. A range of methods to determine and analyse void content are presented. Published work on establishing vibration-assisted composite manufacturing is also reviewed.

2.1. Defects and Properties of Composite Materials

Hancox (1977, 1981) studied shear properties of solid CFRP rods and tubes containing flaws and voids, and conclude that voids have a serious degrading effect on shear modulus and strength, reducing properties to 30% of their void free value at 5 vol% voids. He also reported how the shear modulus, strength and strain at failure of carbon fibre reinforced plastics respond when exposed to the effects of temperature and temperature plus water. The effect of low (<1%) and high (>5%) void contents on the torsional properties of CFRP exposed to both dry and wet environments was studied, showing that that specimens with high voiding absorbed considerably more water than those with low-void content. Mechanical testing revealed that excessive voiding reduced the interlaminar shear strength of the composite by approximately 30%.

Judd and Wright (1978) reported a brief summary of void types and their causes, methods of measurement of void contents, and the influence of voids on the mechanical properties of composites. They concluded that voids in composites are caused by a) volatiles arising from the resin or its components during cure, b) from residual solvents, c) or from trapped air. The first two can be obviated by choosing a resin system, which does not evolve volatiles during cure and which does not need a solvent, especially of a high boiling point and polar nature. The last also depends upon resin characteristics, e.g. flow, viscosity, gel time, and also upon the care exercised in processing the material. Their research shows that there are decreases in mechanical properties in the presence of voids. The properties affected include interlaminar shear strength, longitudinal and transverse strength and modulus, fatigue resistance and high-temperature oxidation resistance. The authors reviewed 47 papers and conclude that there was considerable scatter in results, that the

ILSS of composites decreases by about 7% for each 1% voids up to at least 4% void content level, beyond which the rate of decrease diminishes, they add that other mechanical properties may be affected to a similar extent, that this is true for all composites regardless of the resin, fibre or fibre-surface treatment used in their fabrication.

Cantwell and Morton (1992) state that voids are arguably the greatest problem because they are difficult to avoid, particularly at the corners of composite components, and are detrimental to mechanical properties. Voids are inadvertently created in a number of ways, including by the formation of bubbles from volatile by-products produced during the cure reaction of the polymer matrix, by the use of a high-viscosity resin, by closely packed fibres which are not completely wetted by the resin, by entrapment of air, and by fabrication mishaps such as a leaking vacuum bag or poor vacuum source. They report that fibre-reinforced composites fail in a large number of modes involving the fibres, matrix and interphase region. In general, failure modes that involve fracture of the matrix offer low fracture energies, whereas fibre-dominated modes of fracture involve greater dissipation of energy. The tensile strength of long-fibre composites is sensitive to fibre damage, but the compressive properties are influenced by matrix fracture, most particularly delamination.

Studies of the detrimental effect of void content on the mechanical properties of carbon/epoxy laminates by Ghiorse (1993) indicate that in a manufacturing setting, a 2% void-content increase will cause an approximately 20% decrease in both interlaminar shear strength and flexural strength, accompanied by an approximate 10% drop in flexural modulus. He concluded that void content has been shown to be a major consideration in composite materials' quality control, regardless of the loading mode.

Lundström and Gebart (1994) studied the effects of process parameters on void formation in RTM, with vinylester resin and glass fibre reinforcement in focus. They found that void content increased with increasing flow lengths but that void content could be reduced by continuing resin flow after initial mould fill, thus 'washing' voids out of the mould. In this way, the resin advects out voids and more time is allowed for dissolving any binder or excessive sizing on the fiber surface. In industrial practice this procedure has commonly been referred to as bleeding. Void content increased with increasing temperature, despite decreasing resin viscosity, but the bubbly region at the flow front was relatively constant. They suggested that the mechanism for this might be thermal expansion of the voids but this was deemed unlikely as both mould and fibres were allowed to reach thermal equilibrium. An alternative explanation might lie in the evolution of volatile components. They also indicated that surface-tension effects were found to be negligible as temperature increased.

Surface treatments were found to significantly affect void content: fibres with the sizing removed became softer and easier to spread, which could possibly lead to better filling. Increasing pore-space complexity was found to produce higher void contents due to an increase in complex flow paths as would be expected. Probably the most important conclusion reported is that void content is strongly reduced by an applied vacuum and can be almost completely eliminated. Using vacuum assistance during mould filling was efficient for both the magnitude of the void content and for the extent of the void region. The lowering of the void content with vacuum assistance can be interpreted as a result of compression of voids when the vacuum is released and higher mobility of voids created at a lower pressure. The investigation of the influence of different lay-ups and different micro-

geometry indicates that a more complex flow path will give a higher void content. This could be a result of an increased number of bubble traps.

In summarising the variables that are known to contribute to voids and porosity in composite parts, Campbell et al. (1995) present a simple theory for void formation in addition curing thermoset composite materials that ties void formation to volatile vapor pressure. If the volatile vapor pressure in the curing laminate exceeds the actual pressure on the liquid resin (i.e. the hydrostatic resin pressure) prior to gelation, than void formation and growth will occur. Variables that are known to influence void formation and growth are chemical composition of the resin system, resin mixing and prepregging operations, lay-up variables, pressure operations, tooling variables, and finally, cure-cycle variables.

Olivier et al. (1995) examined the effects of various curing pressures (resulting in different void contents) on mechanical properties of carbon/epoxy laminates. They demonstrate that even if two laminates show the same void content, their respective response to an identical mechanical loading can be different, this being mainly due to void sizes and locations. The voids are principally located between the plies of the laminates where strength is lowest. No voids developed in a direction perpendicular to the plies. For any theoretical prediction of mechanical properties as a function of void content, it is absolutely necessary to consider voids as a volume variable. Plots of void-sensitive mechanical properties, ILSS and bending modulus, as a function of the time at which pressure was increased, enable them to suggest an optimal curing-pressure route, which minimizes void content and maximizes the mechanical properties of unidirectional laminates.

Varna et al. (1995) investigated the effect of void content and geometry on the transverse mechanical behavior of unidirectional glass-fibre-fabric/vinyl-ester laminates. Those laminates with the highest average content of voids had a transverse strain to failure as high as 2%, whereas low-void content laminates failed at 0.3%. Only a few large and well-defined transverse cracks formed in low-void content laminates before final failure. Multiple transverse cracks with irregular shape, as well as numerous smaller cracks, formed in the high-void content laminates. The irregularity of these cracks resulted in lower stress concentration and stress levels in the small amount of weft bundles orientated in the loading direction. Higher vacuum (lower pressure) resulted in lower void content. The highest void content was obtained at the edge of the laminate, and the void content then decreased away from the edge.

Ranganathan et al. (1995) propose a novel approach to model the consolidation process of thermoplastic composite plies, consolidation that incorporates relevant void growth and transport phenomena. The model is capable of predicting the final void fraction and the final thickness of a composite part as a function of the processing speed and the consolidation pressure under non-isothermal conditions. This work was based on the assumption that the composite can be modeled as a compressible continuum. Figure 2.1 depicts possible void mechanisms explored by the authors.

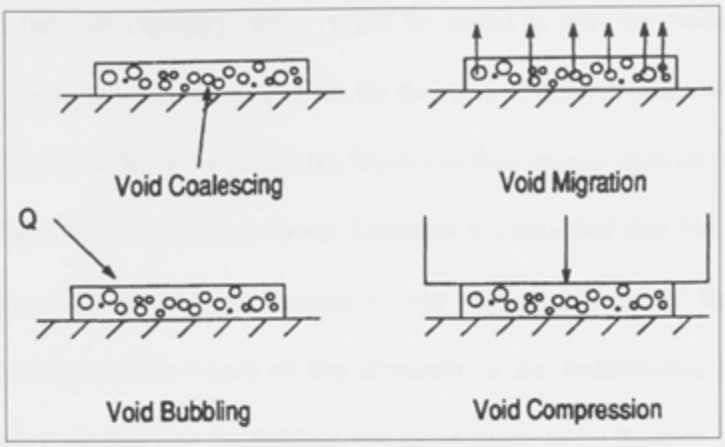

Figure 2.1: Void mechanisms in in-situ consolidation [Ranganathan et al. (1995)].

Ye et al. (1995) investigated consolidation quality and corresponding mechanical properties of GF/PP thermoplastic composites manufactured from a commingled yarn system. This model predicts the current void content as a function of bundle geometry and processing variables, i.e., temperature, applied pressure and holding time.

Studies by Davies et al. (1996) report the influences of water absorption on interlaminar shear strength and shear-fracture toughness of glass/epoxy. The composites were immersed in water for up to eight months at temperatures up to 70°C. Unreinforced matrix resin samples were also immersed for periods up to 2 years, with sea water absorbed less rapidly than distilled water. The interlaminar shear strength of the composite was reduced by prolonged immersion in water. Below 1% weight gains the shear strength was unaffected by water exposure. The mode II delamination toughness also decreased after immersion of the composite in water.

Lundström (1996, 1997) studied the advection of the bubbles by a model theory and experiment. He simulated void transport through fiber reinforcements in RTM by studying

bubble transport through capillary tubes. What he found is that the pressure required to deform bubbles through a constriction is set by the ratio of the constriction radius and the tube radius, the length scale of the geometry, liquid-surface energy and, in certain cases, the contact angle of gas-liquid-solid interfaces. Lundstrom concluded that bubbles are carried if: i) the pressure gradient is high enough, ii) the surface tension of the liquid is low enough, iii) the cross-sectional area of the channels in the reinforcement is sufficiently uniform. The theory reveals that the bubbles are more likely to be trapped on a small scale, i.e. within fiber bundles rather than on a large scale, i.e. between the bundles.

In a later paper Lundstrom considers the dissolution of cylindrical voids trapped between fibres during the resin transfer moulding process. It was found that in RTM not only pressure but also flow contributes to the dissolution of the trapped bubbles. The length of the voids decreases and voids disappear in minutes due to molecular diffusion. From the experiments it was found that high pressure, high flow rate and low initial gas concentration in resin (properly degassed resin) are favorable parameters for the dissolution of the voids. Further, from the experiments with pure resin it was found that air dissolves much faster in the vinyl-ester resin tested than in the epoxy at the evaluated conditions, as shown in Figure 2.2 where the square of dimensionless radius as a function of normalized time is plotted.

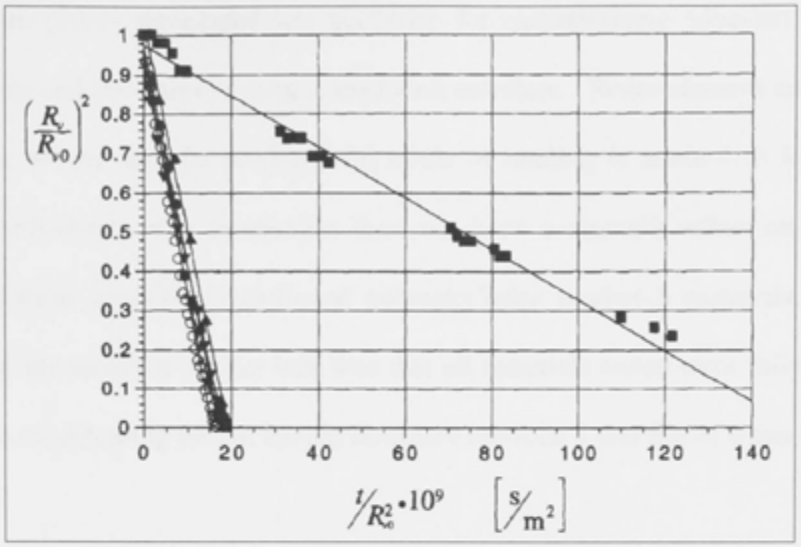

Figure 2.2: The dissolution rate is much slower for bubbles in epoxy (squares) than for bubbles in vinyl-ester resin (circles and triangles) [Lundstrom (1996)].

Compston and Jar (1998) investigated the effect of fibre lay-up and matrix toughness on mode I and mode II interlaminar fracture toughness (*G*Ic and *G*IIc) of marine composites. Results from both modes showed toughness variation that is consistent with matrix toughness. They also concluded that composites with woven roving fibres showed similar mode I delamination characteristics to the unidirectional composites, but their mode II delamination characteristics, after crack initiation, were quite different.

In another paper Compston and Jar (1999) investigate the influence of the fibre-volume fraction on the mode I interlaminar fracture toughness, *GIc,* of a glass-fibre/vinyl ester composite. Composite laminates were made by hand lay-up in an open mould, then evacuated using the vacuum-bag technique. Their results showed that *GIc* values for crack initiation are independent of the fibre-volume fraction and similar to matrix resin *GIc.*

Cantwell et al. (1999) developed test geometry for characterising adhesion between the composite skin and the balsa core in a sandwich structure. Finite-element analysis of the geometry has shown that the predominant mode of loading is mode I. It has also been shown that prolonged water immersion does not have a dramatic effect on the fracture properties of these glass-fibre-reinforced polyester/balsa sandwich materials. Continuous monitoring of the moisture uptake indicates that all materials tested were fully saturated at the end of the conditioning period having absorbed between 4 and 5% of water by weight.

The edgewise compression, flexure and shear properties of small GFRP/PVC foam sandwich composite specimens was investigated by Mouritz and Thomson (1999) to gain insight into the damage tolerance of a large minehunter ship. Compression strength decreases rapidly with increasing gauge length, and the failure mechanism changes suddenly from compressive fracture of the skins to shear crimping of the core when specimen length reaches ~100 mm. Interfacial cracks only affect the strength of the sandwich composite when they cause a change in the failure mechanism. The stiffness and strength of the sandwich composite decrease with increasing impact energy and impact-damage area except when the composite is loaded in bending-tension. The properties are most severely degraded when the depression in the impacted surface causes the composite to fail by skin wrinkling, which occurs in edgewise compression and bending-compression.

In another study Mouritz (2000) investigated the effect of increasing void content (up to 30%) on the ultrasound attenuation coefficient, interlaminar shear strength (ILSS) and Mode I interlaminar fracture-toughness properties of a glass fibre-reinforced polymer (GFRP) composite, and came to the conclusion that all properties degrade with increasing

void content. He has found that interlaminar shear strength and interlaminar fracture toughness decreased rapidly with increasing void content; see Figures 2.3 and 2.4.

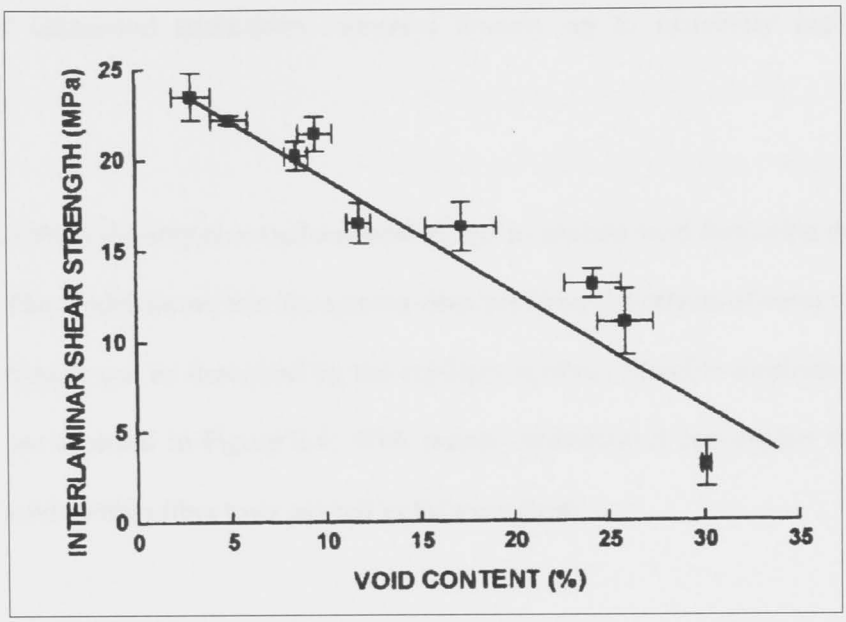

Figure 2.3: Variation in ILSS with void content [Mouritz (2000)].

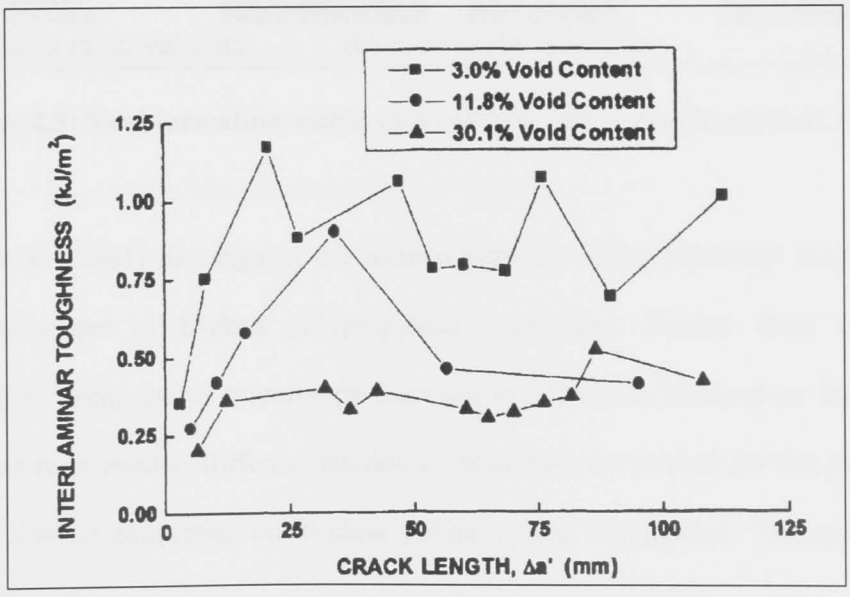

Figure 2.4: Curves for composites with various void content [Mouritz (2000)].

While previous studies showed that the attenuation coefficient of aerospace composites increases rapidly with void content up to ~12%, Mouritz showed that the attenuation coefficient continues to rise rapidly with void content up to ~30%. This study has also shows that ultrasound attenuation increases linearly up to extremely high thickness (~150mm).

Kang et al. (2000) developed a mathematical model to analyze void formation during RTM processes. The model shows that for a given fiber preform, the effects of resin velocity and capillary pressure can be described by the capillary number. Possible mechanisms of void formation are depicted in Figure 2.5. With proper calibration it can predict the size and content of voids within fiber tows as well as between them.

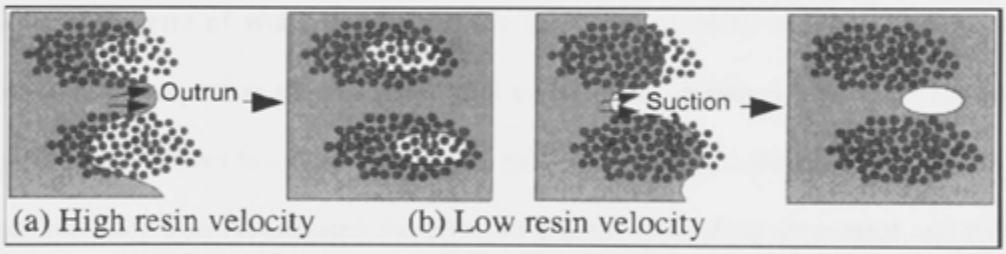

Figure 2.5: Void formation within and between fibre tows [Kang et al. (2000)].

Santulli et al. (2001) investigated the relation between void content and mechanical and impact properties of E-glass polypropylene composites. Results from void-content measurement using optical microscopy were put in relation to interlaminar shear strength and impact tests results. Different moulding parameters are critical for the attainment of sufficient impact properties on E-glass polypropylene composites. The application of

higher transfer time or inappropriate tool temperature may also affect material microstructures, resulting in a higher void content.

Fundamental mechanisms of matrix shrinkage and evolution of viscoelastic properties under given processing conditions were investigated by Eom et al. (2001). They constructed a process window for the manufacture of void-free thermoset composite parts, taking into account the dynamics of resin curing, including its shrinkage, and the mechanical-property evolution of the resin, as well as the structural resistance of the fiber network.

Costa, Almeida and Rezende (2001, 2005, 2006) performed a series of experimental programs to characterize the effect of voids on the strength of composite laminates. They report that the rate of water uptake and the maximum level of moisture absorption in carbon/epoxy composites depend upon void content and specimen geometry. Laminates with high void-content levels absorbed more moisture, leading to deterioration of laminate properties. They also investigated the effect of matrix, type of reinforcement and type of loading on the critical-void content, and showed that laminate properties depreciate with increasing void content. The influence of porosity was also studied, showing that the resin system affects the shape and size of voids in composite laminates and the associated fracture parameters.

Santulli et al. (2002) performed measurements in E-glass/polypropylene commingled laminates by analyzing images from optical micrographs. They analyzed the morphology of voids present, classified voids based on their size and orientation, and discussed the

difficulties in carrying out void content measurements in laminates. A statistical analysis of the relation between the representative number of photomicrographs to be analyzed and the consequent accuracy of the obtained measurement was also provided.

Scudamore and Cantwell (2002) investigated the combined effect of prolonged seawater exposure and high loading rates on the fracture properties of a range of sandwich structures used in marine and offshore applications. Their examination showed that the balsa system absorbed the greatest amount of water, which is a reflection of the hydrophilic nature of the balsa core. The linear PVC foam absorbed significantly more moisture than its crosslinked counterpart, suggesting that the three-dimensional network structure in the latter has inhibited moisture ingress. The aluminum honeycomb structure absorbed less than 2% by weight of moisture, reaching saturation in a relatively short timescale.

Hamidi and Altan's (2003) work indicates significant spatial variation in void content and morphology for resin transfer moulded E-glass/epoxy composites. These variations seem to correlate well with the local velocity of the fluid front during filling, which can be analyzed through the capillary number. More than 40% reduction in capillary number leads to more than 60% reduction in the void content. The slower moving fluid front traps less and more circular voids, whereas the voids might be sheared into more elliptical and irregular shapes near the parts' surface and inlet gate.

Barraza et al. (2004) applied various postfill pressure levels to glass/epoxy parts moulded at high volumetric flow rates as a method to reduce their void content. Overall void area fractions were found to be a function of the modified capillary numbers and flow front

velocities. The postfill pressure also seemed to have a strong influence on the shape and size of the voids. Basically, the overall content of irregular voids is substantially reduced with increasing levels of pressure. The same holds true for both the elliptical and circular voids, which are almost completely eliminated as the packing pressure increases. It is worth noting that void morphology also changed as a function of radial position, with increasing proportions of circular voids being located towards the vent openings.

A mathematical model developed by Jinlian et al. (2004) describes the mechanism of void formation during the RTM process, and the location of the void predicted by this model agrees quite well with experimental results. The model also shows that the ratio of weft's axial permeability and warp's transverse permeability is a determinant for the formation and size of voids.

Hagstrand et al. (2005) point out that voids may actually have positive effects on the properties of a structure, bearing in mind that for a given mass of material, voids will increase the dimensions and as a result, for example, the moment of inertia. This hypothesis has been evaluated by studying the influence of void content on the flexural properties of beams manufactured by compression-moulding multiple unidirectional commingled glass/polypropylene fibre tows. They conclude that there is a certain negative effect on the flexural modulus and strength, but a clear positive effect on beam stiffness.

Hamidi et al. (2005) investigated three-dimensional features of void morphology in resin transfer moulded composites. Relatively large cylindrical voids are observed in cigar shapes in the planar surfaces, whereas these voids only appear as small irregular or

elliptical voids on through-the-thickness surfaces. Along the radial direction, combined effects of void formation by mechanical entrapment and void mobility are shown to yield a complex radial void distribution. It is shown that fewer voids are trapped mechanically with increasing distance from the inlet and most of the medium and small voids that are mobile migrate towards the exit during resin injection. Void content contribution of voids located at different locations of the composite is presented in Figure 2.6.

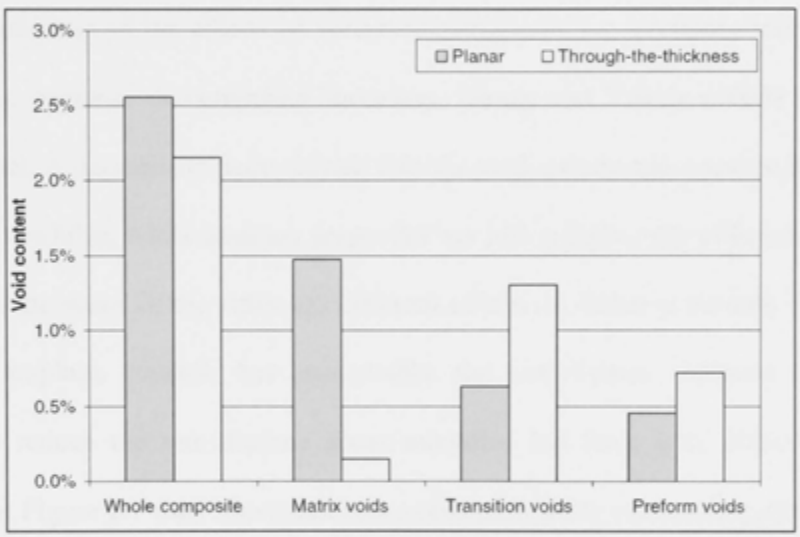

Figure 2.6: Planar and through-the thickness void content contribution of voids located at different locations of the composite [Hamidi et al. (2005)].

Hamidi et al. (2005) also investigated effects of applying packing pressure on void content, void morphology, and void spatial distribution for resin-transfer moulded E-glass/epoxy composites. The packed composite was found to contain almost 92% less void content than the unpacked composite. In addition, the average void size was observed to decrease from approximately 60 μm in the unpacked composite to approximately 32 μm in the packed composite, a decrease by a factor of 2. Furthermore, reduction rates of voids appear to be affected by their shapes. While circular voids experienced the highest removal rate, 99%,

cylindrical and elliptical voids registered lower but still significant reduction rates of 83% and 81%, respectively. Irregular voids, on the other hand, showed a slightly lower void-removal rate of 67%. The proximity of voids to fiber bundles was also observed to affect their removal rates, as voids located inside fiber tows sustained slightly lower reduction rates. Along the radial direction, removal of voids with different proximities to fibers seems to depend on their arrangement at the end of the filling stage.

In their examination of the effects of void microstructures, i.e. geometry and distribution, on the elastic response of composite laminates, Huang and Talreja (2005) used a finite element model. A parametric study reveals that the void content has a severe impact on the out-of-plane modulus, while in-plane properties are less significantly affected. For a given void content, the shape of the voids has different effects on different moduli. Flat voids are benign for in-plane moduli, but undesirable for out-of-plane stiffness. Long voids significantly reduce the out-of-plane shear modulus, but have little effect on in-plane properties. In Figure 2.7 they illustrated how voids push aside surrounding fibers and resin as they expand.

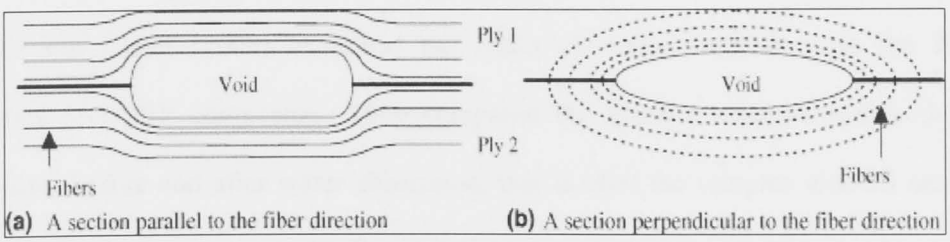

Figure 2.7: Schematic illustration of voids in composite laminates [Huang & Talreja (2005)].

Marriati and Chum (2005) concluded that lower resin/fiber ratios produce glass-fibre reinforced plastic plaques with higher fiber-volume fraction, fiber-weight fraction and void content. Furthermore, higher fiber volume content results in higher flexural strength and modulus in GFRP composites; see Figure 2.8. Additionally, higher void content resulted in higher weight gain and higher water-saturated levels, therefore water absorption decreased the flexural strength and modulus of GFRP composite laminates.

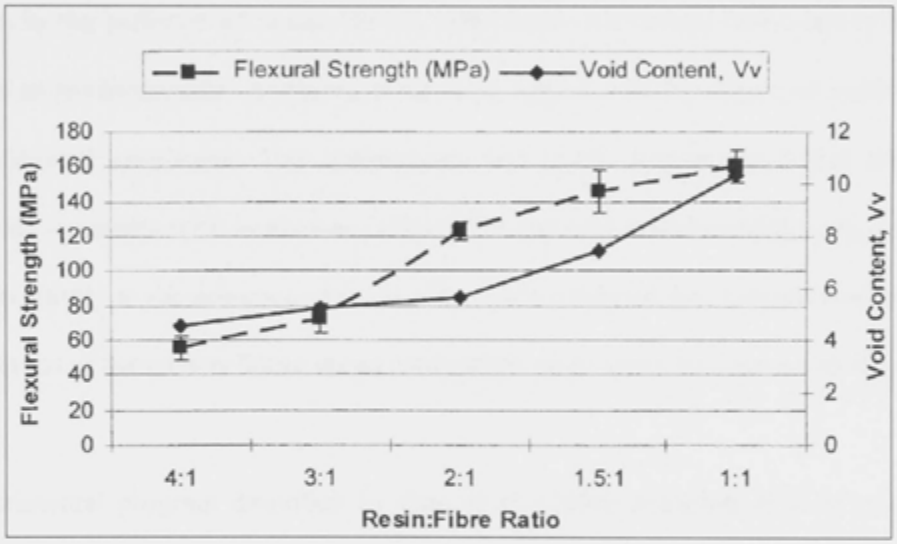

Figure 2.8: Flexural strength and void content vs. resin:fiber ratio [Mariatti & Chum (2005)].

Mariatti and Chum (2005) examined the effect of water absorption on the flexural properties of GFRP composites. They compared the flexural strength and modulus of composites before and after water absorption, that is after the samples reached saturation point (22 days). As expected, the flexural strength and modulus decreased with moisture absorption. It was also noted that severe debonding may occur at the fiber-interface and, as a result, the flexural strength and modulus of the composite reduced. The flexural modulus of all samples decreased by 5–27% after exposure.

Costa et al. (2005) presented experimental results on the combined effect of voids and moisture in polymer composites. Two types of reinforcement (eight harness satin fabric and unidirectional tape), two types of resin systems (epoxy and bismaleimide), and two types of loading (interlaminar shear and compression) were considered. Both temperature and humidity affect the interlaminar shear and compressive strength of composite laminates. The results for interlaminar shear strength showed that hygrothermal conditioning does not significantly affect the fracture parameters of the carbon-tape epoxy and carbon-fabric BMI laminates in the presence of voids. On the other hand, the carbon fabric-epoxy laminates subjected to environmental conditions were more sensitive to the effects of voids than the non-conditioned specimens. The compression test results demonstrated that the carbon fabric-BMI laminates with voids were affected by environmental conditioning, presenting higher sensitivity to the presence of voids. The effect of the environmental conditioning on the toughness of the carbon fabric-epoxy and carbon tape-epoxy laminates was negligible.

An experimental program described by Guo et al. (2006) describes aims at establishing acceptance levels for an attenuation level in the ultrasonic inspection of composite laminates. They focused on (1) obtaining an optimal cure cycle as well as evaluating the effects of pressure conditions on void content (Figure 2.9) and mechanical properties, (2) presenting the results of an experimental program to investigate the effect of voids on the mechanical strength of composite laminates, (3) assessing the adequacy of the fracture criterion to represent the experimental data for the effect of voids on the flexure, tensile, and shear strength of composite laminates, and (4) discussing the effect of the type of loading, flexure vs. interlaminar shear, on the critical void content of composite laminates both in terms of volume fraction and ultrasonic attenuation.

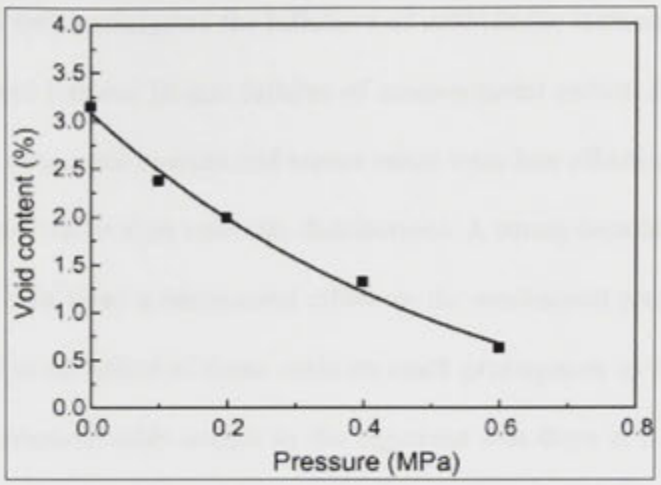

Figure 2.9: Void content as a function of cure pressure [Guo et al. (2006)].

Liu et al. (2006) designed a number of curing cycles to evaluate the effects of different pressure-induced voids on mechanical properties of carbon/epoxy laminates and optimum cure pressure time. A composite laminate produced by different cure pressures presented void contents from 0-3.5%. A decreasing relationship was obtained between void content and cure pressure, as shown in Figure 2.10.

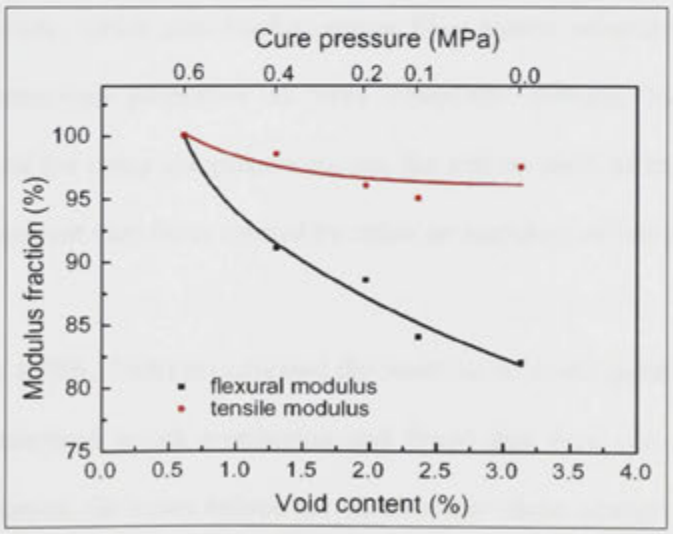

Figure 2.10: Relationship between modulus and void content (or pressure) [Liu et al. (2006)].

Chambers et al. (2006) investigated the influence of voids in the initiation and propagation of static flexural and flexural fatigue failures of unidirectional carbon-fibre composites. It was observed that mean void content and aspect ratios were less effective in explaining the mechanical property results than void-size distributions. A strong correlation between large voids (area > 0.03 mm^2) and a detrimental effect on the mechanical properties was found, and was attributed to the effect of these voids on crack propagation in the resin-rich inter-ply regions. This research adds weight to the argument that there is a critical void level below which mechanical properties do not further improve, but shows that the concept of critical-void content is too simplistic.

Zhang and Fox (2006) compared delamination resistance and nanocreep properties of 2/2 twill-weave, carbon-epoxy composites manufactured by hot press, autoclave, and Quickstep processes. The Mode I and Mode II interlaminar fracture-toughness results showed that the Quickstep process (QS) provided comparable delamination resistance to those laminates manufactured by autoclave. The QS was found to have the highest glass transition temperature, which also implies strong fiber–matrix adhesion of this material. Analyzing the nanocreep properties of three composite systems, based on both the analytical result and the creep compliance curves, the authors showed that the QS material was more creep resistant than those formed by either an autoclave or hot press.

Kousourakis et al. (2006, 2008) investigated the insertion of small galleries into laminated composites for structural health monitoring and found that they can significantly alter interlaminar properties. Galleries reduce the interlaminar shear strength of carbon-epoxy laminates. Interlaminar shear strength decreases with increasing size and volume content of

galleries inside the laminate, and loss in strength was attributed to reduced interlaminar load-bearing area due to the open-hole design of the galleries. Mode I delamination toughness is improved by the galleries blunting the crack tip. Low-energy impact damage resistance can also be improved by galleries blunting delamination cracks.

In a later paper (2008) the inclusion of open-hole galleries in polymer laminates for structural health monitoring was studied and it was concluded that galleries can degrade tensile and compressive properties of laminates when they exceed a critical size. Galleries alter the microstructure of the laminate by reducing fibre-volume content, due to swelling, reducing load-bearing area, and increasing ply waviness, with these changes adversely affecting mechanical properties. The reduction in elastic properties is more severe when galleries are aligned in the transverse direction, with this because of increased waviness of the load-bearing plies, which does not occur when galleries are aligned in the longitudinal direction.

Frishelds et al. (2008) modeled bubble motion through interbundle channels in biaxial non-crimp fabrics and explained that bubbles move with the resin through these channels and are trapped if the channels become too narrow. The paths of the bubbles depend significantly on the position of the threads keeping the fabric together and the number of fibres crossing the interbundle channels. The voids will move with the resin if they are not hindered by the reinforcement. The local speed of the resin, the size of the void and the detailed geometry of the reinforcement are thus important parameters for this transport. Splitting of bubbles is possible only if the gap is long and narrow. The bubbles can also rejoin. Another result is that the pressure difference over a trapped bubble increases by 50% in 3D geometry, possibly helping the bubble to escape, and that, on average, bubbles

movement is biased to the direction of the tows. Probabilities of bubble trapping and splitting are shown in Figure 2.11 where d_b is the bubble diameter.

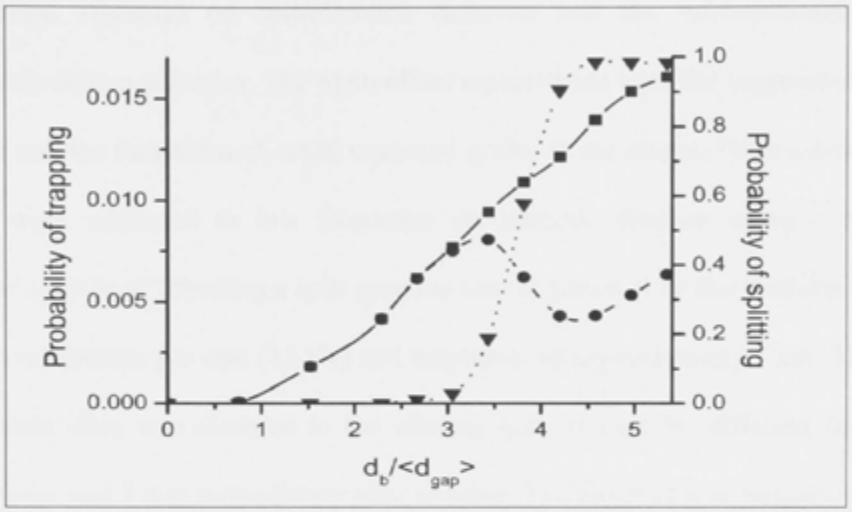

Figure 2.11: Probability of bubble trapping (squares and circles) and probability of bubble splitting (triangles) versus bubble size [Frishelds et al. (2008)].

2.2. Vibrations in Materials Manufacturing

Pillai (1972) presented results of an investigation on the effect of low-frequency mechanical vibration on solidification behavior and the microstructure of modified aluminum-silicon eutectics. The main effect reported has been the suppression of columnar growth and the formation of small equiaxed grains in the alloys. The normal and modified alloys were subjected to low frequency mechanical vibration using a simple electric vibrator capable of vibrating a split graphite mould mounted on the platform at a frequency of 720 oscillations per min (12 Hz) and amplitude of approximately 1 cm. The mould with the molten alloy was clamped to the vibrator and vibrated for different durations, viz. 1 min, 3 min, and 5 min immediately after pouring. The effect of low-frequency vibrations on the microstructure of normal and modified Al-Si alloys was quite marked. Silicon particles in the normal Al-Si eutectic alloys were refined with increasing duration of vibration. The eutectic silicon particles in modified Al-Si alloys were coarsened with increasing duration of the vibration. Since the eutectic constituent in the normal alloys has been found to be rather refined instead of coarsened, the alternate theory that vibration reduces the magnitude of undercooling during solidification and hence leads to coarsening of eutectic constituents stands as discredited.

Shukla et al. (1980) investigated the influence of vibration, when applied to metallic melts during solidification, on modification of conventionally obtained macro- and micro-structures of three aluminum alloys. Vibrations of different intensities were imposed on solidifying melts in the peak acceleration range of 1 to 20 g at 30 Hz and 5 to 120 g at 150 Hz frequencies. The mould was kept vibrating at preset values of frequency and peak acceleration throughout the entire period of pouring and subsequent solidification, with

castings also made in stationary moulds. The pouring temperature (750°C), the mould preheat temperature (350°C) and other conditions were kept identical in preparation of the castings both in static and vibrating moulds. Vibration imposed on solidifying melts has significant influence on ingot porosity in the case of all the three alloys studied. It is seen that under existing experimental conditions vibration could not bring about complete elimination of porosity in any of the three alloys.

This investigation showed that application of vibration can reduce porosity in solid solution types of aluminum alloys. This improvement in ingot soundness, however, occurs only in specific peak-acceleration ranges and, therefore, control of vibration parameters is necessary in order to gain beneficial effects. They concluded that the application of vibration during solidification of eutectic aluminum-silicon alloys was not found to be beneficial.

Campbell (1981) reviewed the literature on the effects of vibration on solidification metals in terms of a unifying concept, the frequency-amplitude f-a map. He categorized methods of application of vibrations (mould or liquid, continuous or intermittent), modes (vertical, horizontal, rotational), structural changes and properties of vibrated alloys, flow and resonance effects, solidification, as well as explained pressure variations in melt, viscous adhesion, cavitation threshold and collapse. One of the conclusions reported is that porosity is generally reduced by vibration during solidification but there seemed a small risk of increased porosity if the cavitation threshold was exceeded. Thus, for grain refinement the recommended frequency range lay below 200 Hz. Campbell also pointed out important advantages of the application of vibrations to solidifying castings.

Prosperetti et al. (1982, 1984, 1999, 2000) surveyed many topics on bubble dynamics in the presence of an oscillating pressure field, such as pressure fluctuations caused by mechanical vibrations. The mechanisms by which pressure fluctuations affect the bubble's growth process are essentially two: rectified diffusion and coalescence. A bubble containing pure vapour collapses in a static pressure field under the action of pressure and surface-tension forces and there is no static equilibrium radius in this case. However, the bubble can be stabilized by a sound field inducing volume pulsations. During most of the bubble's lifetime, internal pressure is very small and its dynamics mostly governed by external pressure. Because of the density difference between liquid and vapor, the pressure gradient causes the bubble to acquire relative velocity with respect to the liquid, with significant effects on heat transfer and radial dynamics. Due to the tendency of the system to conserve impulse, this relative velocity is amplified when the bubble collapses and reduced when it expands. As a consequence, the bubble's tendency to avoid high pressures and move toward low pressures is magnified in the former case and reduced in the latter.

Young, in his book, (1999), gives detailed analyses of cavitation, starting with different kinds of cavitations (hydrodynamic, acoustic etc), their formation and possible mechanisms for size changes (growth/collapse) with reference to pressure, temperature and diffusion. It also contains general explanations and equations of bubble dynamics, threshold and equilibrium conditions, Rayleigh-Plesset, mass and thermal diffusion, spherical stability, damping, Bjerknes force and sound propagation in liquids.

Ghiorse and Jurta (1991) applied vibration during the pre-gelation period of the cure cycle of vacuum-bagged, carbon/epoxy laminated plates. Their exploratory process was referred

to as vibration-assisted vacuum-composite processing (VAVCP). They characterized two test groups of laminates: the VAVCP group and a static-cure control group. All preforms were cured on the same tool plate under identical bagging and processing conditions, isolating vibration as the sole variable-processing parameter. All preforms were laid up and vacuum bagged on the release-coated tool plate and the assembly placed in an air-circulating oven. The VAVCP test set-up utilized a simple, air-driven mechanical shaker table. The vibratory frequency ranged from 40-50 Hz. Amplitude was not monitored. The shaker was run from the start of the cure cycle until 30 min after the preform core temperature reached 177°C, when the resin had fully gelled (after 2.5h). The vibration was then stopped and the cure-cycle completed with the tool plate static. VAVCP cure cycle is presented in Figure 2.12. The static cure-control group was processed the same way without vibrations. Microscopy void-counting and sizing was done at 100 magnification on 25mm^2 of laminate cross-section per specimen.

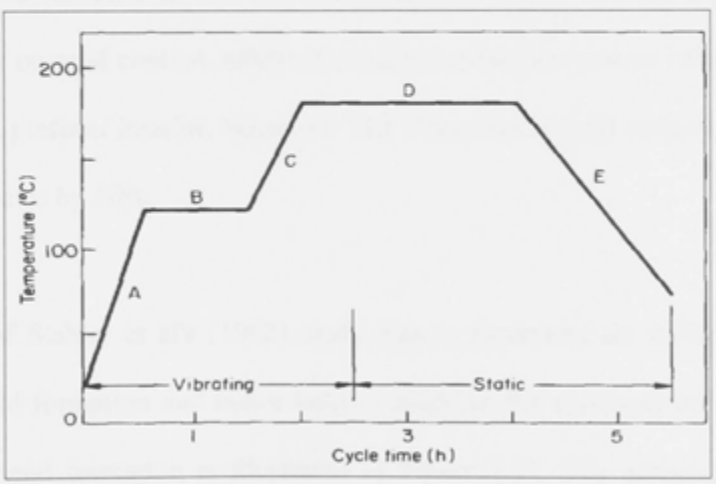

Figure 2.12: Vacuum cure cycles for the VAVCP process [Ghiorse & Jurta (1991)].

What they found was a decrease in void content in excess of 50% with an accompanying 10% increase in the size of the remaining voids, as well as an increase by 0.5%. to laminate densification The average 54% decrease in void content using the vibratory-cure process (VAVCP) versus the static-cure process was a key finding. The authors believed that the void reduction was brought about by applied vibration.

Ghiorse (1993) investigated several composite-materials void-reduction techniques. These included vibration-assisted vacuum-composite processing (VAVCP), porous scrim layering (PSL), microporous membrane processing (MMP), and Narmco Materials, Inc.'s Thick Laminate Prepreg (TLP). In VAVCP, low-frequency vibration was applied during the pregelation period of the cure cycle of vacuum-bag processed carbon/epoxy laminates. This process affected only established gas bubbles. Decreased void content in excess of 50% and increased laminate densification of 0.8% were measured. Data also indicated an approximate 10% increase in size of the remaining voids. The PSL process had no detectable effect on void content. MMP showed the ability to remove volatile water vapor from within the preform interior. Narmco's TLP lowered the void content of vacuum-bag processed laminates by 50%.

The objective of Stabler et al's (1992) study was to determine the effects of processing variables on void formation and hence help to establish the reason(s) for void formation. Mechanism of void formation is illustrated in Figure 2.13. The processing variables of interest were: application and the amount of mould-release agent (i.e. surface waxing) on the mould used in the RTM; the initial bubble content of the epoxy resin entering the mould during filling; the vibration frequency of the mould during filling; the fill pressure of the

equipment, and the fill time. For conditions of good surface waxing and low initial bubble content, voids were minimized. Vibration at 10 Hz reduced voids significantly in samples having high specific voidage and became less significant when near-perfect samples were produced. Operating variables that did not affect void formation were fill time and pressure. To study the effect of vibration on void content, the mould was mounted vertically on a vibration table, and the mould was filled from the bottom during vibration. A frequency range between 5 and 50 Hz was studied. The amplitude of the vibration was typically 5 mm. To test the effect of vibration on void content, only resin with high bubble content was used in the vibration testing. And that was considered as the worst-case test. A minimum in void formation was observed at approximately 10 Hz. Vibrations at frequencies other than approximately 10 Hz neither helped nor hindered void formation. Studies with vibration were also performed under the best of conditions (i.e. low bubble content in the resin fee, excellent waxing) with and without vibrations. The significance and importance of vibration became less in the elimination of voids as perfect samples and samples of low specific voidage were obtained without vibration.

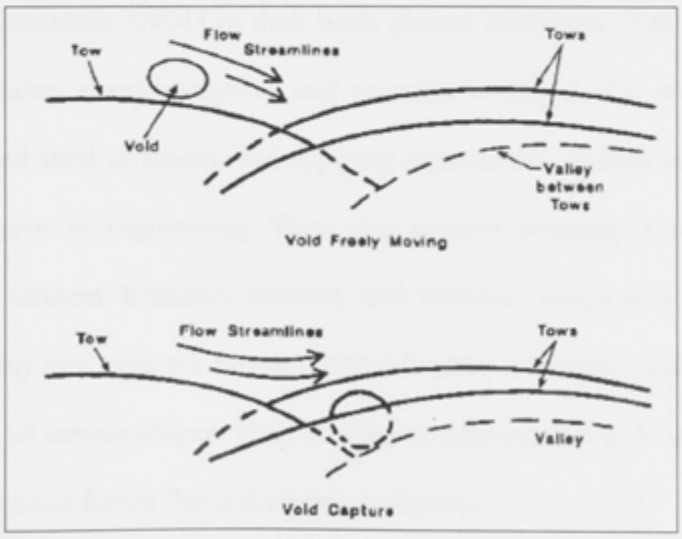

Figure 2.13: Drag induced void formation [Stabler et al. (1992)].

Grinis and Monin (1999) found that application of vibrations to the liquid phase serves to overcome the surface-tension forces and assist the break-up of bubbles. In their paper they describe the influence of vibration on bubble size and established that the energy transferred from the vibrating channel to the bubbles is well correlated to the speed of vibration. They proposed the use of vibration as a means of obtaining the desired bubble size.

Lauterborn et al. (1999) address all issues that deals with experimental and theoretical bubble dynamics, such as mechanisms of bubble appearance in liquids, descriptions of bubble dynamics in a sound field relating to the Rayleigh-Plesset model, frequency dependence, shock-wave radiation, spherical stability and bubble dynamics, rectified diffusion, Bjerkness forces, etc. Their findings also emphasise that sound waves consist of pressure and tension phases, and thus strong waves are able to rupture a liquid in their tension phase, giving rise to the phenomenon of acoustic cavitation.

Ventsel and Krauthammer (2001) in their book present principles of thin plate and shell theories, emphasizing novel analytical and numerical methods for solving linear and nonlinear plate and shell problems, and applying them to the analysis and design of thin plate-shell structures in engineering. They also present computer processes for finite difference, finite element, boundary element, and boundary collocation methods. In thin plates chapters they deal with the fundamentals of small-deflection, plate-bending theory, bending of plates of various shapes, plate bending by approximate and numerical methods, as well as with free and forced flexural vibration of plates.

Graham (2002) reported that rudimentary vibrations were employed in early work on QS plants, such as hitting the mould gently with a hammer, to assist with the removal of gas bubbles from a highly fluid resin in the early stages of processing. Once time had elapsed to permit gellation to take place they stopped. It was believed this effect would act as a liquid hammer blow to more closely fit fibre to fibre thus improving inter-laminar bonding and, as a by-product, produce a somewhat more consolidated package.

Quickstep dismissed ultrasonics because of its excellent mixing characteristics and searched for something that would simulate the tapping of a finger on the side of a beaker of resin to remove entrained gas or tapping to help settle out solids in a beaker of flocculated suspended solids.

The first approach sought was to find a high-speed valve that could be placed in the line to create a water-hammer effect. The next approach was to use a Vibra-ball high-speed vibrator, used in mining and industrial applications to help solids move along chutes out of bins etc. This gave 12,000 vpm (vibrations per minute) that was too far away from tapping the side of the beaker to be of use.

Finally there was a system found which appeared to meet the tapping specification, an air cylinder cycled by a quick-reversal valve. By appropriately sizing a cylinder, valve, air lines and pressure, a varying pulse in a piston set in a diaphragm within the liquid of the QS moulds was created. This gave a more consistent and better-consolidated product with lower-void content than could be achieved by not using vibration. Supplying plenty of air to the unit by putting it directly on the compressed air line was found to be better than using throttled air.

It is believed that there is probably an optimal vibration frequency and mode of vibration that is applicable to a particular mould set, and hence the need to investigate whether the

up-stroke should be faster than the down-stroke, the vpm be 300 or 1300, how much of the mould area is covered by a single unit, etc.

Alonso-Rasgado et al. (2002) established that die vibration can be used to polish surfaces as they form during solidification, with tangential vibration at certain frequencies and amplitudes influencing surface finish. It was shown that by varying the position and number of sources of vibration, conditions required for polishing can be approached and that die vibration can be used to generate surfaces with a quality significantly superior to that of the die. Frequencies employed were 80 Hz and 350 Hz.

Krishna and Ellenberger (2003) studied the influence of low-frequency vibrations on the water phase, in the 50-400 Hz range, on the size of air bubbles and oil drops formed at a single orifice. A special device, a vibration exciter, was mounted at the bottom of the 0.1 m diameter column that was filled with water. Vibration was transmitted to the water phase by means of a piston. Both the amplitude of the vibration and its frequency had been adjusted accurately. The application of vibration to the water phase has been seen to reduce the size of air bubbles by 40-50% and that of the oil drops by 70-80%. The authors concluded that application of low-frequency vibration has the potential to improve contacting in fluid-fluid dispersions.

Ellenberger and Krishna (2003) report that vibrations have a beneficial effect in gas–solids fluidisation. Application of low-frequency vibrations, in the range 40–120 Hz, causes a 40–50% reduction in bubble sizes formed in a single capillary. It was concluded that

application of low-frequency vibration has the potential to improve gas-liquid contacting in bubble columns.

The possible improvement of RTM process with mould-inducing vibrations and vacuum assistance was investigated by Pantelelis (2004). Reported results showed that with the Vibration Assisted Resin Transfer Molding, VIARTM, method a considerably better quality product part could be manufactured when frequencies of 15-30 Hz are used, in conditions of higher pressure and fibre-volume fractions. Even though the process considerably reduced dry spots as well as air-traps and bubbles, drawbacks were experienced in the design and construction of vibration mechanisms for heavy moulds.

Doinikov (2005) researched the area of primary and secondary Bjerkness forces on bubbles in acoustic fields, interrelation of oscillatory and translational motions of bubbles, surface bubble modes, and dynamics of many-bubble systems in strong fields. In his earlier work he explored interactions of gas bubbles in a compressible fluid and acoustic radiation pressure exerted by a spherical wave on a bubble in a viscous fluid.

Kocatepe (2007) summarises research into the effect of low-frequency mechanical vibration on the porosity of unmodified and metallic-sodium modified LM25 [Al–Si 7.15%] and LM6 [Al–Si 12.30%] alloys. Vibration at varying frequencies between 15 and 41.7 Hz and amplitudes between 0.125 and 0.5 mm has been applied to both unmodified and metallic-sodium modified LM6 and LM25 alloys during solidification. Results indicate that the number and size of pores increased with increasing vibration intensity in unmodified LM25 and LM6 alloys. Vibration of sodium-modified LM25 and LM6 alloys

increased the number and size of pores. Vibration at frequencies of 31.7–41.7 Hz, and amplitudes of 0.375–0.5 mm, produced large holes on the top of the ingot in unmodified and modified LM25 and LM6 alloys. In this experimental study, vibration did not reduce cavitations in the ingots.

Jimenez-Fernandez and Crespo (2006) investigated the collapse of gas bubbles taking into account the general Rayleigh-Plesset equation. They studied the collapse of spherical bubbles in viscoelastic fluids, induced by an imposed pressure difference between the internal gas pressure, and the external pressure of the continuous phase. It was concluded that the dynamics of single bubbles is unaffected by the rheological properties of the host fluid, except for in the proximity of rigid boundaries or in the case of non-spherical bubbles.

Xu et al. (2008) investigated the effect of ultrasonic vibration injected into the melt at various stages of solidification, on grain refinement and particle distribution in a Zn-based solidified composite-filler metal. Perfect grain refinement was obtained with the application of continuous ultrasonic vibration, but serious SiC particle segregation occurred in the solidified composite filler. Uniform distribution of SiC particles as well as grain refinement was obtained when proper intermittent ultrasonic treatment was applied. The investigation's purpose was to collect information relevant to handling the solidification process during joining or casting of SiC-reinforced metal-matrix composites with the aid of ultrasonic vibration.

2.3. Physical Chemistry in Composites

Thomason (1995) studied the influence of the fiber-matrix interface on the properties of composites. He found that the level of ILSS in unidirectionally reinforced glass-fibre/epoxy resin composites was dependent on the void content; the magnitude of this dependence varied in the range 2-10 MPa loss per 1% voids, depending on the fibre/matrix combination. The interfacial strength (proportional to the ILSS at fixed void content) is dependent on the nature of the glass-fibre coating and on the type of curing agent in the resin formulation.

Thomason also describes the effect of voids, the fibre-surface coating and the nature of the fibre-matrix interface on water absorption in glass/epoxy composites. The presence of only 1% voids in a composite can more than double the amount of water it absorbs; see Figure 2.14. The nature of the matrix system was also found to have an effect, in particular the epoxy-resin/curing- agent ratio played an important role. He concluded that the interfacial strength and the fibre surface coating also had an influence, but to a much lesser extent.

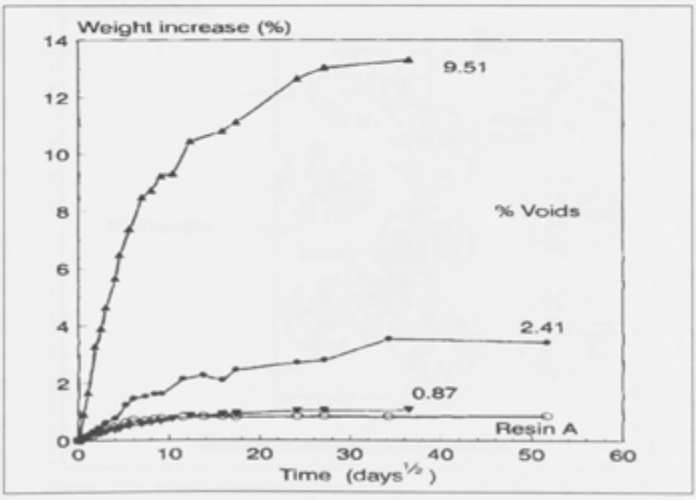

Figure 2.14: Water absorption curves for composites with different void contents [Thomason (1995)].

Additionally, Thomason showed that application of a coupling agent to a glass fibre improved fibre-matrix adhesion in composites.

Chen et al. (1995) followed the flow front in RTM and qualitatively measured entrapped air bubbles by image analysis. Voids were found to move axially along fibres until they find a pore space to escape into or settle down or merge with another void. Figure 2.15 depicts two levels of impregnation in RTM process and the behavior of voids. Voids were found to shrink when subjected to pressure but not necessarily become mobilized. They concluded that optimum processing parameters of fiber wetting for resin transfer moulding and structural reaction injection moulding are low viscosity, vacuum, high-mould temperature, and high pressure.

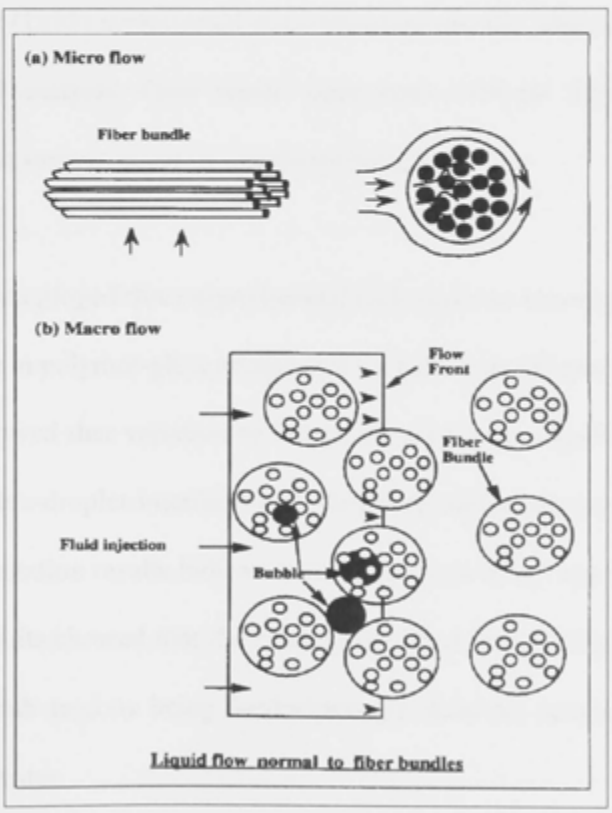

Figure 2.15: Two levels of impregnation in RTM process: a) micro flow-bundle level; b) macro flow-mat level [Chen et al. (1995)].

Saidpour and Richardson (1997) used four different silane- and one titanate- coupling agents, at three different concentrations, to achieve optimum mechanical properties in unidirectional glass reinforced vinyl-ester composite materials, finding that when glass fibre had no coupling-agent protection in the coating, the tensile strength of the composite was significantly reduced.

Keusch et al. (1997) investigated the influence of differently sized glass fibres on the mechanical properties of glass fibre/epoxy resin composites. Their results showed that the type of sizing has considerable influence on composite's properties, including interfacial shear strength, interlaminar shear strength and transverse tensile strength.

Keusch and Haessler (1999) investigated glass-fibre/epoxy-resin adhesion in composites by dynamic mechanical analysis. Their results once again indicate that aminosilane-sizing fibre treatment lead to improvement of interfacial bonding.

Hodzic et al. (2001) employed three experimental techniques to investigate the influence of the interphase region in polymer-glass composites on bulk material properties. Results from microdroplet test showed that variation to interphase properties significantly affects stress distribution at the fibre-droplet interface, and, therefore, stress redistribution in composite materials. Nano-indentation results indicate interdiffusion in water-aged interphase regions. The nano-scratch results showed that the harder interphase region dissolved into the softer interphase region (both regions being harder/stronger than the matrix) and expanded its width after aging in water.

Hodzic and Stachurski (2001) performed surface-tension measurements based on the angle of contact between resin and fibre. Their method proposes different geometry and consequently a simpler solution to the problem, with an additional advantage of verification of droplet equilibrium and accuracy of measurements.

Suri et al. (2001) investigated the coupled effect of ageing and surface treatment on the fracture and tensile properties of a glass/vinyl-ester composite. Interlaminar fracture toughness is most sensitive to interface properties. Absorbed water caused serious damage at the interface, leading to degradation of mechanical properties. The surface treatment of glass fibers had an indirect influence on the properties of the composite, an influence amplified by ageing.

Iglesias et al. (2002) observed the influence of different aminosilane fiber coatings on the resistance of epoxy-based composite materials using a fractographic test and fluorescence methodology. They reported their conclusion that the mechanical properties of glass-fiber reinforced epoxide-composite materials are strongly dependent on the molecular structure of the coupling region. Crosslinking density and, therefore, rigidity, increase as the accessibility of the functional groups of the coupling layer increases, with the hydrolytic damage rate depending up on the surface reinforcement treatment.

Plonka et al. (2004) analysed ageing effects on sized glass fibres. Their tests show that interfacial strength strongly depends on the chemical nature of the fibre surface, the sizing formulation, and surface roughness, with micro-mechanical tests appearing to be very sensitive to surface-property changes due to aging.

Hodzic et al. (2004) investigated the influence of water degradation on bulk material properties. The aim of this work was to investigate different polymer/glass composite systems at micro and macro levels, in order to obtain the link between their local micro-properties and the fracture toughness of the bulk materials.

Chen et al. (2006) studied the influence of fiber wettability on interfacial properties of composites. Results indicate that higher surface free energy can enhance the wettability between fiber and matrix, and that humid resistance and interfacial adhesion can be improved at the same time.

Comte et al. (2006) investigated the origin of voids in sheet-moulding compound sheets using different glass-fibre sizing. The quality of impregnation and void elimination was found to be dependent on bundle characteristics, rigidity and surface energy, conferred by their sizing and over sizing.

2.4. Summary of Literature Review

This chapter provides an introduction to the general aim of this study: the development and the understanding of vibrations in composite materials manufacturing so as to fully enable their successful utilization.

Much previous work has concentrated on how void content affect mechanical properties of laminates. Literature reviewed indicates degradation of mechanical properties with any type of defects and flaws associated with composite laminates. Type of defects and their formation are also reviewed; it is difficult to avoid them but there are means to minimize the void content in composite laminates.

Variables that are known to influence void formation and growth are chemical composition of the resin system, resin mixing and prepregging operations, lay-up variables, pressure operations, temperature and humidity, tooling variables, cure-cycle choice and vacuum assistance. Flow rate (for RTM), properly degassed resin, applying packing pressure or postfill pressure are other factors also taken into account.

A strong correlation between voids and a detrimental effect on the mechanical properties was found.

Studies on vibration-assisted materials production have mainly focused on the use of low frequency vibrations and how they affect materials properties. It is found that vibrations can be beneficial when lowering void content is the target. There are summaries of methods and modes of vibrations, as well as theoretical explanations to some phenomena associated with mechanical vibrations.

General explanations and equations of bubble dynamics in presence of vibrations, their formation and possible mechanism for size changes, with reference to pressure, temperature and diffusion are presented.

Findings of void content decrease and mechanical properties increase with low-frequency vibrations use are disclosed; generally, frequencies reported are in the range of 5-200 Hz.

Promising behavior in reducing the porosity in composite laminates is investigated, with some studies looking at metallic melts.

Additional investigations of fibre-matrix interface, fibre coatings and fiber wetting effects on void content of composite laminates were necessary to characterize vibration supported mechanisms involved with bubble removal.

It is found that fiber wetting influences void content and is aided with low viscosity, vacuum, high-mould temperature, and high pressure. Differently sized glass fibres also affect mechanical properties of composites. Effect of ageing and surface treatment on the mechanical properties of composites, as well as the influence of water degradation on bulk material properties, are examined. There is a clear connection of quality of impregnation and void elimination.

Chapter 3 THEORETICAL DEVELOPMENT

This study deals with void content in composite materials and possibilities of its reduction.

The physics of bubble statics and dynamics in a two-phase medium can be a complex matter. Complications arise from:

- gases (air) dissolved in the liquid,
- the bubbles may contain both air and condensable vapor in unknown ratios,
- bubbles with a distribution of sizes are present in the liquid, and
- plies of woven fibres are present in the liquid resin.

Other complications may arise from energy losses involved in damped oscillations of the bubble/liquid system, heat conduction, viscosity, compressibility, surface tension, mass transfer, diffusion, temperature and mass discontinuity at the phase boundary.

Assumptions

It is assumed that the reduction of void's content is achieved mainly through the flow of the bubbles to the surface of the liquid (surface of the laminated sample). The dissolution of bubbles in the liquid is assumed to have negligible effect in comparison to the removal of

bubbles by flow and exit (escape). Hence the main focus is on the means by which a bubble can flow to the surface and disappear.

The presence of the solid fibres in the liquid resin is assumed to present a hindrance to bubble flow, but not affecting the mechanisms of flow. Consequently, the presence of fibres is not considered, other than as an obstacle which delays the bubble's time to escape.

Let us consider the case of a bubble being in a liquid that is not subjected to vibrations. The bubble is submerged in the liquid at depth h, as shown in Figure 3.1. There are four ways by which the bubble can be disturbed from equilibrium:

- Growth due to internal pressure or reduced external pressure
- Contraction due to surface tension
- Rise due to buoyancy
- Dissolution due to diffusion of gas out of the bubble

When exposed to mechanical vibrations other phenomena affect the behavior of a bubble, and these will be considered later.

3.1. Effect of Pressure

A small, free, spherical bubble in a viscous liquid is filled with a mixture of air, liquid vapor and any gases dissolved in the liquid. Such a free bubble will slowly float to the liquid's surface, and gas may diffuse in or out of the bubble, allowing it to either grow or diminish.

Figure 3.1 depicts mechanical equilibrium of a gas bubble in a liquid at depth h.

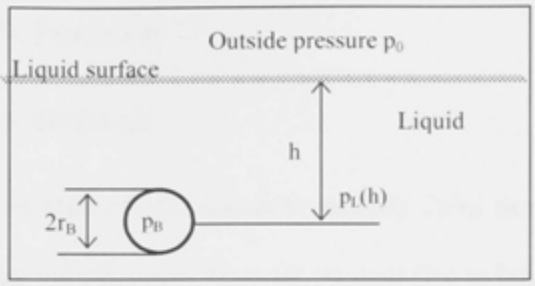

Figure 3.1: Mechanical equilibrium of a gas bubble in a liquid.

The pressure in the liquid, p_L, at depth h is

$$p_L(h) = p_0 + p_h \tag{3.1}$$

where p_0 is the external/outside atmospheric pressure and p_h is the hydrostatic pressure. The pressure inside the gas bubble, p_B, is given by:

$$p_B(h) = p_L(h) + \frac{2\gamma}{r_B} \tag{3.2}$$

where the last term is so-called Laplace pressure, with γ as the surface tension and r_B as the radius of the bubble.

Further in the text, this dependence on depth (h) will be omitted for the ease of reading.

For a given system γ is constant. For epoxy resin it is taken as 45 mN/m [Hodzic & Stachurski (2001)], and for vinyl-ester resin it is 30.4 mN/m [Dirand et al. (1996)].

For any bubble to be in mechanical equilibrium with a liquid the pressure difference across its liquid/gas interface must equal $2\gamma/r_B$, where γ is the surface tension of the liquid and r_B is the radius of the bubble [Campbell (1981)]. Thus, pressure difference, Δp, is

$$\text{internal pressure} - \text{external pressure} = \Delta p = 2\gamma/r_B \tag{3.3}$$

Therefore, possible situations are expansion or shrinkage of the bubble:

$$\Delta p > \frac{2\gamma}{r_B} \Rightarrow \text{Expansion} \tag{3.4}$$

$$\Delta p < \frac{2\gamma}{r_B} \Rightarrow \text{Shrinkage} \tag{3.5}$$

When the left hand side of the equation exceeds $2\gamma/r_B$ then mechanical equilibrium no longer holds and the bubble grows from its original size to larger dimensions.

Typical value for the surface tension is 40 mN/m. Therefore, for a bubble of 10 μm radius: $2\gamma/r_B$ = 8 kPa, small value compared to normal, atmospheric pressure.

Applying gas law to the bubble we have:

$$p_B V_B = NRT \tag{3.6}$$

where volume of the bubble, V_B, is

$$V_B = \frac{4r_B^3\pi}{3} \tag{3.7}$$

Substitution of equation (3.7) into (3.6) gives bubble radius, r_B,

$$r_B = \sqrt[3]{\frac{3NRT}{4\pi p_B}} \tag{3.8}$$

The dependence of radius on pressure (p_B) and temperature (T) is illustrated in Figure 3.2 (a) and (b). The graphs clearly show that as pressure rises the radius of the bubble will decrease, and if the temperature increases the bubble's radius will increase.

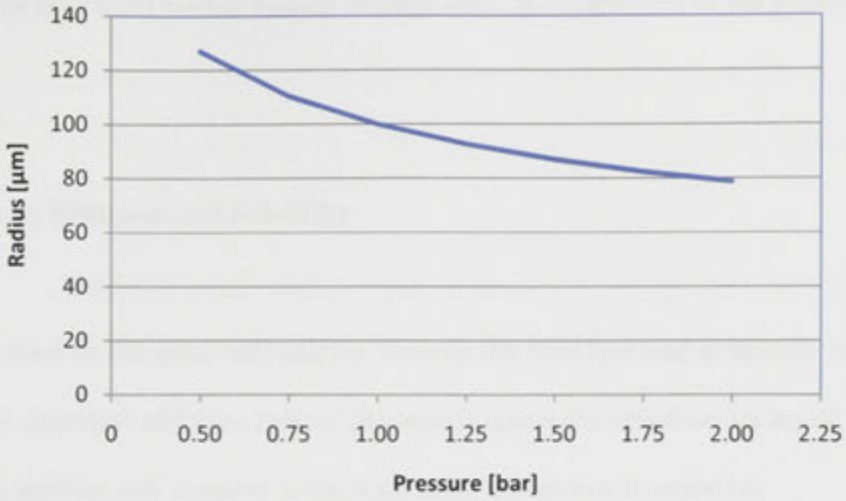

(a)

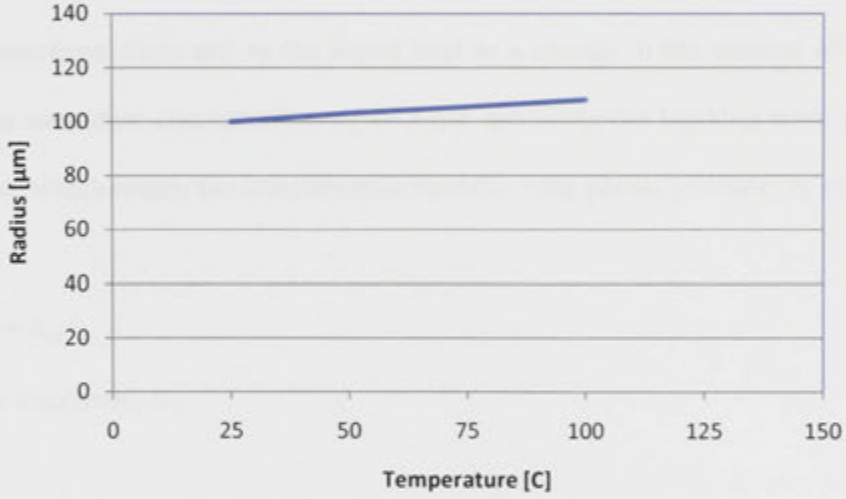

(b)

Figure 3.2: Dependence on pressure (a) and temperature (b) of a bubble's radius with a nominal size of 100µm.

Variations in atmospheric pressure have significant influence on the size of bubbles. We note from Figure 3.2 (a) that decreasing the pressure from 1bar to 0.5 bar results in a 26% increase in the bubble's size.

In the experimental systems studied here, temperature ranged between 25-50°C. Increasing the temperature from 25°C to 50°C would result in a 3% increase to the size of the bubble

which can be neglected for the system studied here, in comparison to the strong effects of pressure.

3.2. Effects of Diffusion and Solubility

Gases dissolved in the resin will diffuse towards the interface and evaporate into the gas bubble until chemical affinities (partial pressures) across the interface are equal. Similarly, gases in the bubbles will dissolve in the resin until the balance is achieved.

Diffusion processes from and to the liquid lead to a change in the amount of gas in the bubble. The saturation concentration, c_s, of a gas species in the liquid is usually given by Henry's law, which relates the concentration linearly to the partial pressure, p_p, of the gas:

$$p_p = k_H c_s \tag{3.9}$$

with Henry's constant, k_H.

Accurate data for solubility of air in liquid epoxy or vinyl-ester resin is not available in published literature. However, assuming that the solubility of air ($0.21O_2 + 0.79N_2$) in epoxy resin is similar to that in oils, the solubility is presumed to be of the order of 0.1 g/kg of resin at 25°C [Logvinyuk et al. (1970)]. The Thomson-Freundlich effect predicts that the concentration of the gas dissolved in the liquid matrix adjacent to a bubble depends inversely on the radius, r_B, of the bubble [Paul (1990)]:

$$C_{rB} = C_e[1 + \left(\frac{2V_m\gamma_{int}}{kT}\right)\frac{1}{r_B}] \tag{3.10}$$

where: kT is the Boltzmann constant and absolute temperature, respectively, γ_{int} is the interfacial surface tension, V_m is the molar volume (22.4 x 10^{-3} m^3) of the solute gas at normal pressure and temperature, and C_e is the equilibrium concentration of the gas in the liquid epoxy.

Equation (3.10) predicts that the concentration of the solute gas around small bubbles will be greater than that around large bubbles. Consequently, a concentration gradient will exist between the bubbles.

The composition gradient between adjacent bubbles will cause a net flow of the solute gas from small toward the larger bubbles. In a system containing a distribution of bubble sizes, smaller bubbles will tend to diminish, whilst the larger bubbles will grow at their expense. The solution of the diffusion problem leads to a general equation known as the Liftshiftz-Slyozov-Wagner equation [Glickman et al. (2002), Yin et al. (1996)]:

$$\left(\bar{r}_B\right)^3 = \left(\bar{r}_B\right)_0^3 + K(T)\cdot t \tag{3.11}$$

where: K(T) is a (temperature dependent) constant related to the parameters of the system, the bars over the radii indicate an average over the distribution, and the subscript, 0, indicates the initial value of the average radius.

3.3. Effect of Temperature

A rise in temperature will cause lowering of viscosity, $\eta(T)$, (Arrhenius equation):

$$\eta(T) = \eta_0 exp\left(\frac{E_A}{RT}\right) \tag{3.12}$$

with η_0 as constant and E_A activation energy. Therefore, a change in viscosity at different temperatures can be calculated from

$$ln\left(\frac{\eta(T_1)}{\eta(T_2)}\right) = \frac{E_A}{R}\left(\frac{1}{T_1} - \frac{1}{T_2}\right) \tag{3.13}$$

The viscosity of different resin systems influences the mobility of voids and higher mobility of voids is expected at lower viscosity.

An epoxy-resin system, when mixed with hardener, has a viscosity of approximately 540 mPa·s at 25°C, and approximately 334 mPa·s at 50°C.

The viscosity of vinyl-ester resin system at 25°C is approximately 370 mPa·s.

3.4. Effect of Buoyancy

A free spherical gas bubble in a viscous liquid will float to the liquid surface due to buoyancy. There are two forces acting on it: buoyancy, F_b, and drag force, F_d. The buoyancy force acts upward, tending to float the bubble; the drag force acts downwards, resisting the rise. If the bubble moves at a constant velocity, then according to Newton's law we can write:

$$-F_d + F_b = 0 \tag{3.14}$$

According to Archimedes principle the buoyancy force is equal to the weight of displaced fluid:

$$F_b = \frac{4}{3} r_B^3 \pi \rho_f g \tag{3.15}$$

where: ρ_f is the density of liquid, and g is gravitational acceleration. The density of the gas in the bubble is approximately three orders of magnitude less than that of the liquid, and therefore it is neglected in equation (3.15). The drag force is given by Stoke's law.

$$F_d = 6\,\pi r_B \eta v \tag{3.16}$$

where: η is the dynamic viscosity, v is the velocity of the bubble relative to the fluid. Substitution and rearrangement of the terms leads to the relationship for velocity of the rising bubble, v:

$$v = \frac{2}{9}\frac{\rho_f g}{\eta} r_B^2 \tag{3.17}$$

This relationship is depicted in Figure 3.3.

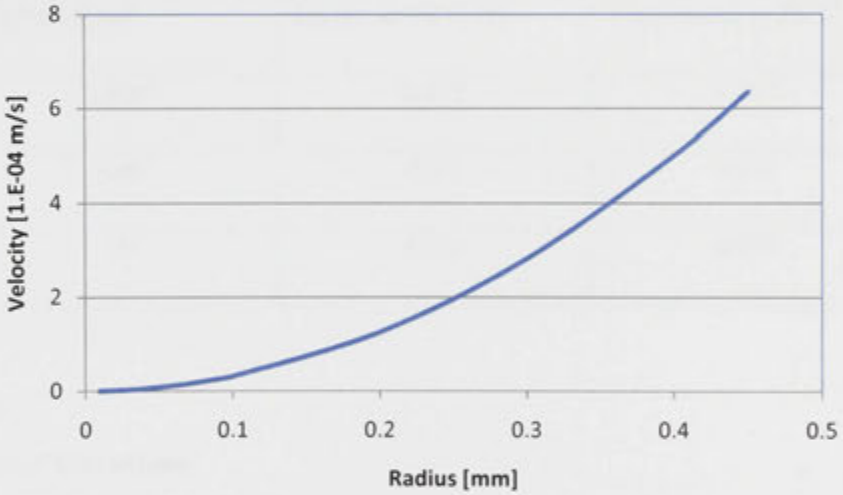

Figure 3.3: Velocity of bubble's rise depending on the radius.

As seen from Figure 3.3 small bubbles rise slowly in a liquid, while the larger bubbles reach the surface of a liquid in a shorter period due to their higher velocity.

Inverting equation (3.17) gives the time, t, needed to reach the surface from depth h:

$$t = \frac{9}{2}\frac{\eta}{\rho_f g}\frac{h}{r_B^2} \tag{3.18}$$

Strictly, equation (3.18) needs integration since the radius of the bubble depends on depth, h, and the velocity, in turn, depends on bubble radius. However, in the experiments carried out here the liquid depth (thickness of laminates) was typically 3 mm, and never more than 5 mm. Therefore the change of velocity with depth is considered to be small, and equation (3.18) is used to estimate the times for a bubble to reach the liquid surface. These estimations are shown in Table 3.1.

Table 3.1. Exit times for bubbles of different sizes from epoxy resin at 50°C and vinyl-ester resin at 25°C.

Radius (μm)	Epoxy at 50°C (s)	Vinyl-ester at 25°C (s)
1000	0.412	0.487
100	4.12	4.87
10	4120	4870

3.5. Effect of Vibrations

A bubble in a liquid can be viewed as an oscillator that can be set into radial oscillations by vibrations. For small pressure amplitudes, these oscillations can be considered to be linear about the equilibrium radius of the bubble [Lauterborn et al. (1999)]. Bubble oscillation amplitude depends on the fluid parameters, the resonance frequency of the bubble, and the frequency of external driving.

When a bubble is subjected to an oscillating acoustic field, the bubble undergoes periodic, coupled volumetric pulsation and translational motion [Hao & Prosperetti (1999)]. As the bubble expands and buoyancy becomes stronger, the bubble accelerates while the oscillations continue.

Pressure inside a bubble subjected to dynamic effects, $p_B(r,t)$, is described by [Prosperetti (1984)]:

$$p_B(r,t) = p_L(r,t) + 2\gamma / r_B + 4\eta\left(dr_B / dt\right) / r_B \tag{3.19}$$

where: $p_L(r,t)$ is pressure in the liquid just outside the bubble, γ is the surface tension between the liquid and the gas inside the bubble, and η is the liquid viscosity. The second term is only significant for very small bubbles (<1 μm), whereas the third term comes from the flow of the resin around the bubble during its oscillations. With applied acoustic vibrations, the pressure in the liquid can be described by:

$$p_L = p_0 + p_A \cos(\omega t) \tag{3.20}$$

where: p_0 is the steady pressure in the absence of the acoustic field, p_A is the pressure amplitude and ω is the angular frequency.

The response of the bubble to the pressure variations can be derived from gas law, equation (3.6):

$$V_B(\omega, t) = \frac{NRT}{p_0 + p_A \cos(\omega t + \delta)} \tag{3.21}$$

where: δ is phase lag. As the bubble pulsates, the surrounding liquid near the bubble is set into motion, which will enhance the diffusion process. Such a 'shell effect' contributes to diffusion rates and may intensify the bubble's growth. If p_0 and p_A are of comparable

magnitude then the sinusoidal oscillations become distorted (for both volume and surface area) as shown in Figure 3.4.

Note that the surface area of the bubble during expansion interval is larger than that during contraction. This leads to a difference in surface area between the expansion and contraction intervals, ΔS_B, given by:

$$\Delta S_B = 4\pi (r + \Delta r)^2 - 4\pi (r - \Delta r)^2 = 16\pi r|\Delta r| \tag{3.22}$$

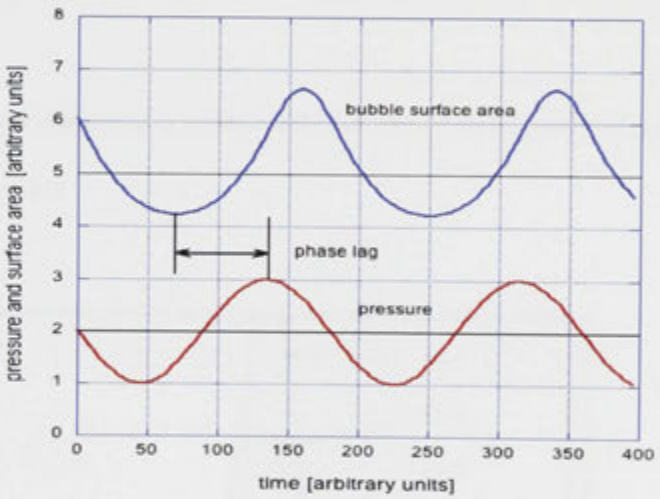

Figure 3.4: Schematic diagram of oscillations of pressure and bubble surface area.

During the oscillation, the bubble volume, bubble surface, and pressure inside the bubble change periodically and cause, via Henry's law, a variable gas concentration in the liquid layer at the bubble wall. These variations contain certain symmetry: the surface area during expansion, and low pressure inside the bubble, is larger than during contraction, and high pressure, as shown in Figure 3.4. Because the diffusion rate is proportional to the interfacial

area, the inward gas flow may be greater than the outward diffusion, depending on the concentration of dissolved gas adjacent to the bubble.

Effect of Frequency

A system that has elasticity and mass will exhibit a resonance frequency. Bubbles provide elasticity while liquid provides mass. Damped resonance frequency, f_d, exhibited by such system is given by:

$$f_d = \frac{1}{2\pi}\sqrt{\frac{k_e}{m} - \frac{b^2}{4m^2}} \tag{3.23}$$

where: b is the damping coefficient, k_e is elastic rigidity, and m is mass.

The amplitude of oscillation of a bubble will depend on frequency (ω) and damping (Q), as shown in the Figure 3.5.

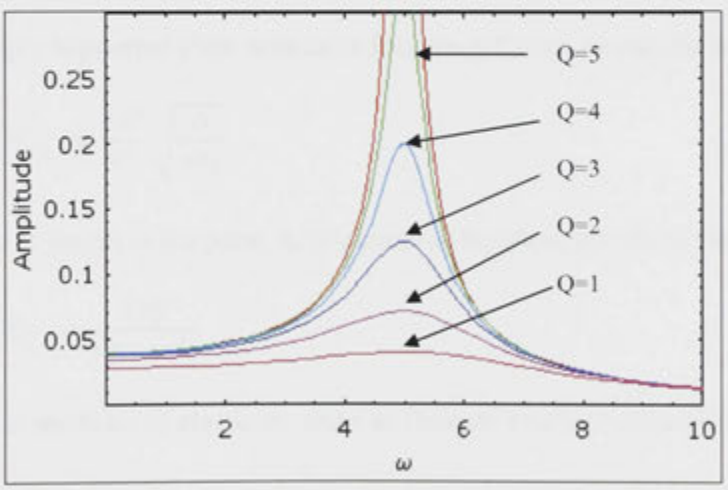

Figure 3.5: Resonance curves with increasing levels of damping.

When bubbles are driven, they oscillate in size at their natural frequency. The corresponding equation for the resonance frequency of a small bubble, f_0, characterized by surface tension γ, is given by [Leighton (1994)]:

$$f_0 = \frac{1}{2\pi r_0}\sqrt{\frac{3p_0}{\rho} + \frac{4\gamma}{\rho r_0}} \tag{3.24}$$

where r_0 is the steady state radius, p_0 is the steady state pressure and ρ is the mass density of the surrounding liquid.

Bubbles of 10-500 μm radii have resonance frequencies in kHz ranges. As frequency becomes close to resonance frequency, pressure amplitude increases, dissipation increases and temperature rise increases. Near-resonance frequency bubbles should dissolve, disperse and disappear faster.

For simply supported plate resonance frequency f_{11} can be calculated from:

$$f_{11} = \frac{2\pi^2}{a^2}\sqrt{\frac{D}{\rho h_p}} \tag{3.25}$$

where a is length of the plate, h_p thickness of the plate, and D_f is flexural rigidity

$$D_f = \frac{E h_p^3}{12(1-\nu^2)} \tag{3.26}$$

with E as modulus of elasticity, and ν as Poisson's ratio [Ventsel & Krauthammer (2001)].

Bjerkness Forces

A bubble with volume V immersed in a pressure gradient, ΔP, is subjected to a force approximately given by $-V\ \Delta p$. For an acoustic pressure field, the average force, often called the Bjerknes force [Young (1999)], is:

$$\langle F \rangle = \langle V \Delta P \rangle \tag{3.27}$$

where the brackets indicates the average over a cycle. The Bjerknes force may be large enough to overcome buoyancy, thus trapping the bubble in the sound field.

In the case of two oscillating bubbles in a sound field there is a secondary Bjerknes force between them, which arises because one bubble experiences a primary Bjerknes force due to the field radiated by the other. The consequence is that there will be an attractive force between the two bubbles if they are oscillating in phase and a repulsive force if they are oscillating out of phase.

This effect has not been studied in details in this project, but it's possible effect is acknowledged.

3.6. Effect of Energy Dissipation

Under the action of the acoustic field, there is net transport of heat into the bubble that causes the temperature rise and a consequent diffusive heat-flux out of the bubble. A steady regime is reached when the two fluxes balance each other [Hao & Prosperetti (1999)].

Oscillating bubbles are very effective in redistributing and dissipating the vibrational energy, raising the temperature of the system.

The dissipated work, W_d, per unit volume per second is

$$W_d = \pi K \sigma \omega sin\delta \tag{3.28}$$

where $sin\delta$ is related to internal friction, ω is angular frequency, σ is stress, and K is bulk modulus. Since dissipated work is transformed into heat energy, the temperature will rise accordingly

$$\frac{dT}{dt} = \frac{W_d}{\rho_f C_p} \tag{3.29}$$

where Cp is the heat capacity of the liquid.

Energy dissipation weakens vibration effects but temperature is still considered as one of the important parameters in experiments, not only due to viscosity decrease but, as shown here, due to internal energy dissipation and its effects.

Chapter 4 EQUIPMENT AND METHODOLOGY

This chapter details the processes involved in the manufacture of laminates, and includes a description of equipment and materials used, sample preparation and methods for the measurement of laminate properties, including mechanical testing, computed tomography and optical and electron microscopy.

4.1. Equipment

This thesis describes four stages in experimentation that utilise four different experimental set-ups.

4.1.1. Stokes Bubble Cell

Stage one involved the use of a Stokes Bubble Cell, a transparent box filled with epoxy resin was exposed to vibrations with the intention of observing and determining bubble movement inside a liquid when vibrations were employed. A high-frequency piezoelectric crystal was used as a vibration source.

The Stokes Bubble Cell (SBC) was made from a transparent polycarbonate material as a transparent box with dimensions of 220x220x50 mm and filled with viscous fluid up to 160mm; see Figure 4.1. The fluid used was epoxy resin, 105R West system (viscosity of

800 mPa.s and density of 1.115 g/cm^3). The upper side of SBC was open so that air-bubbles could be injected with suitable air-pump and a tube, and also to allow air-bubbles to float to the surface freely.

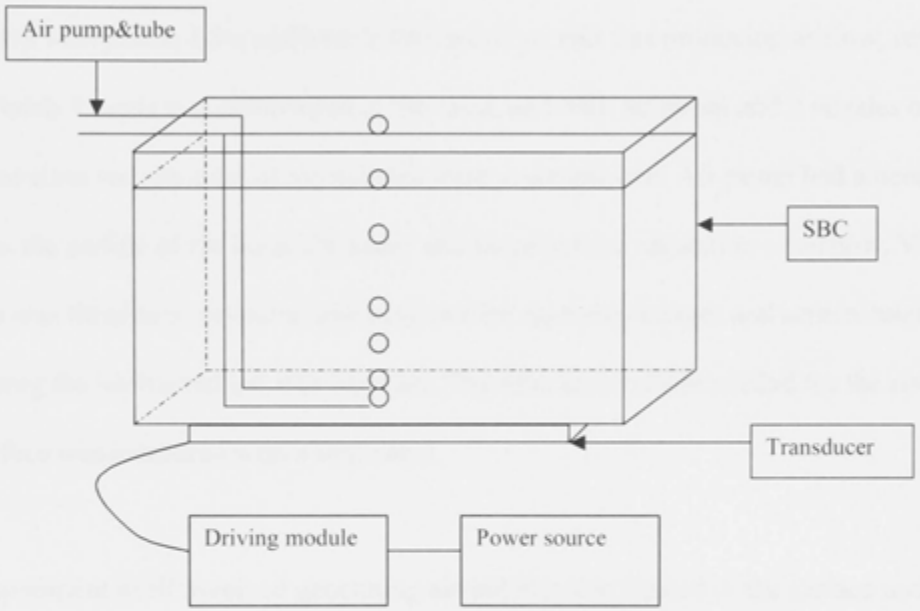

Figure 4.1: Schematic diagram of Stokes Bubble Cell.

Piezoelectric transducers were attached to the base of the SBC that generated vibrations in the viscous fluid. Transducers chosen were of 50W power operating at 40 kHz, and they were connected to power supply via driving module, as shown in Figure 4.1.

Piezoceramic material used in transducers was PCM 41, hard power "hard" material (PZT piezoceramic material), suitable for high power ultrasonic applications.

Two transducers, each with piezoelectric crystal attached to Al plate, were glued with epoxy to the bottom of SBC, and placed in a plastic box (for safety). The electric box with driving module was equipped with a fan for cooling.

Air-pump with plastic hose and nozzle fitting on one end was producing airflow, regulated with a knob. Nozzle was submerged in the resin, and with air-pump and 2 nozzles of different sizes various sizes of air-bubbles were accomplished. Air-pump had a needle valve in the middle of the hose, for easier and more precise regulation of airflow. Video camera was fitted to a computer, and program for capturing images and screen-ruler (for measuring the bubble radius) was installed. The time each bubble needed for the rise up to the surface was measured with a stopwatch.

The experiment itself involved generating air-bubbles that floated to the surface under Archemides principle. It was expected that the induced vibrations would affect the bubbles and their floating regime to the surface.

The air-bubble rising to the surface with reliance on the Stokes law, measuring the time-period each bubble needed to reach the surface, was analyzed.

The size of bubbles was also taken into consideration and at first there was only one air-bubble flow.

Then by changing the frequency of transducers, defining the effect of vibrations on the time-period bubble needed to reach the surface of the fluid was in the focus.

Video camera, ruler and microscope were used to help to determine bubble radius and trajectory length of bubbles.

4.1.2. High-frequency Piezoelectric Crystal

The second stage saw the use of a piezoelectric crystal, 40 kHz, and aluminum moulds for laminate production.

Two aluminum plates of the same size were used as moulds, the first employing a piezocrystal transducer, with 50W power operating at 40 kHz, attached by epoxy glue on the bottom and connected to the power supply via a driving module. The piezoceramic material used in transducers is PCM 41, a PZT piezoceramic material, suitable for high-power ultrasonic applications. The second aluminum plate did not include a transducer. The intention in the use of these plates systems was the observation of differences between laminates produced where one group was made using high frequency vibrations and the other was not.

After cutting and polishing with P400and P1200 emery papers samples were placed in water in an ultrasonic cleaner. Laminate samples were examined under optical microscopy at 40 and 400 magnifications, with scanning electron microscopy, SEM, providing up to 500 magnifications and all SEM samples being carbon coated before use.

4.1.3. Electromagnetic Shaker

Working with lower frequencies was made possible by the use of an electromagnetic shaker, which was adapted with the inclusion of a removable flat mould on its top, named top plate, as shown in Figures 4.2 and 4.3.

Experiments in the production and analyses of the effects of mechanical vibration applied to the curing system of subject composite materials were performed as follows.

The frequencies of vibrations employed ranged from 2 Hz to 8 kHz for periods of vibration of 10 and 30 min. Samples were cured with and without the top plate, as without the top plate bubbles would be allowed to freely escape to the surface, whereas with the top plate in place curing would imitate closed-mould conditions. The top plate was of the same dimensions as the mould, but made from transparent plastic for ultraviolet (UV) curing and secured in place with rubber bands (see Figure 4.3). Vacuum bagging was subsequently introduced into the experimental system.

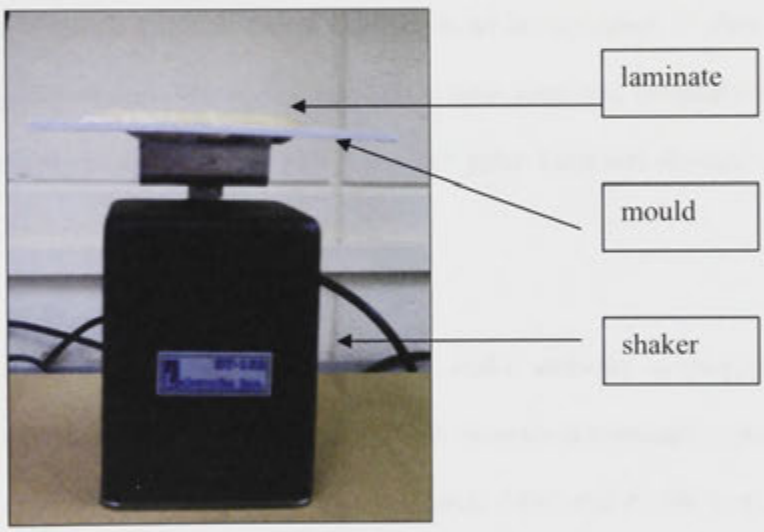

Figure 4.2: Experimental set-up with EM shaker.

The vibration system consisted of a shaker (Labworks Inc, ET-132, frequency range of 1-9000Hz), a power amplifier (Labworks Inc, pa-119), and a signal generator, Figure 4.5 (b). A flat mould (120mmx 120mm) was attached to the shaker's top, as shown in Figure 4.2.

After experiments with the power range 0.1 - 1.4 W, and finding no difference in laminates' void content, 100mW was established as a constant parameter.

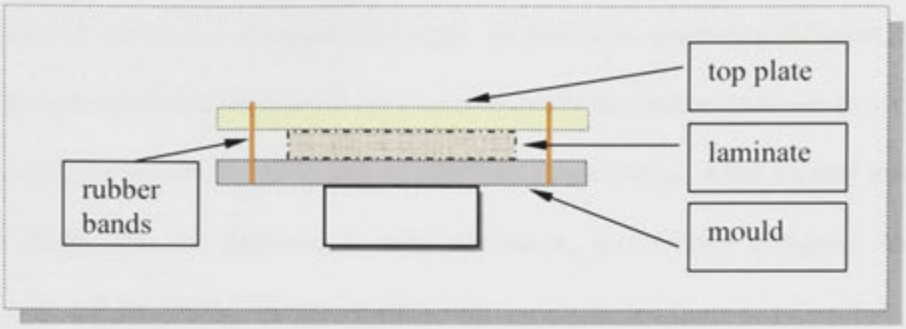

Figure 4.3: Schematic diagram of EM shaker mould with the top plate.

Composite laminates were made by hand lay-up using 12 plies of E-glass fibre (JPS glass, plain weave). The epoxy vinyl-ester resin used was Derakane 411-350 (FGI F01110) with photoinitiator Irgacure 819 (Ciba, 0.5 pph). Laminate dimensions were 100mm x 100mm, with thickness 2.8mm ± 0.1mm.

Sample laminates were produced under ambient room-temperature conditions, using vibrations for 10 or 30 minutes, with samples immediately cured by the use of a UV lamp, cut with a diamond saw, polished with P400 and P1200 wet and dry emery papers, and examined under optical microscopy, at 64 magnifications, and SEM to determine types and quantities of defects.

4.1.4. The ANU-Quickstep Machine (ANUQSM)

The most sensible and advantageous way to proceed with experimentation of vibrations on QS mould and curing was discussed at length. In particular, exploring different placement of shakers in the plane of the mould, for example one in the centre, two, one in each corner, six, etc, with the possibility of curing at elevated temperatures. After careful analysis the decision made was to construct a new apparatus, specifically designed for further experiments and flexibility. Technical drawings and final decisions were realized with the ANU departmental technical staff and the apparatus, ANUQSM, was built. ANUQSM is shown in Figures 4.4 and 4.5.

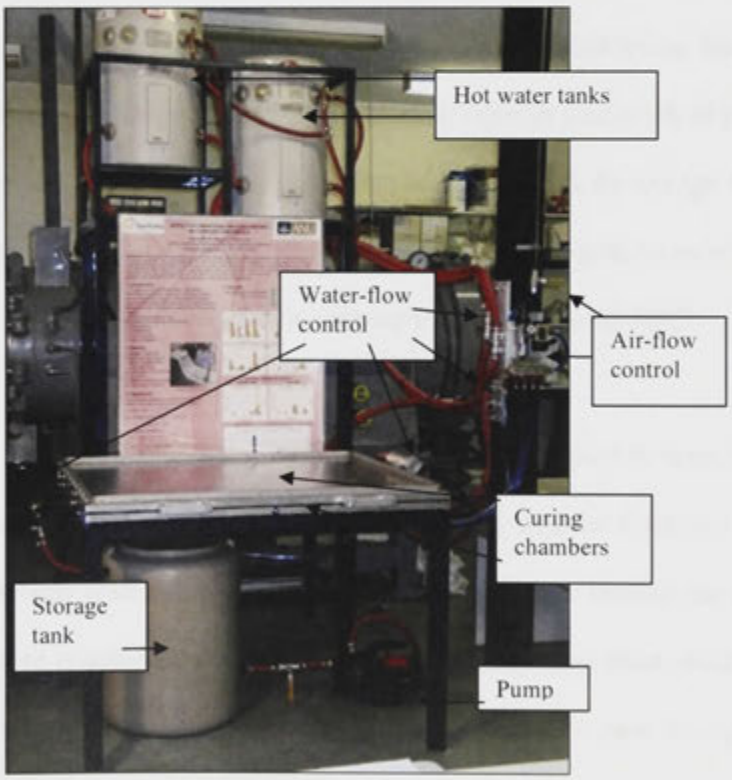

Figure 4.4: The ANUQSM experimental system.

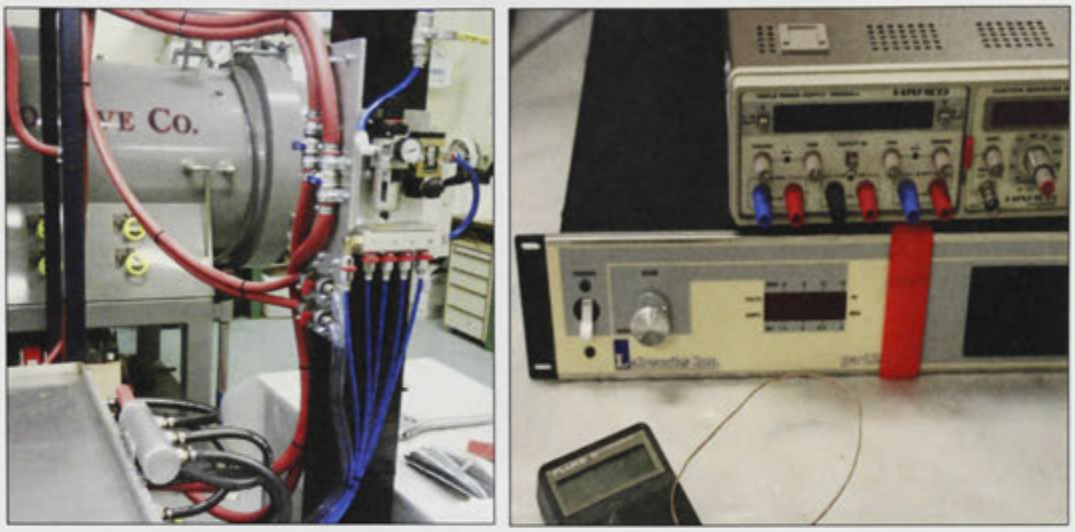

(a) (b)

Figure 4.5: Water and airflow control (a), power amplifier and signal generator (b).

The ANUQSM consists of two curing chambers sitting on a metal-frame base. Both chambers are filled with hot water provided by two heaters, through a network of pipes and hoses. The water runs constantly when the apparatus is in use, with its storage tank and pump connected to the heaters. Water-tank heaters are at different heights to provide equal pressure inside each chamber, with the heater's working temperature set at 50°C.

The curing chambers have a silicone membrane on one side, see Figure 4.6, through which heat is radiated from water flow to a composite lay-up. The interior thickness of each chamber, and the fluid flow within it, is 20mm. Introducing vibrations through the liquid to the mould and a laminate is achieved through a 1.5mm thick aluminum sheet, thick enough to contain the fluid, yet thin enough to allow the vibration energy to pass through to the fluid and laminate.

Figure 4.6: Silicone membranes and fluid inside the chambers.

Five air-driven vibrators were attached on the underside of the chamber, one in each corner and one in the center (as shown in Figure 4.7). Each is a pneumatic, unidirectional Olivibrator, type K22 vibrators with internal steel piston and adjustable compressed air inlet (Figure 4.5 (a)) and maximum working pressure of 6 bars. When all five vibrators were in use it was not possible to fully control frequency; with three diagonally in line it was not possible to achieve lower than 60 Hz, with certain of the sample laminates manufactured this way and employing 10 and 20 minutes of vibrations.

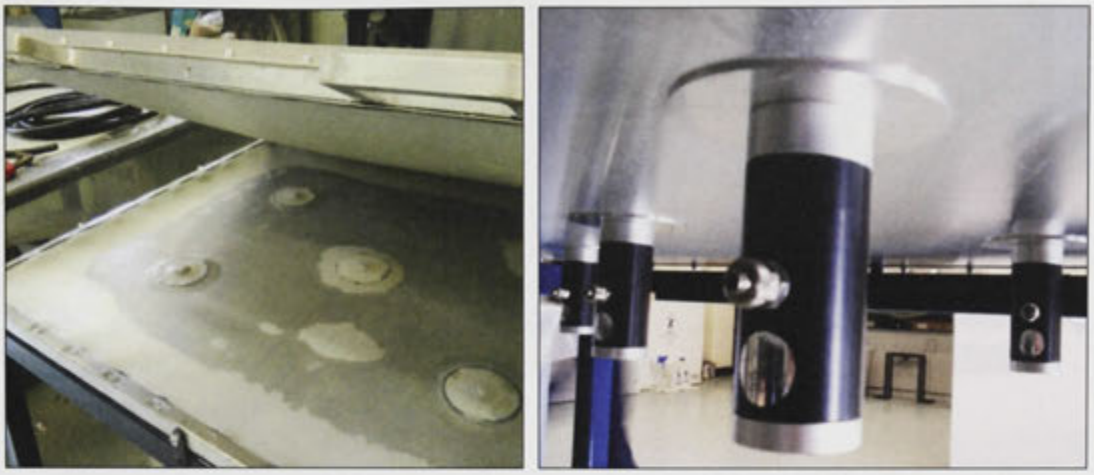

(a) (b)

Figure 4.7: Air-driven vibrators viewed from the top (a) and the bottom (b).

A 15 inch (Redback, 150W power max) subwoofer speaker was introduced into the system, see Figure 4.8, along with the previously used power amplifier and signal generator. Initially it was attached to the underside of the mould and was in contact with the bottom chamber. This configuration did not produce satisfactory results because of constraints on the movement of the speaker as well as the presence of air in the heating fluid (water) which it was not possible to eliminate at this point in the experimental program. The speaker was then mounted on the top of the chamber where it was possible to move it freely.

(a) (b)

Figure 4.8: Subwoofer speaker (a) and in place on the top of the chamber (b).

At this point a vacuum pump was introduced, to provide vacuum assistance as required through the experimental program.

A short cure cycle was not the prime concern in the thinking underlying this program as three tanks for fast fluid exchange (like in the Quickstep process) were not available. The idea underlying the construction of this apparatus was the curing of composite laminates at higher than room temperature while utilising vibrations, with examination of void presences subsequently.

Full explanation of the operating procedure of ANUQSM can be found in Appendix B.

4.2. Methodology of Laminate Production

Wet hand-lay-up was used throughout the whole project. Resins were impregnated by hand into glass fibres that were in the form of unidirectional or woven fabrics. This was achieved by the use of rotating rollers and a bath of resin.

Fabrication of 4-ply composite plaques in Stage 2 employed the hand lay-up method, with E-glass fibres impregnated with Derakane epoxy vinyl-ester resin and cured with UV light. The thickness of laminates was 1.4mm ± 0.1.

Stage 3 involved hand-lay up 12-ply laminates with an EM shaker, using E-glass fibres and Derakane epoxy vinyl-ester resin for UV curing. Vacuum bagging and top plate were also introduced at this point in Stage 3. For manufacturing detail please see Appendix C.

The use of ANUQSM in Stage 4 of this program was as follows:
Hand lay-up of 12-ply composite laminates, i.e. the cutting of fibres of specific dimensions, the mixing resins and hardeners in appropriate ratios, the application of the mixture to each fabric and impregnating them into the fibres by rolling it on a mould, the application of auxiliary materials, i.e., peel ply, breather, the placing of the assembled composite in a vacuum bag made specifically for each experiment, and the inserting the bag into the ANUQSM for vibration-assisted curing.

Laminated panels were fabricated using woven E-glass and Vinyl-Ester or Epoxy resin. A flat, 2mm thick aluminum plate, dimensions 300mm x 380mm was used as the mould

surface for the lay-up of the laminated panels. The mould surface was treated with a self-release agent; on the top of the fabric preform a peel ply and a breather were stacked. The fabric preform consisted of 12 plies of E-glass, measuring 200 x 200mm. A vacuum sealant tape was placed around the edges of the assemblage to create the vacuum bag, with preform on the mould inside it, creating a sealed mould (Figure 4.9). The vacuum port was sealed, the whole assembly was placed inside the chambers of ANUQSM, and the vacuum pump was used to evacuate the sealed mould.

Laminated samples were subjected to vibrations at frequencies in the range 2Hz to 8,000Hz, with vibration periods of 10, 20 and 30 minutes at 50°C with vacuum assistance.

For UV curing of vinyl-ester resin laminates ANUQSM was not heated, with room temperature ranging from 25-29°C.

The speaker, see Figure 4.8, with previously set frequency via the signal generator, was turned on and the power of vibrations was adjusted to a constant value, with voltage of 10V pk and current 1A rms.

After exposure to vibrations the preform laminate was removed from the vacuum bag. The epoxy-resin laminates were then cured in an oven at 50°C for 4-6 hours, and allowed to post-cure overnight at room temperature. Vinyl-ester resin laminates were ex posed to sunlight for 5 min, and then left to complete curing for a few hours at room temperature.

All materials were weighed prior to use, with this data being useful for fibre-volume calculations. All data, including frequency and power of vibrations, length of time, temperature changes, were constantly observed and noted. Each laminate was identified and marked.

Final thicknesses obtained for E-glass/Epoxy and E-glass/Vinyl-ester panels were respectively 3.0mm ± 0.1 and 2.8mm ± 0.1. For manufacturing details see Appendix C.

Laminated samples tested to determine apparent interlaminar shear strength were manufactured as previously but using 20 plies of unidirectional glass fibres and epoxy resin. Ten minutes of vibrations with vacuum assistance and elevated temperatures of approximately 50ºC were constant parameters. The thickness of the laminates was 8mm ± 0.3mm.

Fiber-Volume Fraction

The mass of each panel, including fiber fabrics, resin and auxiliary materials, was determined by weighing on a precision balance. The ratio of the fiber volume to the specimen volume in each sample is the fiber-volume fraction. The fiber-volume fraction for the E-glass/Vinyl-ester and E-glass/Epoxy resin panels was calculated as 49% ± 2 by weight.

4.3. Materials Used

4.3.1. Matrices

This project used two different resin systems: a two-part epoxy resin, consisting of the West System 105R epoxy resin and the matching West System 209H super-slow hardener, and an epoxy vinyl-ester resin, Derakane 411-350 (FGI F01080), and a photo initiator, Irgacure 819 (Ciba, 0.5 pph).

The weight of the resin/hardener mixture was measured with an accuracy of ± 0.1 g, using a balance, Precisa^{TM}, Switzerland, model 30000D SCS.

The resin/hardener mixture was stirred in an open plastic cup, using a wooden spatula, for approximately one to two minutes, ensuring thorough mixing and that the sides and the corners of the mixing cup were scraped. Appropriate care was taken whilst stirring to ensure that the mixture was not aerated. The mixture was left to de-gas for 5-8 min prior to use for impregnation.

The Epoxy resin system

The West System® R105 epoxy resin is a clear, pale yellow, low-viscosity liquid epoxy resin. Formulated to be used in conjunction with a hardener, it can be cured over a wide temperature range to a high-strength solid with excellent moisture resistance, for bonding with wood fibre, fibreglass, reinforcing fabrics and metals. The H209 super-slow hardener is a low-viscosity epoxy-curing agent and is formulated for general coating and bonding applications in extremely warm and/or humid conditions, or when ex tended working time

is desired at room temperature. The resin has a viscosity of 800 mPas and density of 1.115 g/cm^3 at 25ºC. When combined with R105 resin in a by weight 3.5-parts resin to 1-part hardener ratio, at room temperature (21°C) the resin/hardener mixture has a pot life of 50 to 60 minutes, or 15 to 20 minutes at 35ºC. It cures to a solid state in 6-8h at 35ºC, or over 20-24 hours at 21ºC. Further hardening occurs over the next 4 to 9 days.

The Vinyl-ester resin system

The matrix system used was the Derakane Classic 411-350 epoxy vinyl-ester resin (Ashland) and UV photoinitiator Ciba Irgacure 819.

Irgacure is a versatile photoinitiator for radical polymerization of unsaturated resins upon UV light exposure. The amount of Irgacure powder hardener needed in respect of resin weight was 0.5 g per 100g of resin.

The manufacturer's certified properties of Derakane resin are density 1.046 g/cm^3, and viscosity 370 mPas at 25ºC. It has a styrene content of 45%.

4.3.2. Reinforcements

Throughout this program, except for shear-testing samples, glass fibres used were woven E glass (JPS), plain-weave finish S912, style 7533, with density of 2.2 g/cm^3.

Unidirectional E-glass fibres, Owens Corning R25H, with an aerial weight of 300g/m^2 were used for shear testing.

The weight of glass fibres was measured with a Precisa^{TM} balance with accuracy of ± 0.1g.

4.3.3. Auxiliary Materials

Mould release agent is a material applied to mould surfaces to facilitate the release of the moulded laminate. Airtech Safelease 30, a water-based PTFE mould-release agent was used in this project.

Peel ply is a smooth, woven fabric that will not bond to epoxy, polyester or vinyl-ester resins. It is used to separate the breather layer and the laminate in vacuum-bagging applications. Excess resin can wick through the release fabric and can be peeled off after the laminate has cured, ex posing a smooth surface.

A breather layer is used to maintain a breather path throughout the bag to the vacuum source, so that air and volatile gases can escape, allowing continuous pressure to be applied to the laminate.

The vacuum port is a metal fitting that connects the vacuum bag to the vacuum pump through a reinforced hose.

The sealant tape is a rubberised adhesive tape used to provide the seal at the peripheries of the vacuum bag. It is sticky on both sides and has the ability to remain soft and pliable at high temperatures.

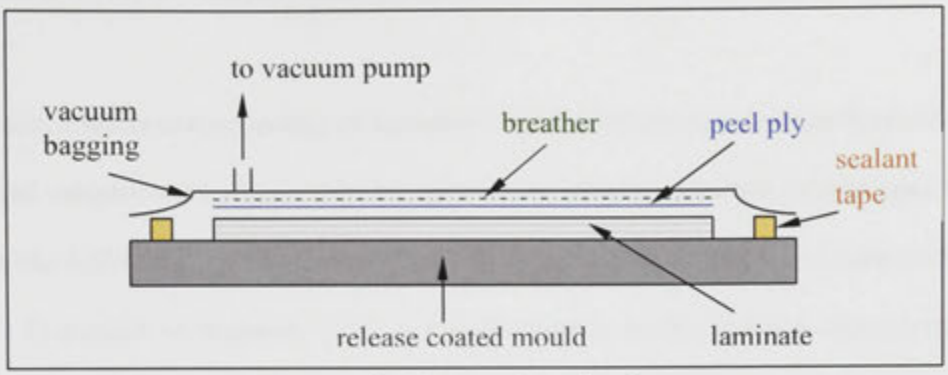

Figure 4.9: Vacuum bagging layers.

The three main reasons for vacuum bagging include the following: facilitation of the flow and absorption of resin, the application of compaction pressure to consolidate plies, and the ex traction of moisture, solvents, and volatiles from the curing composite.

The vacuum bag allows the extraction of gases. Pressure is applied to the laminate to improve sample consolidation once lay-up is completed. This is achieved by sealing a plastic film over the wet laid-up laminate. The air under the bag is extracted by vacuum pump, thus up to one atmosphere of pressure can be applied to the laminate in its consolidation.

4.4. Sample Preparation and Characterisation

To obtain a better understanding of laminates' internal structures, cross sections of cut and polished samples were observed under optical and scanning electron microscopes (SEM), within the ANU Electron Microscopy Unit, Research School of Biological Science (RSBS), ANU. Computed tomography (CT), a non-destructive testing method that provides 3D insight into sample structures was carried out in the Adelaide Microscopy, the University of Adelaide.

4.4.1. Preparation

The laminate's thickness and width were measured using a Mitutoyo digital micrometer series 193.

All laminates were cut to size using a diamond saw. Two test strips along the center line of each laminate were each cut into four sections; four inner samples were used for optical microscopy observations and void-content measurements. Further cutting of later laminates provided 6 additional strips for mechanical testing, three for bending and three for tensile measurement. Subsequent laminates were cut into 12 strips and divided into two sets, each of six specimens. One set was aged by immersion in water for 7 days at 50°C. Three samples of each set were subjected to tensile and three for flexural measurements.

Optical microscopy used samples of dimensions length 47mm ± 2, width 13.5mm ± 0.2, and thickness 2.8mm ± 0.2. The surface of each cross section was polished using wet P400 and P1200 emery papers, and marked for identification.

Scanning electron microscopy samples were carbon coated prior to analysis.

Samples for tensile and flexural mechanical testing were cut into strips of length 210mm, width 12.6mm and thickness 2.8mm ± 0.1. Tensile-test samples were glued to grips, requiring the polishing of both ends and sides of each sample, as well as the faces of each grip. Epiglue adhesive was used to bond grips and samples. All samples were placed in a Qualtex Solidstat oven for 48 hours at 50ºC for further bonding.

Samples for shear mechanical testing were cut along the fibre direction of their unidirectional fibres and were 9.6mm ± 0.1 wide, 8mm ± 0.3 thick and 53mm ± 1 long. The surface of each cross section was polished using wet P400 and P1200 emery papers and marked for identification. Another, similar set of samples was cut from samples in the direction perpendicular to the axes of their fibres and were prepared for observation using the same sequences.

4.4.2. Scanning Electron Microscopy

A scanning electron microscope, a Cambridge S360 (SEM, 1987), was used to observe laminate's internal structures, fibre wetting, fibre pullout, missing fibres, misalignment of fibres, and small voids. Left-hand side of Figure 4.10 shows magnification of 35 times while the right-hand side picture is at 435x magnification.

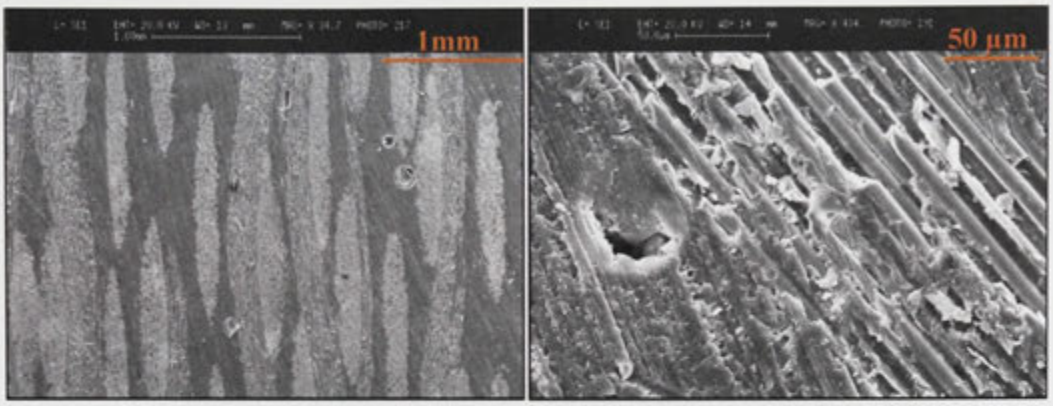

Figure 4.10: Typical SEM images with different magnifications.

4.4.3. Optical Microscopy

Microscopic image analysis is considered among the most precise methods for measuring void contents in composite materials. Furthermore, this image analysis technique has the advantage of providing detailed information of other important parameters such as void distribution, shape, and size that cannot be assessed by either physical or chemical methods. A standard assumption in determining void content with image analysis is that the voids are randomly distributed in the composite. This assumption makes it possible to compute the area fraction of voids and to use this as a statistical value of the volume-fraction of voids.

All voids that could have been identified at the working magnification were included in porosity calculations. Voids entrapped within a particular cross-section were distinguished, their images acquired at 64x magnification and captured using a PC-based CCD camera attached to the optical microscope. At this magnification, each frame displays an area approximately 1.8mm x 1.9mm, with a resolution of 1,500 x 1,500 pixels. Eight frames were captured from each sample composite. The magnification chosen, 64x, enables the assessment of voids as small as the radius of a fibre (up to 20µm); hence all visually

identifiable voids throughout the composite sample are included in the analysis of void content and morphology.

Each captured frame was manually processed using image analysis software which allowed simultaneous measurements of void dimensions.

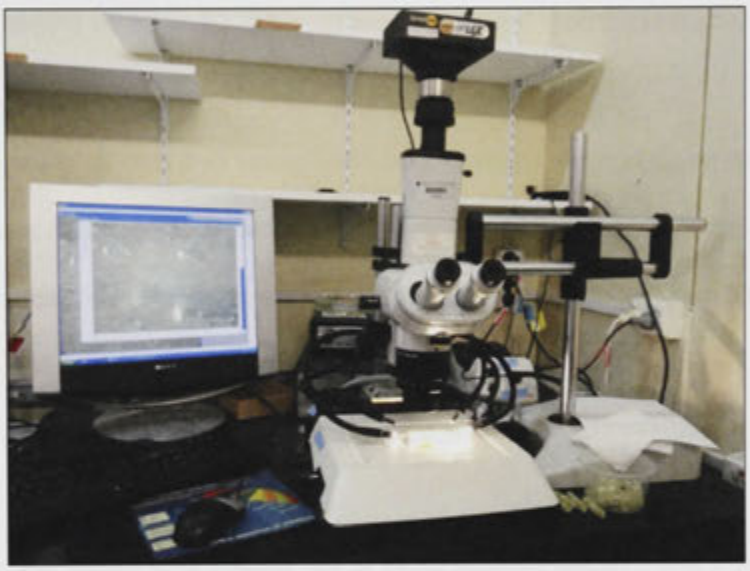

Figure 4.11: Optical microscope at EMU, ANU.

The processing of digital images taken directly from the microscope were possible with the use of an optical microscope, the Wild M400 Photomicroscope with SPOT Flex CCD Camera 14bit 50Mb color CCD camera, the LM Wild PC4-Image Pro-Image Analysis program, and a LEICA illumination base, shown in Figure 4.11. The magnification of the microscope's camera (64x) could be varied by using different magnification lenses. With appropriate illumination and at 64x magnification eight random images were taken from each sample and later analyzed. Each image was processed in the determination of actual length, width or radius of bubbles, and all visible bubbles over 50μm radius in each image

were noted. Smaller-sized bubbles, between 20-50 μm radius were included in void-content calculations but not for comparison with the number of bubbles in each sample.

4.4.4. Void Content Calculation

Optical-micrograph analysis included grouping voids based on their size, organizing tables and charts of samples cured under different conditions, and void content calculation.

After counting voids all data was categorized into 4 groups, depending on the radius of the bubble cross-section. Sizes A, B and C are shown in Figure 4.12, while group D includes bubbles larger than 500 μm diameter. Bubbles with radii smaller than 50 μm were not included in groupings because of light scattering, a phenomenon which can result in small voids, surface imperfections or limitations on resolution.

Void counting and sizing was carried out at eight random points, each 1.8mm x 1.9mm, across the whole specimen cross-section thickness, approximately 100mm^2, totaling 27.4mm^2 of laminate cross-section per specimen.

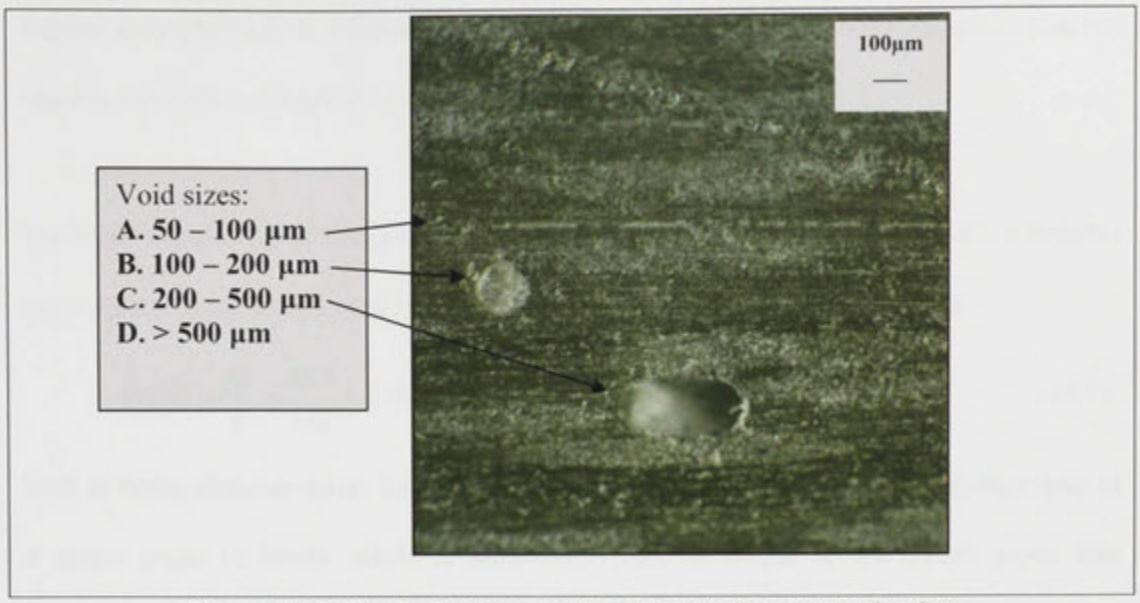

Figure 4.12: Typical micrograph and void-size categorisation of a high-void content sample.

When unidirectional fibres were used for shear testing, specimen cross-section thickness was approximately 400mm, with eight random images giving a total of 27.4mm^2 of analyzed laminate cross-section per specimen.

The image-analysis technique is the most accurate method for determination of true void content but it is dependent upon the resolution of the imaging system. One drawback with image analysis is that only a small area can be investigated which may lead to scatter in the results owing to the stochastic nature of void distribution. The choice of resolution, 64x, was determined by the constraint of microscope used. While there was the need for higher resolution to enable detection of voids of all sizes, voids with areas much smaller than the cross-sectional areas of fibers were impossible to detect. However, a separate investigation with higher magnifications available through SEM showed that few voids smaller than the fibres existed and that their contribution to total-void content was negligible. The distribution of bubble cross-sections as measured is not the same as the distribution of

bubble radii [de Hoff & Rhines (1968)]. However, comparison between samples does not require calculation of bubble radii.

For void-content analysis calibration was done by graph paper to identify radii of bubbles on computer images, and relative bubble size error, RBSE, can be presented as

$$RBSE = \frac{\Delta l}{l} = \frac{0.5}{122} = 0.41 \cdot 10^{-2} \tag{4.1}$$

with Δl being absolute error; that is the greatest possible error – half of the smallest unit of a graph paper (0.5mm), while l, measured value, is length of the graph paper that corresponds to 1mm.

4.4.5. Computed Tomography

Nondestructive testing is testing that which does not destroy the test object. One of the methods for nondestructive testing in this study is computed tomography.

Computed tomography explores the structure of materials by taking a number of x-ray images of a sample from a variety of angles. Computers then combine the images to build a 3D-model of the structure. The X-ray CT can take measurements over three orders of magnitude simultaneously, from microns to millimeters.

During scanning the sample rotates within a fixed x-ray receiver. The x-ray camera then records 2D radiographic information from a range of rotation angles. Computer manipulation of the data allows the construction of a three-dimensional image of the sample's internal structure. The micro-focus x-ray source can produce a wide range of x-

rays, 30-225 kV, suitable for scanning soft, biological materials through to hard materials such as stone or metals.

The x-ray detector is an extremely sensitive 16-bit, scintillator-coupled 2048 x 2048 pixel CCD camera mounted on a linear rail that allows it to be moved back and forth from the sample and x-ray source. Moving the camera gives a range of magnifications from 3x to 100x . The sample is mounted on a precision rotation stage, and the entire apparatus sits on custom-built vibration isolators, allowing the sample, X-ray source and detector to be reliably steady over long time periods. Because the CCD camera is sensitive, and the apparatus stable, the x-ray source can be used at low power for extended periods, from days to weeks, such that structural change over time can be readily monitored.

Nine hundred images per sample were acquired and scanned images were then processed into 2D tomograms. 3D models were created and selected scanned images as time sequences are presented in Figure 4.13.

Dark-gray areas represent resin with lower electron density while light-gray areas are glass fibres with higher electron density. Black areas indicate absence of any substance, there are no electrons inside, and hence these are voids. Scanned images can be seen as slices through a sample and when, for example, extracting slices 400, 410 and 420 of the 900, differences in internal structures can be seen, such as changes to the size and disappearance of bubbles, or the creation of new bubbles at certain points on tomograms. Different-colored rings are superimposed to emphasize the location of bubbles. Note the difference of ring content in each of the three images, for example the red ring. Red rings encircle: existence of a clear void (dark circle) existence in the top image; decrease of the same void (gray circle) in the middle image; and complete disappearance of the void in the bottom image, replaced by fibre tows.

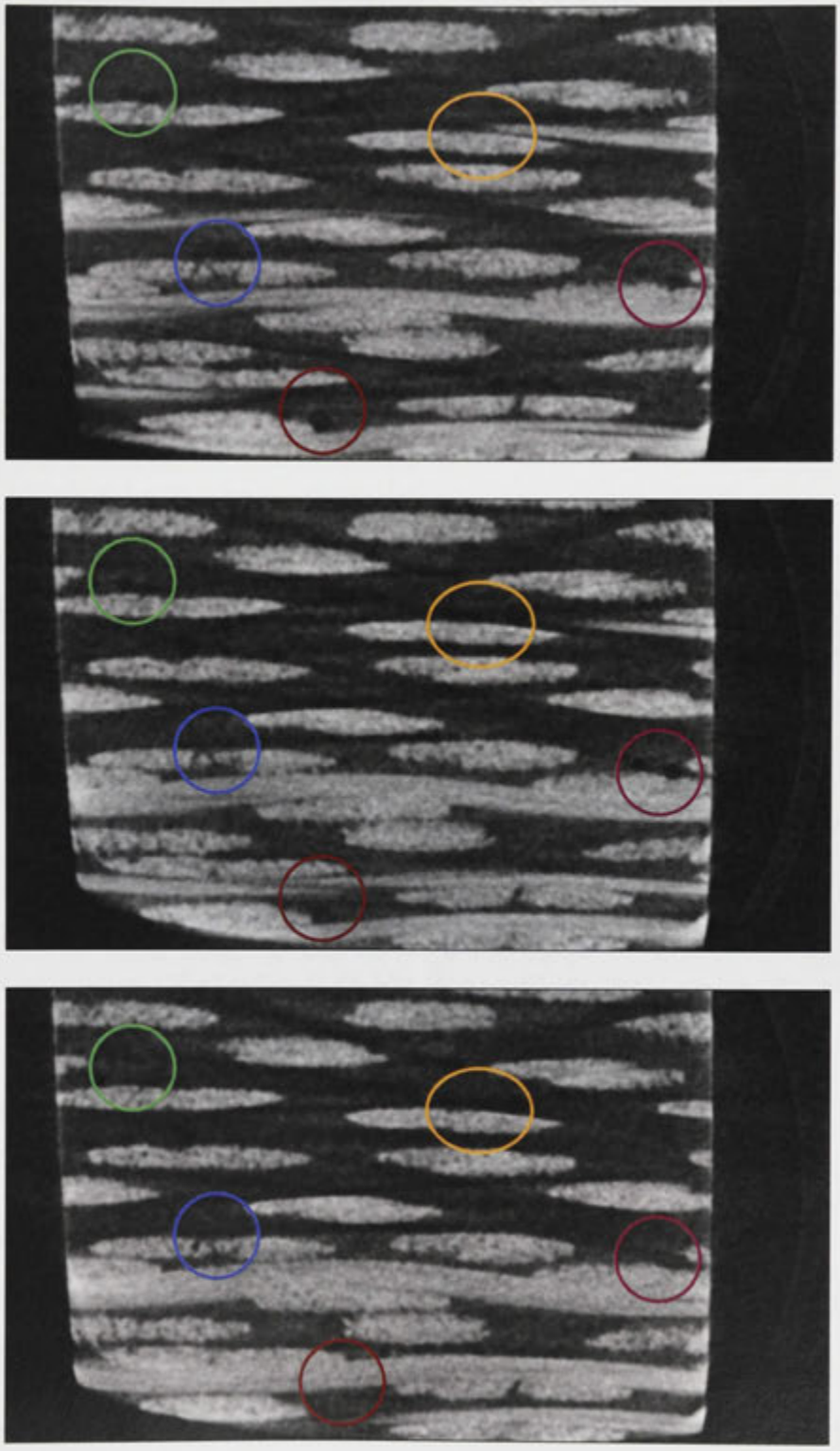

Figure 4.13: CT scans showing changes and disappearance of bubbles.

4.5. Mechanical testing

There are four main direct loads that any material in a structure has to be able withstand: tension, compression, shear and flexure. Tension, flexure and shear testing were performed in this study.

An Instron 5500R Testing machine with Bluehill2 testing software (Figure 4.14 (a)) was used to perform the tests and a load/displacement curve (Figure 4.14 (b)) was produced for each test.

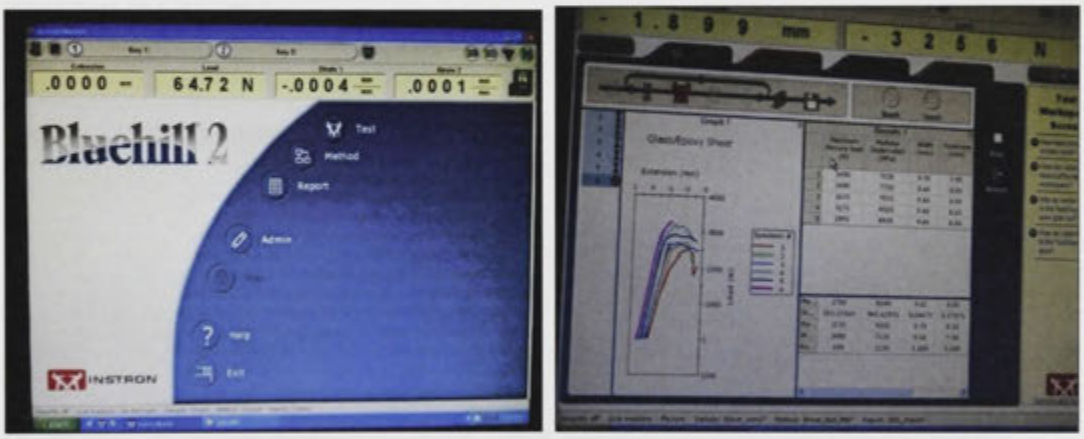

(a) (b)

Figure 4.14: Bluehill2 testing software, (a), and load/displacement curves, (b).

4.5.1. Tension

Figure 4.15 shows a tensile load applied to a composite. The response of a composite to tensile loads is very dependent on the tensile stiffness and strength properties of the reinforcement fibres, since these are significantly higher than the resin system's on its own.

Figure 4.15: Tension.

For tensile testing the testing load cell was 100kN, the crosshead displacement rate was 2mm/min, and end-test extension 5mm. Three samples per specimen were tested, and giving six curves per graph, i.e., the curves from two specimens on one graph. An extensometer was used to measure extension for all specimens for each panel and extensometer removal point was at 1.5mm. Findings of tensile strength and modulus are presented in Chapter 5.

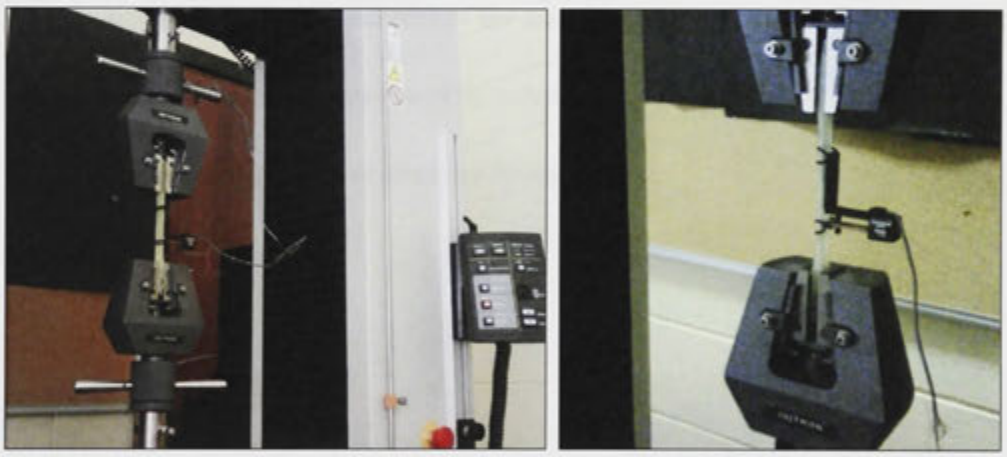

Figure 4.16: Instron machine and tensile testing set-up.

Tensile testing was carried out on an Instron machine shown in Figure 4.16, with a ruler and digital micrometer used to complete the calculation of tensile modulus, E_T, and tensile strength, σ_T. Relative error is as follows:

$$E_T = \frac{FL_0}{A_0 \Delta L} \tag{4.2}$$

$$\frac{\Delta E_T}{E_T} = \frac{\Delta F}{F} + \frac{\Delta L_0}{L_0} + \frac{\Delta A_0}{A_0} + \frac{\Delta(\Delta L)}{\Delta L} \tag{4.3}$$

$$\frac{\Delta A_0}{A_0} = \frac{\Delta t}{t} + \frac{\Delta w}{w} \tag{4.4}$$

$$\frac{\Delta A_0}{A_0} = \frac{0.1}{3} + \frac{0.1}{12.5} = 4.1 \cdot 10^{-2}$$

$$\frac{\Delta E_T}{E_T} = 10^{-5} + 10^{-2} + 4.1 \cdot 10^{-2} + 10^{-4} = 5 \cdot 10^{-2}$$

where relative error of tensile modulus, $\Delta E_T/E_T$, is based on: $\Delta F/F$ - load error determined by Instron machine; $\Delta L_0/L_0$ - error of sample's length between Instron machine grips; $\Delta A_0/A_0$ - error of cross sectional area of the sample is determined by thickness, t, and width, w, and $\Delta(\Delta L)/\Delta L$ is an error measured by extensometer of Instron machine.

Tensile strength and its relative error are found from:

$$\sigma_T = \frac{F}{A_0} \tag{4.5}$$

$$\frac{\Delta \sigma_T}{\sigma_T} = \frac{\Delta F}{F} + \frac{\Delta A_0}{A_0} \tag{4.6}$$

$$\frac{\Delta \sigma_T}{\sigma_T} = 10^{-5} + 4.1 \cdot 10^{-2} = 4.1 \cdot 10^{-2}$$

where relative error of tensile strength σ_T is calculated from load and cross sectional area errors, as previously explained.

4.5.2. Flexure

Flexural loads are a combination of tensile, compression and shear loads. When loaded as shown in Figure 4.17, the upper face is put into compression, the lower face into tension and the central portion of the laminate experiences shear.

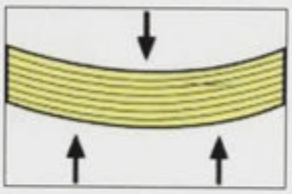

Figure 4.17: Flexure.

Three-point bending was used for flexural testing and required the use of a 5kN load cell, a support span of 100mm, ramp speed of 25mm/min, and end-of-test extension of 20mm. Three specimens per samples were tested, giving six curves per graph. The flexural set-up is shown in Figure 4.18.

Findings of flexural strength and modulus are presented in Chapter 5.

Figure 4.18: Instron machine and flexural test.

Flexural testing was carried out an Instron machine, with a ruler and digital micrometer used use to calculate flexural modulus, E_b, and flexural strength, σ_b. Relative error is as follows:

$$E_b = \frac{FL^3}{4wt^3D} \tag{4.7}$$

$$\frac{\Delta E_b}{E_b} = \frac{\Delta F}{F} + 3\frac{\Delta L_s}{L_s} + \frac{\Delta w}{w} + 3\frac{\Delta t}{t} + \frac{\Delta Def}{Def} \tag{4.8}$$

$$\frac{\Delta E_b}{E_b} = 10^{-5} + 3\cdot 10^{-2} + 80\cdot 10^{-2} + 3\cdot 3.4\cdot 10^{-2} + 5\cdot 10^{-2} = 19\cdot 10^{-2}$$

where flexural modulus' relative error, $\Delta E_b/E_b$, is found from: $\Delta F/F$ - load error determined by Instron machine; $\Delta L_s/L_s$ - error of support span; errors of sample's width and thickness, $\Delta w/w$ and $\Delta t/t$, respectively, and $\Delta Def/Def$ is an error of deflection at load point.

Flexural strength and its relative error are determined from:

$$\sigma_b = \frac{3FL}{2wt^2} \tag{4.9}$$

$$\frac{\Delta \sigma_b}{\sigma_b} = \frac{\Delta F}{F} + \frac{\Delta L}{L} + \frac{\Delta w}{w} + 2\frac{\Delta t}{t} \tag{4.10}$$

$$\frac{\Delta \sigma_b}{\sigma_b} = 10^{-5} + 10^{-2} + 80\cdot 10^{-2} + 2\cdot 3.4\cdot 10^{-2} = 8.5\cdot 10^{-2}$$

where relative error of flexural strength, $\Delta\sigma_b/\sigma_b$, is determined based on load, support span, width and thickness errors, $\Delta F/F$, $\Delta L/L$, $\Delta w/w$, $\Delta t/t$, respectively.

4.5.3. Shear

Figure 4.19 depicts a composite structure experiencing shear load, where the load attempts to slide adjacent layers of fibres over each other. Under shear load the resin matrix plays

the major role, transferring stresses across the composite. For the composite to perform well under shear load the resin matrix must not only exhibit good mechanical properties but must also have high adhesion to the reinforcement fibre. The interlaminar shear strength (ILSS) of a composite is often used to indicate this property in a laminate.

Figure 4.19: Shear.

For shear testing the ASTM method was used. Testing was conducted in accordance with ASTM standard D2344 (1989), with a load cell of 5kN, support span of 40mm, 5 times specimen thickness, and crosshead speed of 1.3mm/min.

Findings of interlaminar shear strength testing are presented in Chapter 5, while the Instron shear testing set-up is shown in Figure 4.20.

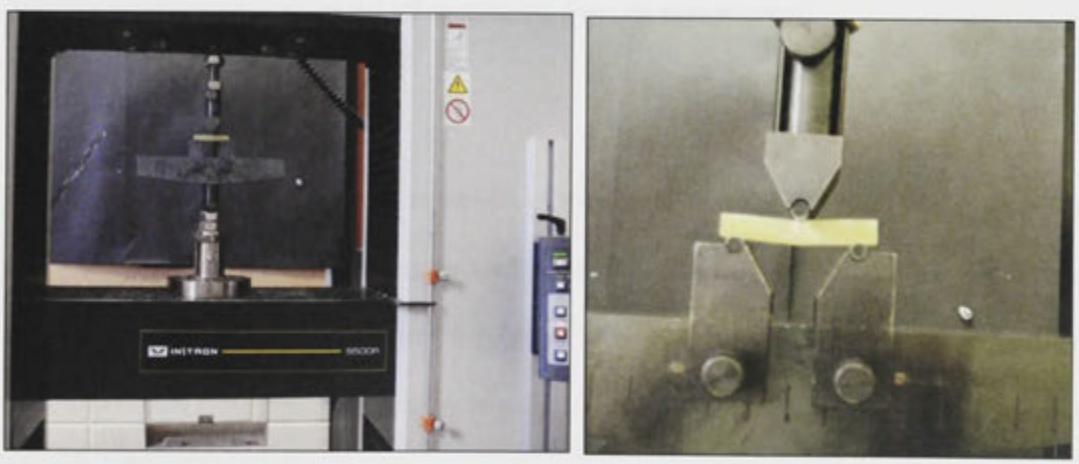

(a) (b)

Figure 4.20: Instron machine (a) and shear test (b).

Shear testing was carried out on an Instron machine, with a ruler and digital micrometer used to calculate shear strength, S_h. Relative error is as follows:

$$S_h = \frac{3L}{4wt} \tag{4.11}$$

$$\frac{\Delta S_h}{S_h} = \frac{\Delta L}{L} + \frac{\Delta w}{w} + \frac{\Delta t}{t} \tag{4.12}$$

$$\frac{\Delta S_h}{S_h} = 10^{-5} + \frac{0.1}{9} + \frac{0.1}{8} = 2.4 \cdot 10^{-2}$$

where $\Delta S_h/S_h$ is the relative error of shear strength calculated from load, width and thickness errors, $\Delta L/L$, $\Delta w/w$ and $\Delta t/t$, respectively.

4.5.4. Water intake

Water absorption experiment involved placing samples in tap water at 45°C for 7 days, with weight measurements performed every 24 hours. An analytical balance, A&D Company, model GR-200, with precision of 0.001g was used. After seven days samples were prepared for tensile and flexural tests using methods previously outlined in Section 4.4.1. The increase in moisture content for all specimens was calculated using:

$$G = \frac{W_s - W_d}{W_d} \times 100\%, \tag{4.13}$$

where G is % of weight gain, W_s is weight of specimen, and W_d is weight of dry specimen. Findings of water-intake measurements are shown in Chapter 5. Water gain was measured with the use of an analytical with a relative error of 10^{-2}, but it should be noted that additional error may have occurred by handling samples with cloth, or from the presence of water residue in laminates.

Chapter 5 RESULTS

Several different experimental systems were used in this study, details of which are found in Chapter 4. The results of those experiments are presented in this Chapter, and they include void content determination and mechanical properties characterization, namely tensile, flexural and shear properties. The influence of water on laminates properties is also presented here.

5.1. Stokes Bubble Cell

Direct measurement of bubble dynamic in liquid was expected to be achieved in Stage 1 of the project.

Table 5.1 presents experimental and calculated results of time-period of bubbles introduced into neat epoxy resin under static conditions (no vibrations) and their ascending time needed to reach the surface of the liquid (trajectory length of 73 mm). Calculation was based on Stokes Law and equation 3.18, as explained in section 3.4., while experimental part is described in section 4.1.1.

Experimental results are in good correlation with theoretical (calculated) ones, as shown in Figure 5.1, indicating that the smaller the bubble is it takes more time to exit the epoxy resin of SBC.

Table 5.1: Experimental (Time exp) and calculated (Time calc) time-periods of bubbles of different radius.

Radius (mm)	Time exp (s)	Time calc (s)
0.50	85.0	93.3
0.75	44.5	41.5
1.25	13.0	14.9
4.00	1.4	1.5

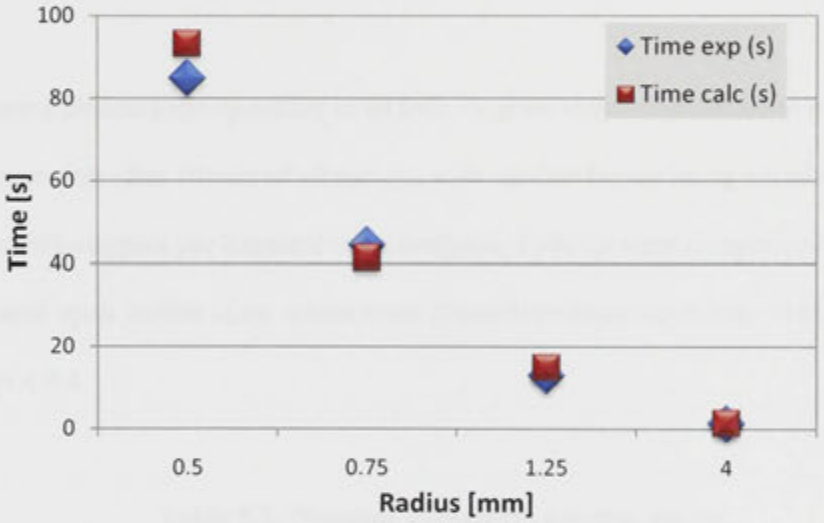

Figure 5.1: Comparison of experimental and calculated data for different-sized bubbles rising to the surface of SBC.

There were intentions of changing the position of vibration source, and also introducing more than two transducers to the system, as well as more powerful transducers, two or more air-bubbles flows enforced into the liquid, etc., but it had to be abandoned at this stage of the project because of difficulties in experimentation faced.

Air-pump with the nozzle and the needle created bubbles too big to work with and it was difficult to regulate the size of bubbles and their movement. Trying to create the steady

flow of air-bubbles was also not very successful. With small airflow (from air-pump) bubbles were not generating. With increasing the airflow the bubbles were too big and there were too many of them to control.

Bubbles generated by air-pump were not sufficiently small, and having vibrations at 40 kHz only did not give good results. To confirm what effect high frequencies have on bubbles movement I moved to the stage 2 of the project.

5.2. High-Frequency Piezoelectric Crystal

Stage 2 saw a piezocrystal operating at 40 kHz. A glass/vinyl-ester laminate was cured at room temperature after 10 min of vibrations, with another lay-up being cured without vibrations. Six samples per laminate were analysed, findings were categorized into four groups based upon bubble sizes, which were themselves based on bubble radii, as outlined in Section 4.4.4.

Table 5.2: Number of bubbles per size group for 0 Hz and 40,000 Hz laminates.

Hz/µm	50-100	100-200	200-500	>500
0	24	10	2	0
40k	16	2	5	5

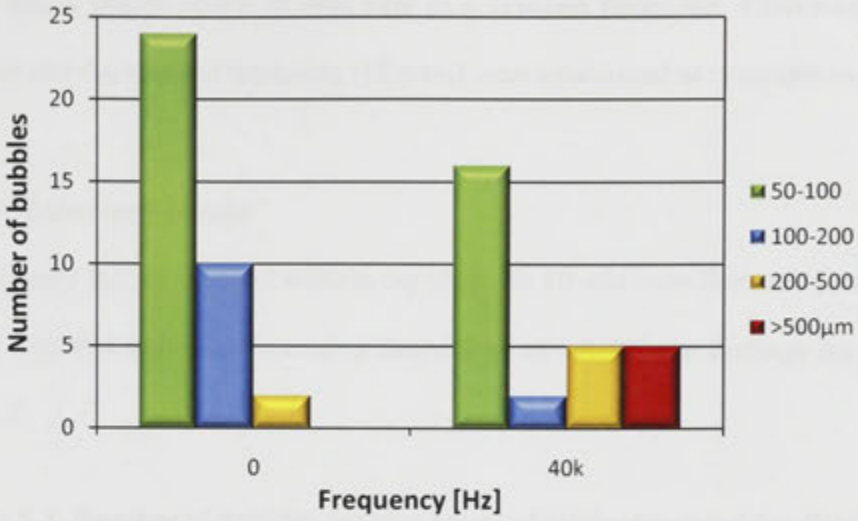

Figure 5.2: Level of porosity of laminates cured without vibrations (0 Hz) and with vibration assistance (40 kHz).

Figure 5.2 shows the porosity levels of laminates, expressed as a number of bubbles per laminate, cured with vibrations of 40 kHz, and without vibrations, 0 Hz, showing that vibrations at 40 kHz are not reducing the porosity to satisfactory extent. While 40 kHz laminates have lower number of small bubbles (green and blue bars) they have higher numbers of large bubbles (yellow and red bars), which indicates no improvement of level of porosity. This leads to the conclusion that despite their dissimilar treatment the two sample groups have similar void content.

5.3. EM Shaker

The Stage 3 experimental system used an electromagnetic shaker as a vibration source for the frequency range 0-8000 Hz. A number of parameters' influences were investigated, such as power of vibrations, length of time of vibrations, vacuum assistance and top plate. Initial experiments revealed no dependence of porosity level of laminates on power of

vibrations hence power of 0.1 W was kept as a constant parameter. Processing at room temperature and thickness of laminates (12 plies) were established as constants as well.

5.3.1. EM Shaker and 10 min

Glass/vinyl-ester laminates cured without top plate, for 10 min were first set of experiments performed with EM shaker and covering frequencies of 0-8,000 Hz; findings are presented in Table 5.3.

Table 5.3: Number of bubbles per size group of laminates cured for 10min at different frequencies.

Hz/μm	50-100	100-200	200-500	>500
0	7	7	3	1
5	9	3	1	0
10	6	6	3	0
30	4	1	1	0
50	7	5	2	0
100	6	7	4	0
1k	6	5	4	1
8k	8	3	1	3

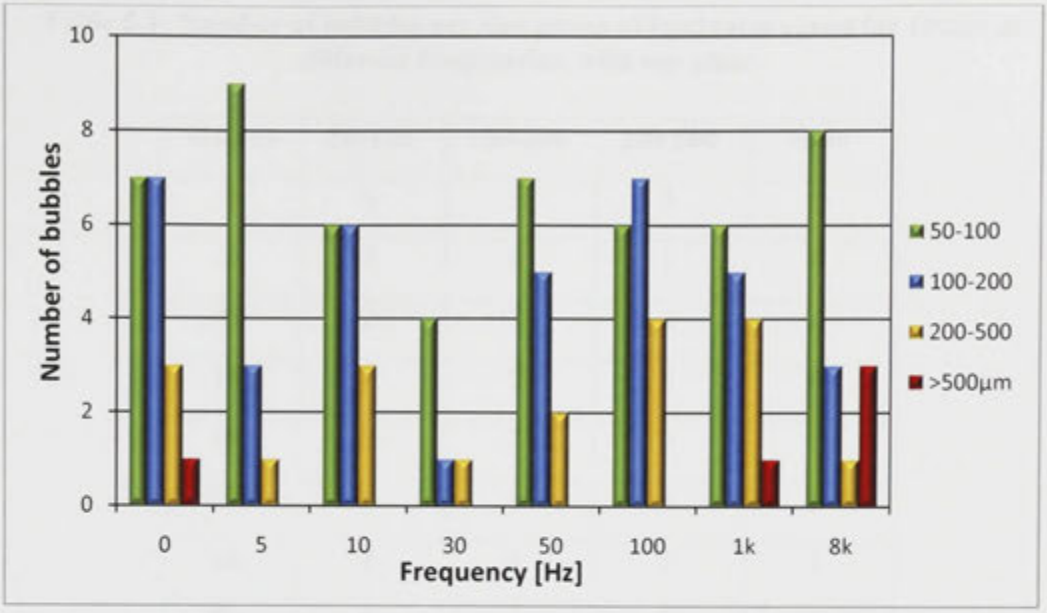

Figure 5.3: Level of porosity for laminates cured with no vibrations and with 10min vibrations at different frequencies.

Figure 5.3 shows that vibration assistance of higher frequencies (kHz) cannot be seen as reducing porosity, when compared with results for that laminate cured under static conditions (0Hz). There is a lower number of bubbles (green, blue and yellow bars) and no large bubbles at all (red bars) for frequencies between 5Hz and 100Hz. These results indicate the need for alteration and improvement to this experimental system as well as the potential of low frequencies as possible means of void reduction.

5.3.2. EM Shaker, 10 min and Top Plate

This group of experiments brought a top plate to the vibration-curing system, having all other parameters the same as in 5.3.1 and results are shown in Table 5.4.

Table 5.4: Number of bubbles per size group of laminates cured for 10min at different frequencies, with top plate.

Hz/µm	50-100	100-200	200-500	>500
0	8	1	3	0
5	5	0	1	0
10	2	7	4	0
30	1	2	2	0
50	2	1	7	0
100	2	1	3	0
1k	2	4	2	1
8k	4	3	6	1

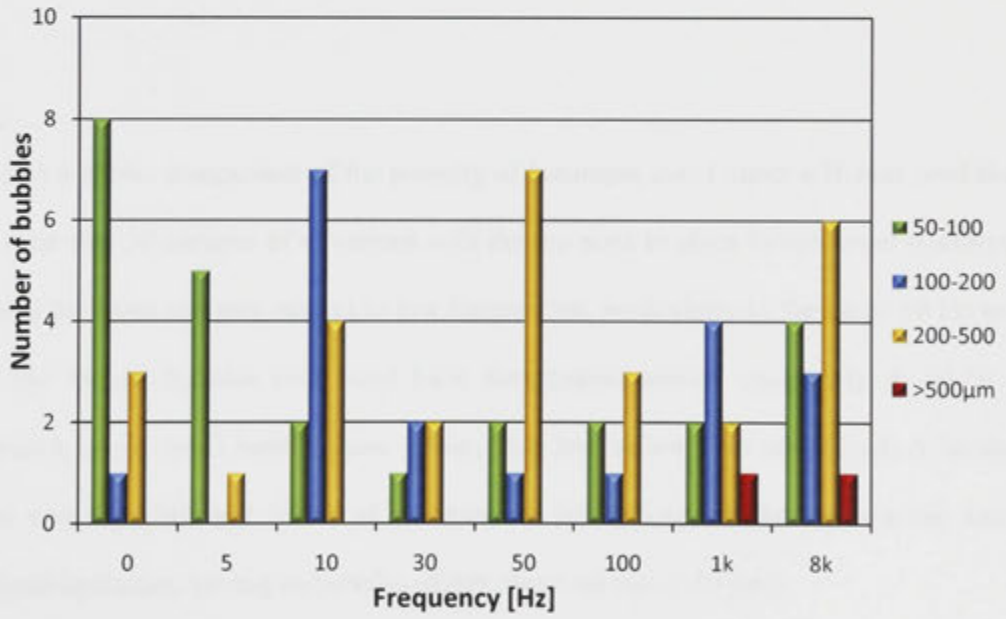

Figure 5.4: Level of porosity for laminates cured with no vibrations and with 10min vibrations of different frequencies, with top plate.

Figure 5.4 presents experimental results which show lower numbers of bubbles (green, blue and yellow bars) in laminates cured under low frequency vibrations, when compared with results seen in Figure 5.3 but with no large bubbles (red bars) other than for those samples subject to 1 and 8 kHz vibrations. All laminates display bubble-number reduction when compared with results of prior experiments in Figure 5.3, with results suggesting that additional refinement of the experimental system is necessary to assist with further void-content reduction.

5.3.3. EM Shaker, 10 and 30 min

In this third group of experiments the length of time-period samples were subject to vibrations was increased from 10 min to 30 min. The use of the top plate was also a shifting parameter. Previous (section 5.3.2) and new results are compared in Table 5.5 and Figure 5.5.

Figure 5.5 shows comparison of the porosity of laminates cured under different conditions. It is clear that 30 minutes of vibrations with the top plate in place brings lower numbers of bubbles for those samples subject to low frequencies, particularly in the range 10 Hz to 50 Hz. The largest bubbles (red bars) have disappeared almost completely in 10-50 Hz laminates, while small bubble sizes (green, blue and yellow) are minimized. A laminate cured with top plate and 30min of vibrations at 30 Hz seemed like the best one among analysed laminates, having no bubbles of any observed size (>50 μm).

Table 5.5: Comparison of the number of bubbles in laminates cured with 10 or 30 minutes of vibrations, with or without top plate.

10min	No top plate				Top plate			
Hz/µm	50-100	100-200	200-500	>500	50-100	100-200	200-500	>500
0	7	7	3	1	8	1	3	0
10	6	6	3	0	2	7	4	0
30	4	1	1	0	1	2	2	0
50	7	5	2	0	2	1	7	0
100	6	7	4	0	2	1	3	0
30min	No top plate				Top plate			
Hz/µm	50-100	100-200	200-500	>500	50-100	100-200	200-500	>500
0	7	7	3	1	2	7	3	1
10	4	2	2	0	0	1	1	0
30	1	2	2	2	0	0	0	0
50	0	0	1	1	0	1	0	1
100	5	4	2	1	4	3	1	2

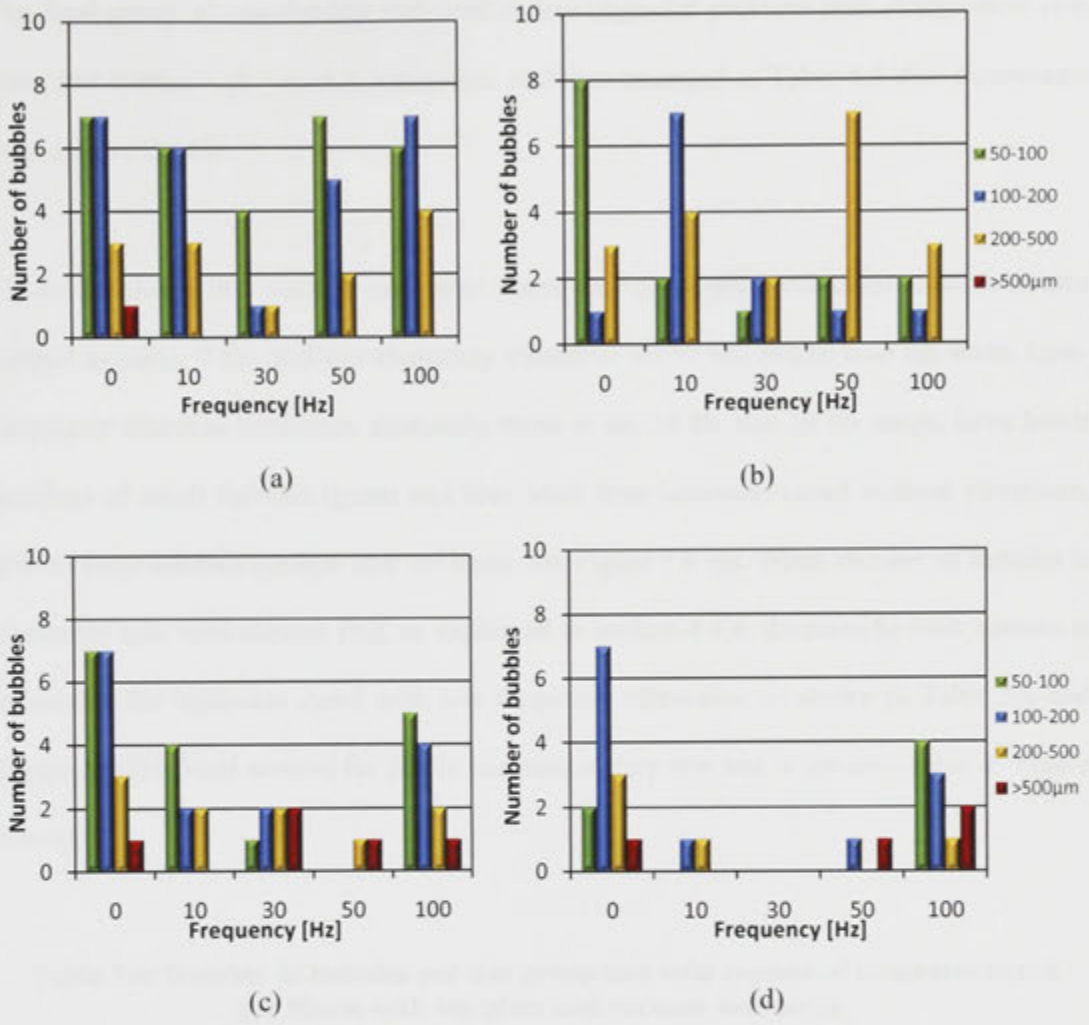

Figure 5.5: Comparison of porosity of laminates cured with no vibrations and with vibrations at low frequencies at 10 min (a and b), and 30 min (c and d); without top plate (a and c), and with top plate (b and d).

5.3.4. EM Shaker, 30min, Top Plate and Vacuum

The final group of experiments with EM shaker upgraded previous best arrangement (top plate and 30min) with vacuum assistance, and data arranged in Table 5.6 also incorporate void content details.

Figure 5.6 shows that vacuum assistance improved void-content reduction in all laminates subject to static, 0 Hz, and low-frequency vibration, 10-50 Hz; please note the scale. Low-frequency vibration laminates, especially those in the 10 Hz and 30 Hz range, have lower numbers of small bubbles (green and blue bars) than laminates cured without vibrations, and no large bubbles (yellow and red bars), see Figure 5.6 (a). When number of bubbles is converted into void content (%), as explained in section 4.4.4, decrease in void content is noticeable for laminates cured with low frequency vibrations, as shown in Table 5.6 and Figure 5.6 (b). Void content for 30 Hz laminate is very low and is not noticeable in Figure 5.6 (b).

Table 5.6: Number of bubbles per size group and void content of laminates cured for 30min with top plate and vacuum assistance.

Hz/µm	50-100	100-200	200-500	>500µm	Void content (%)
0	0	2	2	1	1.363
10	0	1	0	0	0.104
30	1	0	0	0	0.018
50	3	2	3	0	0.543

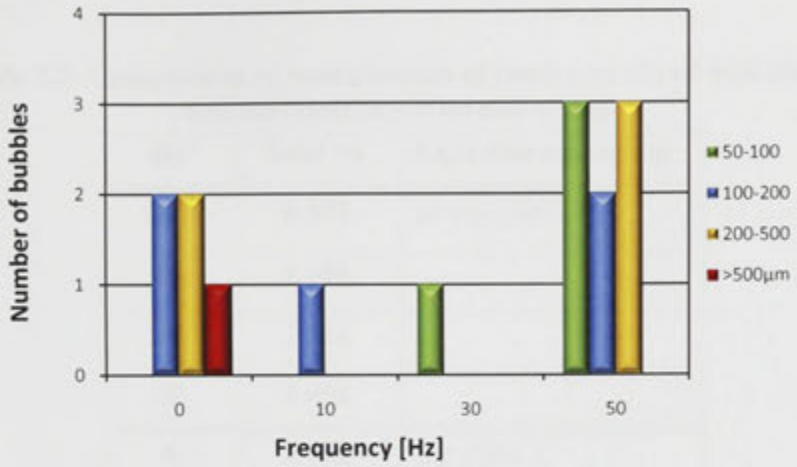

(a)

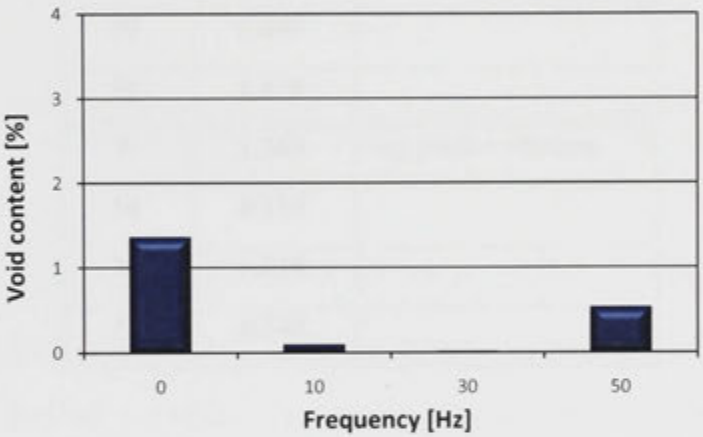

(b)

Figure 5.6: The porosity levels of laminates expressed as number of bubbles (a) and void content (b), cured for 30 minutes with top plate and vacuum assistance.

5.3.5. EM Shaker, Void Content Comparison

This section compares void content (%) of laminates previously explained in sections 5.3.3. and 5.3.4. They are all cured with 30 min of vibrations with the following combinations: (a) with no top plate and no vacuum; (b) with top plate and no vacuum; and (c) with top plate and vacuum assistance, all listed in Table 5.7.

Table 5.7: Comparison of void contents of laminates cured with 30min and different experimental set-up.

Hz	Void %	Experimental set-up
0	8.374	no top plate
10	1.005	
30	2.124	
50	2.656	
0	4.502	top plate
10	0.477	
30	0.040	
50	1.076	
0	1.363	top plate + vacuum
10	0.104	
30	0.018	
50	0.543	

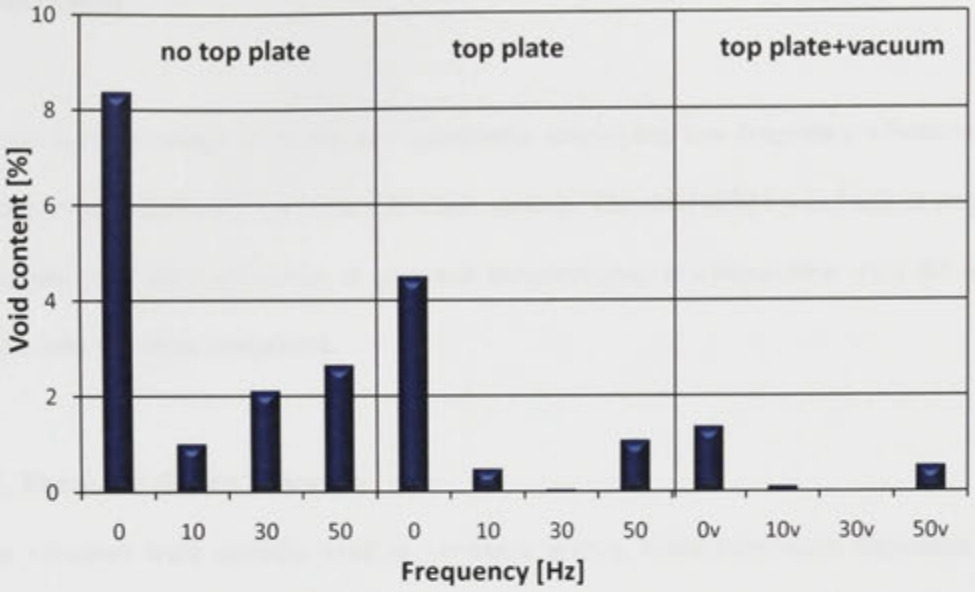

Figure 5.7: Void content of laminates cured with no vibrations and with 30min vibrations of low frequencies: with no top plate (left), with top plate (middle) and top plate and vacuum assistance (right).

Figure 5.7 shows how sample void content is reduced with use of vacuum assistance and top plate for laminates cured with 30min of low frequency (10-50 Hz) vibrations. The left-hand section of the chart (no top plate and no vacuum) shows 10-50 Hz laminates' bars as lower than 0 Hz (no vibrations curing). The same applies to the middle section of the chart (top plate and no vacuum), where bar values are further reduced. The right-hand section of the chart (top plate + vacuum) clearly shows low frequencies as the best for void-content reduction, with values for 10 Hz and 30 Hz bars as much lower than for 0 Hz.

5.4. ANUQSM

In Stage 4, the findings of previous experiments employing low-frequency vibrations and vacuum were incorporated into the QS-alike system. The ANUQSM was built in response to this step and allowed curing at elevated temperatures, in conjunction with the use of vacuum and vibration assistance.

5.4.1. Three Air-driven Vibrators

Three vibrators were initially used as vibration source. Glass/vinyl-ester laminates were cured at room temperature for 10 or 30 min with vibrations and vacuum. The frequency employed in vibrations was constant, 60 Hz.

This group of experiments did not yield promising results, showing high numbers of bubbles for vibration-assisted laminates, with all sizes of bubbles, i.e. all colored bars, for both 10 and 30min. When compared with those of static laminates (0 Hz), see Figure 5.8, no firm conclusion of vibration benefits to curing composite laminate can be made.

Table 5.8: Number of bubbles per size group of laminates cured for 10 and 30min at 60 Hz and room temperature.

	Hz/µm	50-100	100-200	200-500	>500µm
10min	0	7	4	1	0
	60	4	3	1	1
30min	0	1	2	2	6
	60	3	4	2	1

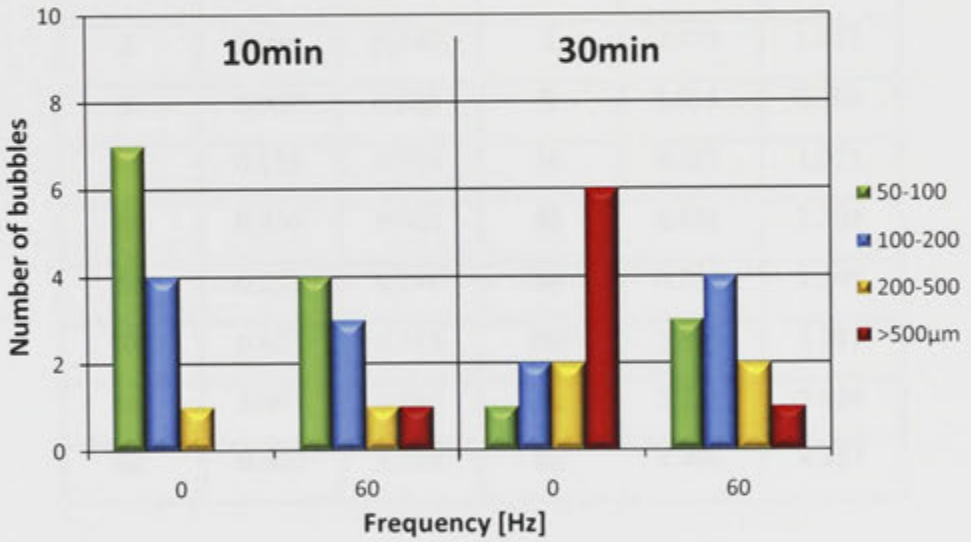

(a) (b)

Figure 5.8: Level of porosity for laminates cured with no vibrations and with vibrations at 60Hz, for 10 min (a) and 30 min (b).

5.4.2. Speaker, Void Content

A new vibration source, the speaker, was included in the ANUQSM apparatus at this point. The speaker was placed on the top of the clamped chambers, and was used for either 10min or 20min. Epoxy resin system was cured at 50°C, and vinyl-ester resin at 25°C, with void content results presented in Table 5.9.

Table 5.9: Void content for vinyl-ester and epoxy laminates cured with altered conditions.

Vinyl	Void %		*Epoxy*	Void %	
Hz	10min	20min	**Hz**	10min	20min
0	0.655	0.513	**0**	3.434	2.780
2	0.090	0.342	**2**	2.175	1.377
5	0.067	0.696	**5**	1.015	0.763
10	0.155	0.175	**10**	0.325	1.073
30	0.036	0.905	**30**	0.881	2.304
50	0.232	0.276	**50**	0.394	1.305
100	0.623	0.115	**100**	2.845	5.781
1k	1.093	0.237	**1k**	2.231	3.604
8k	0.600	1.128	**8k**	1.426	4.457

Figure 5.9 shows glass/epoxy resin laminates cured with vacuum and vibrations that were employed for 10 and 20min; the frequency range covered was 0-8000 Hz. The middle of the chart, with low frequencies (2-50 Hz), indicates lower void content for both 10 minutes (purple bars) and 20 minutes (gold bars) laminates than for no-vibrations (0 Hz) and high-frequency (100-8000 Hz) laminates. Ten minutes laminates (purple bars) have lower void content than twenty minutes of vibrations (gold bars) among frequencies higher than 10 Hz. At the same time 20 minutes of vibrations (gold bars) showed lower void content than 10 min vibration laminates (purple bars) at very low-frequencies, 2 Hz and 5 Hz, and no-vibrations (0 Hz) laminates.

Glass/vinyl-ester resin laminates were produced with UV curing after being in ANUQSM at room temperature (25°C). Vacuum and vibrations were again employed for 10min and 20 min. Low frequencies, 2-50 Hz, showed lower void content when cured with 10 minutes vibration. Figure 5.10 shows that low frequency vibrations of 10 minutes (purple bars) gave better results, i.e. lower void content than high frequencies and no-vibration, 0 Hz, laminates. When comparing glass/vinyl-ester laminates with glass/epoxy lower void content is noticeable for the first ones for all frequencies and time-length.

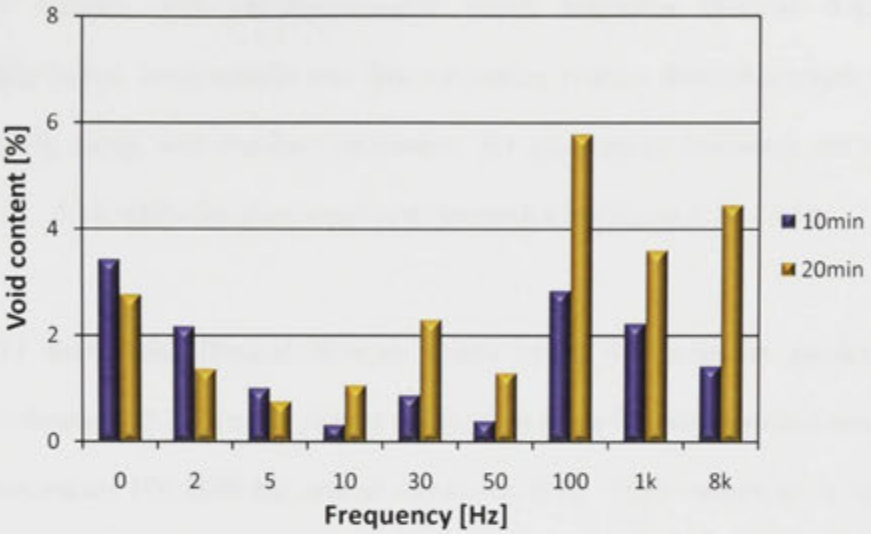

Figure 5.9: Void content for glass/epoxy laminates cured with vacuum and vibration assistance at different frequencies, for 10min and 20min.

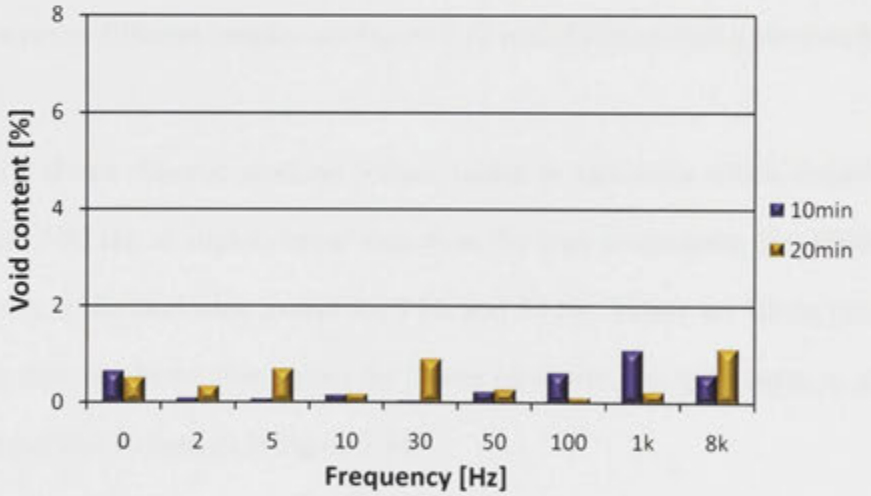

Figure 5.10: Void content for glass/vinyl-ester laminates cured with vacuum and vibration assistance at different frequencies, for 10min and 20min.

5.4.3. Speaker, Flexural Properties

Previously vacuum and vibration-assisted cured laminates (section 5.4.2) were mechanically tested. Void content and flexural testing results- flexural strength (FS) and modulus (FE), along with standard deviations, for glass/epoxy laminates are shown in Figures 5.11 - 5.14, while for glass/vinyl-ester laminates in Figures 5.15 - 5.16.

Figure 5.11 shows that flexural strength values (dots) for laminates employing low frequency vibrations, 2-50 Hz, are slightly higher than those for laminates that were subject to high frequencies, 100-8000 Hz, and no vibrations, 0 Hz. These results are in agreement with void content (bars). Low void content is reflected in higher flexural strength. Values for 10 minutes (purple bars and purple dots) are better than values for 20 minutes (gold bars and gold dots) in almost all cases. To get clearer picture how flexural strength values compare between different samples see Figure 5.12 with different axes scale than 5.11.

Figure 5.13 shows flexural modulus values (dots) in laminates which employed low frequencies, 2-50 Hz, as slightly lower than those for high frequencies, 100-8000 Hz, and no vibrations, 0 Hz, laminates, except for 5 Hz and 50 Hz. Values for 10min (purple bars and purple dots) are better than values for 20min (gold bars and gold dots), in almost all cases, that can also be noticed in Figure 5.14.

Table 5.10: Void content, flexural properties and standard deviation for 10min and 20min of vibration-cured glass/epoxy laminates.

10min					
f (Hz)	void %	FS (MPa)	StDev	FE (GPa)	StDev
0	3.434	226.05	6.299	13.3	0.208
2	2.175	226.79	2.851	12.7	0.351
5	1.015	237.86	9.067	13.7	0.404
10	0.325	229.43	6.191	12.8	0.265
30	0.881	234.94	5.597	12.9	0.265
50	0.394	228.59	6.964	13.3	0.436
100	2.845	224.63	9.026	13.2	0.289
1k	2.231	233.70	2.260	13.4	0.351
8k	1.426	232.02	5.135	13.3	0.404
20min					
f (Hz)	void %	FS (MPa)	StDev	FE (GPa)	StDev
0	2.780	212.14	4.845	11.8	0.153
2	1.377	226.70	1.708	13.2	0.107
5	0.763	222.12	5.836	12.4	0.760
10	1.073	233.20	3.415	12.3	0.851
30	2.304	220.07	10.011	12.4	0.659
50	1.305	235.96	2.836	12.1	0.107
100	5.781	196.47	7.675	12.3	0.250
1k	3.604	216.02	9.247	12.2	0.905
8k	4.457	213.44	8.881	12.2	0.329

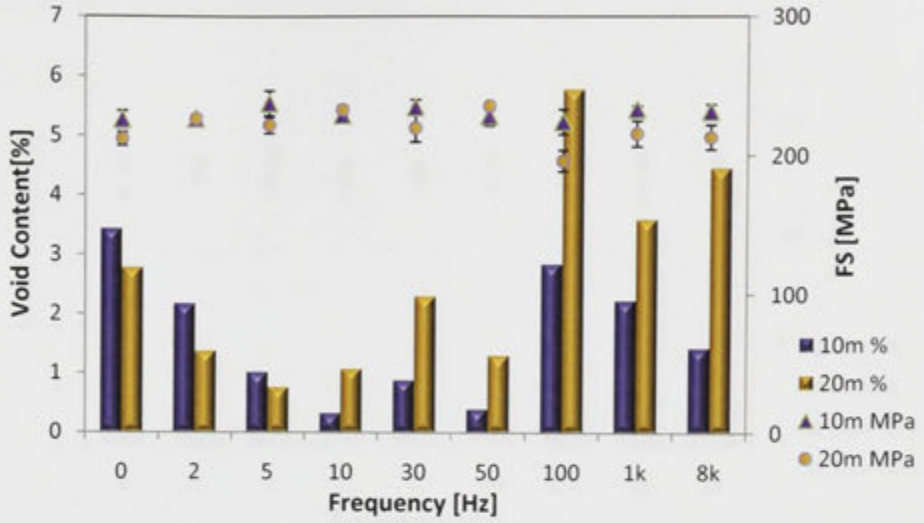

Figure 5.11: Void content and flexural strength of glass/epoxy laminates cured with vacuum and vibration assistance of different frequencies for 10min and 20min.

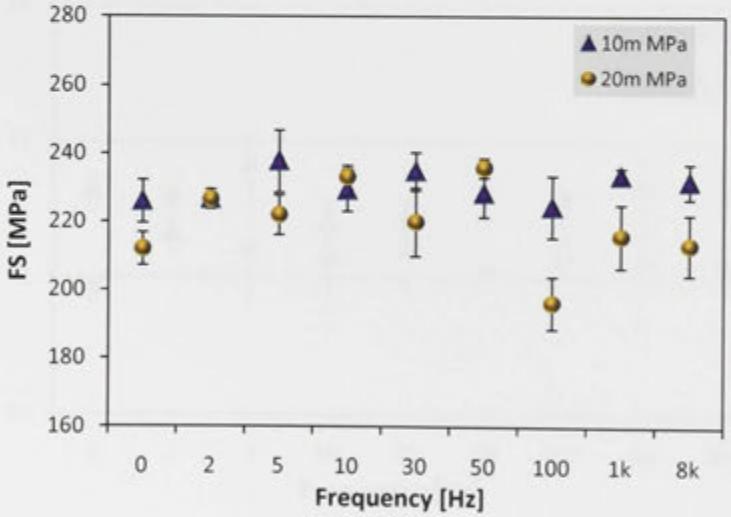

Figure 5.12: Flexural strength of glass/epoxy laminates; note axes scale.

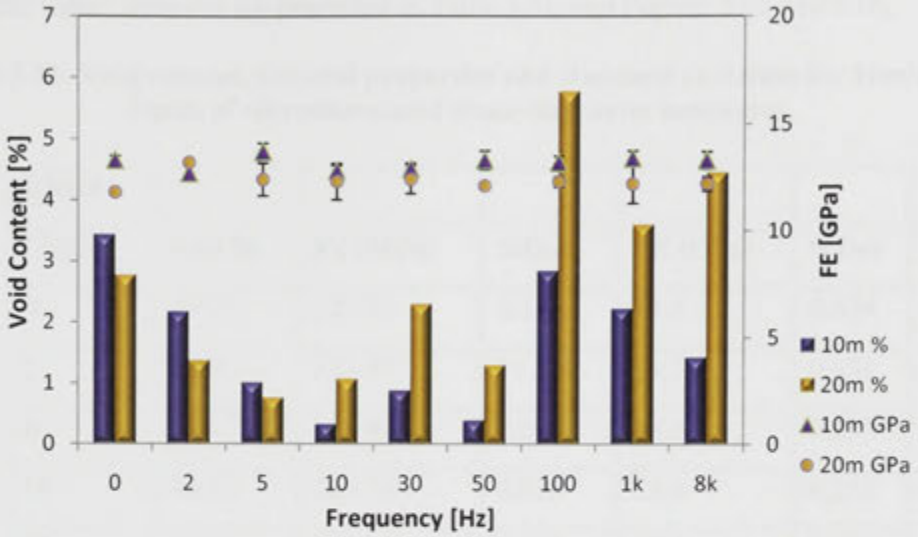

Figure 5.13: Void content and flexural modulus of glass/epoxy laminates cured with vacuum and vibration assistance of different frequencies for 10min and 20min.

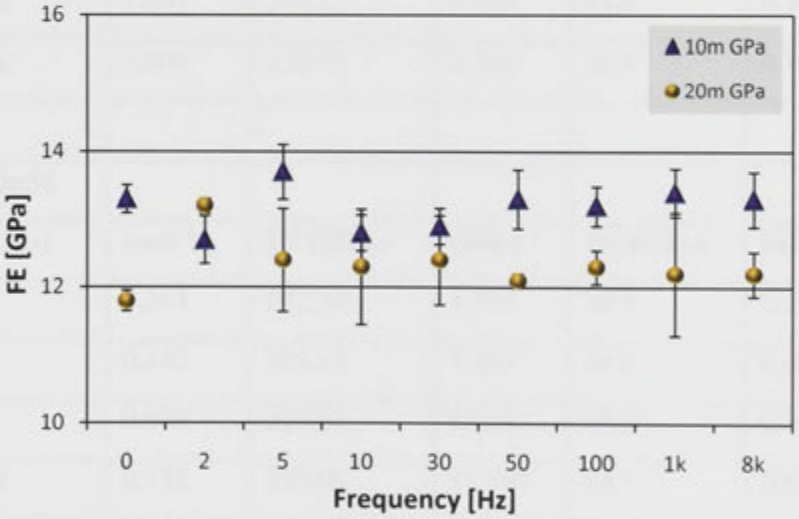

Figure 5.14: Flexural modulus of glass/epoxy laminates; please note axes scale.

Void content and flexural testing results- flexural strength (FS) and modulus (FE) for glass/vinyl-ester laminates are presented in Table 5.11, and Figures 5.15 and 5.16.

Table 5.11: Void content, flexural properties and standard deviation for 10min and 20min of vibration-cured glass/vinyl-ester laminates.

10min					
f (Hz)	**void %**	**FS (MPa)**	**StDev**	**FE (GPa)**	**StDev**
0	0.655	227.18	6.145	13.5	0.624
2	0.090	243.47	11.880	14.7	0.451
5	0.067	232.40	3.899	13.6	0.231
10	0.155	236.70	0.933	13.4	0.252
30	0.036	237.23	1.687	14.3	0.666
50	0.232	222.97	5.698	13.9	0.416
100	0.623	219.27	10.053	12.6	0.854
1k	1.093	234.11	0.565	13.8	0.361
8k	0.600	220.97	3.168	12.8	0.100
20min					
f (Hz)	**void %**	**FS (MPa)**	**StDev**	**FE (GPa)**	**StDev**
0	0.513	242.34	5.177	14.1	0.153
2	0.342	223.17	4.483	14.0	0.404
5	0.696	279.01	8.186	15.0	0.402
10	0.175	257.08	15.395	14.7	0.883
30	0.905	242.68	4.458	14.5	0.107
50	0.276	228.03	1.256	12.0	0.100
100	0.115	238.76	10.632	13.4	0.551
1k	0.237	220.64	1.630	13.5	0.195
8k	1.128	230.02	5.453	14.5	0.150

In Figure 5.15 flexural-strength values (dots) for low frequency (2-50 Hz) glass/vinyl-ester laminates are slightly higher than those for high frequencies (100-8000 Hz) and no vibrations (0 Hz) laminates. That is in agreement with void content (bars). Low void content is reflected in higher flexural strength. Values for 20min (gold bars and gold dots) are higher than values for 10min (purple bars and purple dots), although this trend is not consistent.

Figure 5.16 shows the results of the measurement of flexural modulus values of glass/vinyl-ester laminates. Values of laminates (dots) in which low frequency vibrations, 2-50 Hz, were employed are slightly higher than for those laminates using high frequencies, 100-8000 Hz, and no vibrations (0 Hz). These results are in agreement with void content (bars). Low void content is reflected in higher flexural modulus. Values for 20 minutes (gold bars and gold dots) are higher than values for 10 minutes (purple bars and purple dots), although this trend is not consistent.

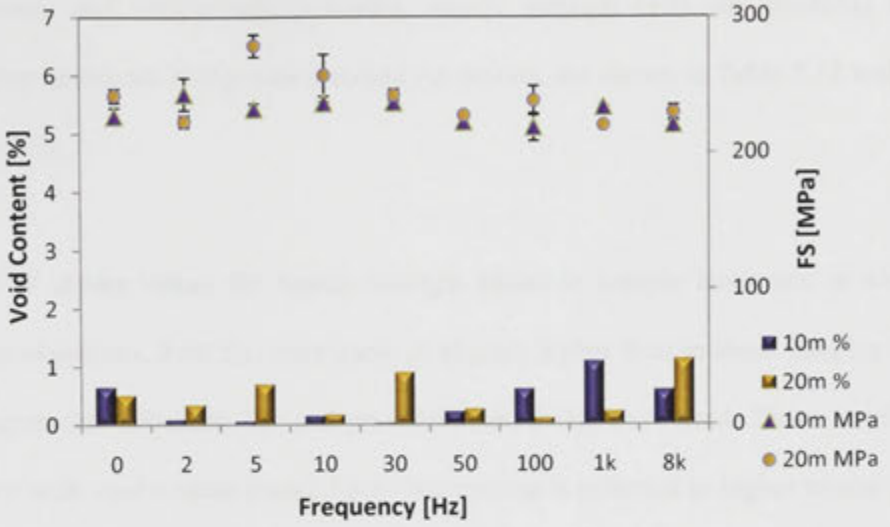

Figure 5.15: Void content and flexural strength of glass/vinyl-ester laminates cured with vacuum and vibration assistance of different frequencies for 10min and 20min.

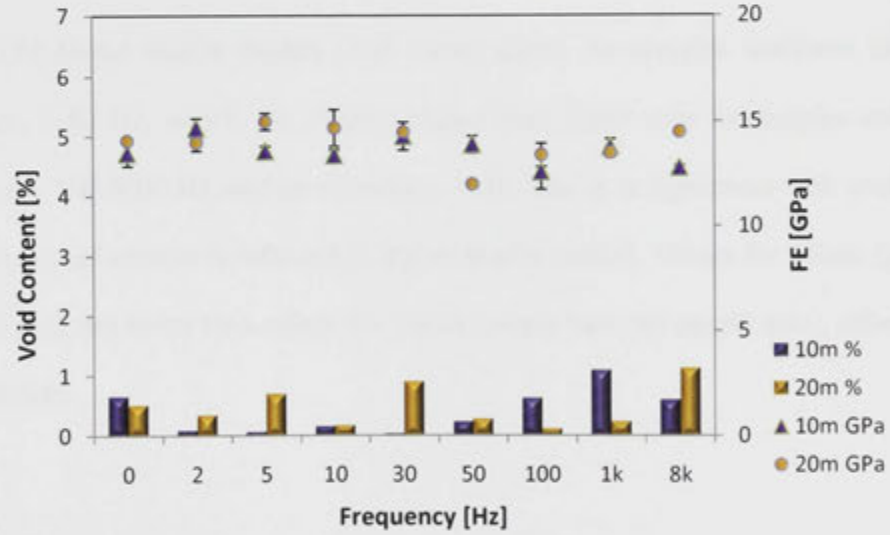

Figure 5.16: Void content and flexural modulus of glass/vinyl-ester laminates cured with vacuum and vibration assistance of different frequencies for 10min and 20min.

5.4.4. Speaker, Tensile Properties

Void content and tensile testing results, tensile strength (TS) and modulus (TE), of glass/epoxy laminates, along with standard deviations, are shown in Table 5.12 and Figures 5.17 and 5.18.

Figure 5.17 shows values for tensile strength (dots) in sample laminates in which low frequency vibrations, 2-50 Hz, were used, as slightly higher than in those samples in which high frequencies, 100-8000 Hz, and no vibrations, 0 Hz, were used. These results are in agreement with void content (bars). Low void content is reflected in higher tensile strength. There is no clear indication whether 10 or 20 min of vibrations give better tensile strength results since the trend is not consistent.

Figure 5.18 shows tensile moduli (TE) values (dots) for samples laminates using low frequency, 2-50 Hz, which are slightly higher than those seen in samples using high frequencies, 100-8000 Hz, and no vibrations, 0 Hz. That is in agreement with void content (bars). Low void content is reflected in higher tensile moduli. Values for 20min (gold bars and gold dots) are better than values for 10min (purple bars and purple dots), although it is not consistent.

Table 5.12: Void content, tensile properties and standard deviation for 10min and 20min of vibration-cured glass/epoxy laminates.

10min					
f (Hz)	**void %**	**TS (MPa)**	**StDev**	**TE (GPa)**	**StDev**
0	3.434	175	13.856	13.4	2.546
2	2.175	163	14.742	13.1	2.517
5	1.015	176	9.074	14.0	5.399
10	0.325	179	6.110	13.8	8.566
30	0.881	166	7.810	13.6	4.338
50	0.394	176	11.930	14.2	4.726
100	2.845	164	9.539	13.1	1.000
1k	2.231	171	3.055	13.1	4.221
8k	1.426	184	5.856	13.7	6.110
20min					
f (Hz)	**void %**	**TS (MPa)**	**StDev**	**TE (GPa)**	**StDev**
0	2.780	171	0.643	13.0	0.351
2	1.377	181	0.300	14.6	0.168
5	0.763	173	0.173	13.8	0.750
10	1.073	171	0.872	13.8	0.600
30	2.304	168	0.462	14.0	1.291
50	1.305	176	0.208	13.9	0.297
100	5.781	180	0.116	13.5	0.265
1k	3.604	170	0.964	13.2	0.184
8k	4.457	165	1.168	13.5	0.329

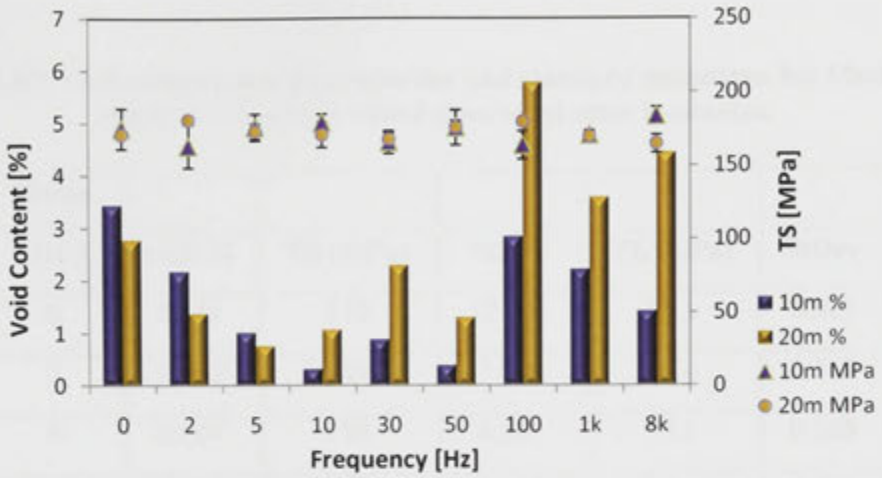

Figure 5.17: Void content and tensile strength of glass/epoxy laminates cured with vacuum and vibration assistance of different frequencies for 10 and 20 minutes.

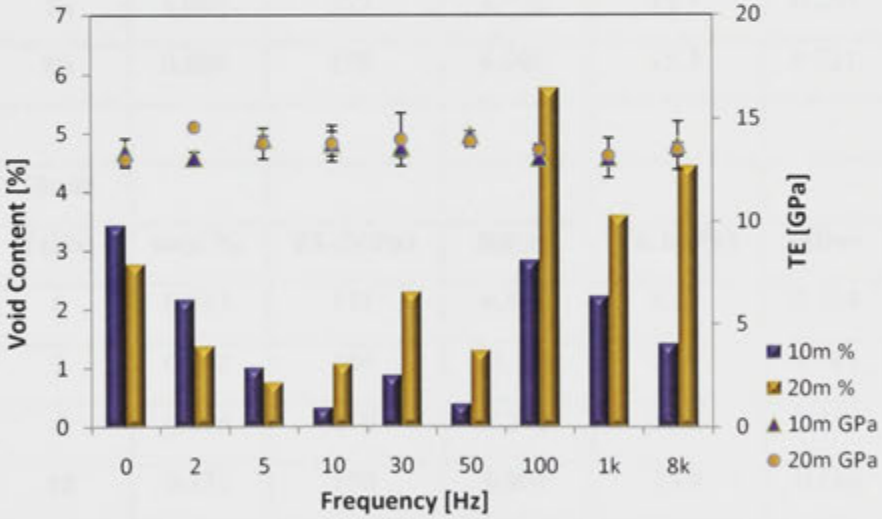

Figure 5.18: Void content and tensile modulus of glass/epoxy laminates cured with vacuum and vibration assistance of different frequencies for 10min and 20min.

Findings of glass/vinyl-ester laminates are presented in Table 5.13 and Figures 5.19 - 5.20.

Table 5.13: Void content, tensile properties and standard deviations for 10min and 20min of vibrations cured glass/vinyl-ester laminates.

10min					
f (Hz)	**void %**	**TS (MPa)**	**StDev**	**TE (GPa)**	**StDev**
0	0.655	170	12.741	15.1	0.815
2	0.090	184	7.810	15.6	0.352
5	0.067	174	8.505	15.1	0.265
10	0.155	176	8.327	15.0	0.529
30	0.036	177	11.314	16.4	2.984
50	0.232	170	4.583	13.9	0.493
100	0.623	180	3.786	14.4	1.531
1k	1.093	173	4.726	15.7	0.265
8k	0.600	178	6.000	15.3	0.721
20min					
f (Hz)	**void %**	**TS (MPa)**	**StDev**	**TE (GPa)**	**StDev**
0	0.513	171	6.501	15.1	0.574
2	0.342	164	23.136	16.1	1.711
5	0.696	210	7.371	16.2	0.310
10	0.175	158	6.801	15.9	0.518
30	0.905	177	15.313	17.0	0.651
50	0.276	189	14.668	15.5	0.900
100	0.115	182	2.309	15.4	0.250
1k	0.237	168	9.002	16.2	1.468
8k	1.128	163	10.599	15.1	0.299

Figure 5.19 shows that tensile strength values (dots) for laminates using low frequency vibrations, 2-50 Hz, are slightly higher than for those laminates in which high frequencies, 100-8000 Hz and no vibrations, 0 Hz, were used. These results are in agreement with void content (bars). Low void content is reflected in higher tensile strength. Values for 10 minutes (purple bars and purple dots) are intermittently better than values for 20 minutes (gold bars and gold dots).

Figure 5.20 depicts tensile moduli (dots) for sample laminates that used low frequency vibrations, 2-50 Hz, in their fabrication, and which are slightly higher than those samples using high frequencies, 100-8000 Hz, and no vibrations, 0 Hz. That is in agreement with void content (bars). Low void content is reflected in higher tensile moduli. Values for 20 minutes (gold bars and gold dots) are higher than values for 10 minutes (purple bars and purple dots).

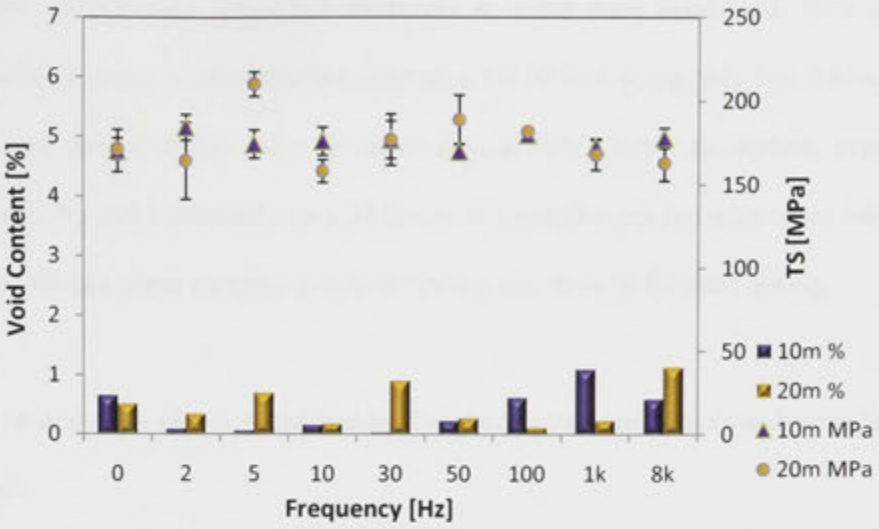

Figure 5.19: Void content and tensile strength of glass/vinyl-ester laminates cured with vacuum and vibration assistance of different frequencies for 10min and 20min.

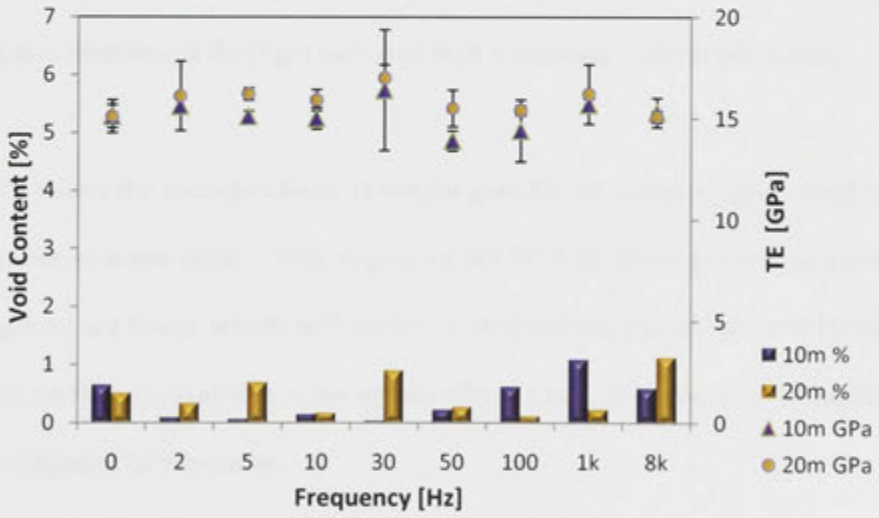

Figure 5.20: Void content and tensile modulus of glass/vinyl-ester laminates cured with vacuum and vibration assistance of different frequencies for 10min and 20min.

5.4.5. Speaker, Water Absorption

Experiments of exposing composite laminates to water were conducted. New laminates were cured with vacuum and vibration assistance for 10 min, using only low frequencies. Samples were soaked in tap water for seven days at 50ºC. Water absorption, expressed as water uptake, %, was measured every 24 hours. Six samples per laminate were subjected to mechanical testing, three samples to tensile testing and three to flexural testing.

Tables 5.14 and 5.15 shows water uptake for glass/epoxy and glass/vinyl-ester laminates, respectively.

Figure 5.21 shows the weight gain mean values of six samples glass/epoxy laminates for each frequency, due to water uptake. Weight gain values for 5 Hz (light green) and 30 Hz (dark green) are lower, indicating lower sample void content than of those laminates which employed no vibrations, 0 Hz (light red), and high vibrations, 100 Hz (dark red).

Figure 5.22 shows the average values of weight gain for six samples (glass/vinyl-ester) per frequency, due to water uptake. Weight gain values for 5 Hz (light green) and especially 30 Hz (dark green) are lower, which indicate lower void content than those for 0 Hz (light red) and 100 Hz (dark red). Note that water uptake after 4 days, 96 hours, was the highest for all laminates subjected to vibrations.

Table 5.14: Water uptake (%) of glass/epoxy laminates measured every 24h for 7 days.

Epoxy							
Hz/h	**24**	**48**	**72**	**96**	**120**	**144**	**168**
0	0.038	0.047	0.065	0.083	0.079	0.077	0.080
5	0.032	0.042	0.052	0.073	0.073	0.072	0.073
30	0.042	0.044	0.060	0.077	0.075	0.074	0.074
100	0.037	0.050	0.062	0.085	0.084	0.082	0.083
StDev							
0	0.0098	0.0052	0.0105	0.0052	0.0075	0.0052	0.0063
5	0.0117	0.0075	0.0075	0.0103	0.0082	0.0075	0.0082
30	0.0121	0.0082	0.0089	0.0052	0.0084	0.0082	0.0082
100	0.0052	0.0063	0.0075	0.0105	0.0082	0.0075	0.0052

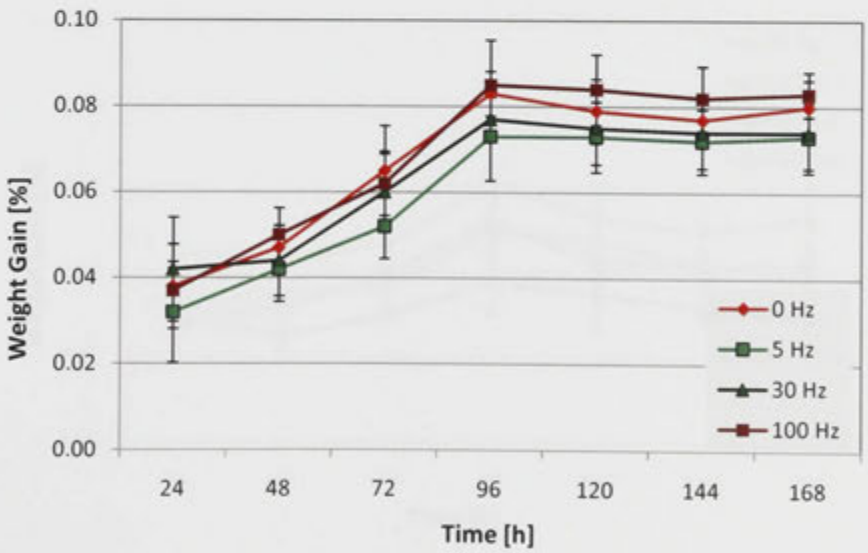

Figure 5.21: Weight gain of glass/epoxy laminates cured with vacuum and 10min vibration assistance, exposed to water for 7 days.

Table 5.15: Water uptake (%) of glass/vinyl-ester laminates measured every 24 hours for 7 days.

Vinyl							
Hz/h	**24**	**48**	**72**	**96**	**120**	**144**	**168**
0	0.045	0.043	0.047	0.062	0.053	0.050	0.053
5	0.032	0.035	0.037	0.050	0.048	0.042	0.042
30	0.030	0.025	0.030	0.038	0.035	0.032	0.030
100	0.028	0.032	0.040	0.052	0.043	0.042	0.042
StDev							
0	0.0105	0.0121	0.0052	0.0041	0.0082	0.0063	0.0082
5	0.0075	0.0055	0.0082	0.0063	0.0075	0.0041	0.0041
30	0.0000	0.0055	0.0000	0.0075	0.0084	0.0041	0.0000
100	0.0075	0.0041	0.0089	0.0041	0.0052	0.0041	0.0041

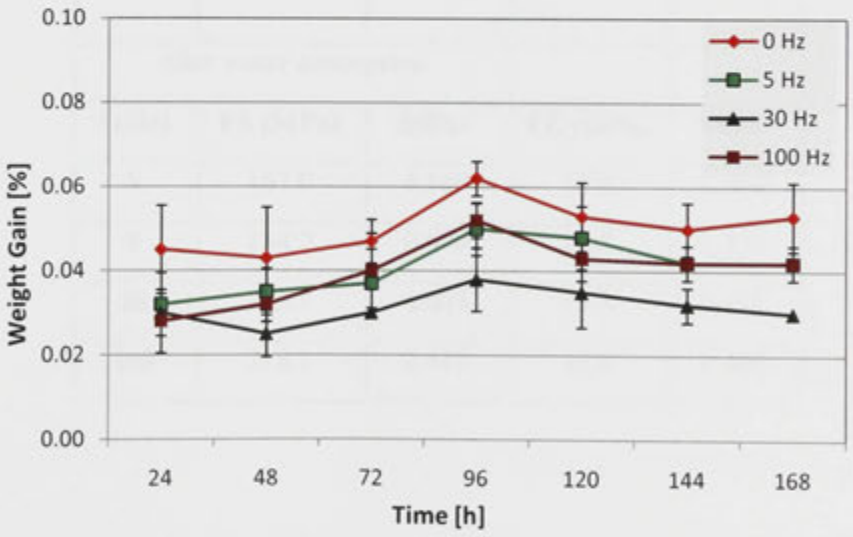

Figure 5.22: Weight gain of glass/vinyl-ester laminates cured with vacuum and 10 minutes vibration assistance, exposed to water for 7 days.

5.4.6. Speaker, Water Absorption and Flexing

Glass/vinyl-ester laminates that were previously in water (section 5.4.5) were subjected to flexural testing. Flexural strength (FS) and modulus (FE) for glass/vinyl-ester laminates (cured with 10min of vibrations), were determined before (denoted as 1) and after (denoted as 2) water absorption. Standard deviations were also calculated and are presented in Table 5.16.

Table 5.16: Flexural properties of glass/vinyl-ester laminates subjected to water.

Before water absorption				
f (Hz)	**FS (MPa)**	**StDev**	**FE (GPa)**	**StDev**
0	203.4	3.835	12.9	0.100
5	227.8	17.204	13.2	0.473
30	247.9	5.541	13.4	0.361
100	234.4	4.903	13.1	0.252
After water absorption				
f (Hz)	**FS (MPa)**	**StDev**	**FE (GPa)**	**StDev**
0	167.0	4.509	12.8	0.400
5	164.7	0.694	12.7	0.231
30	223.3	6.003	13.3	0.289
100	218.3	2.411	12.8	0.400

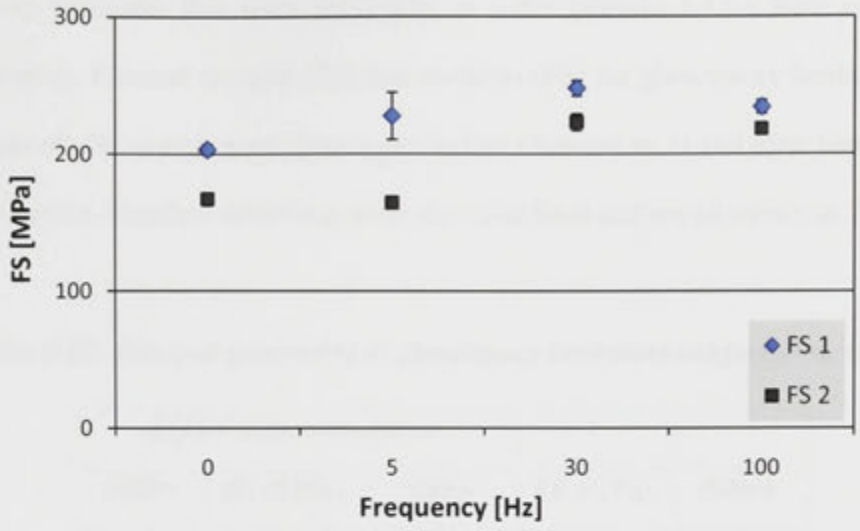

(a)

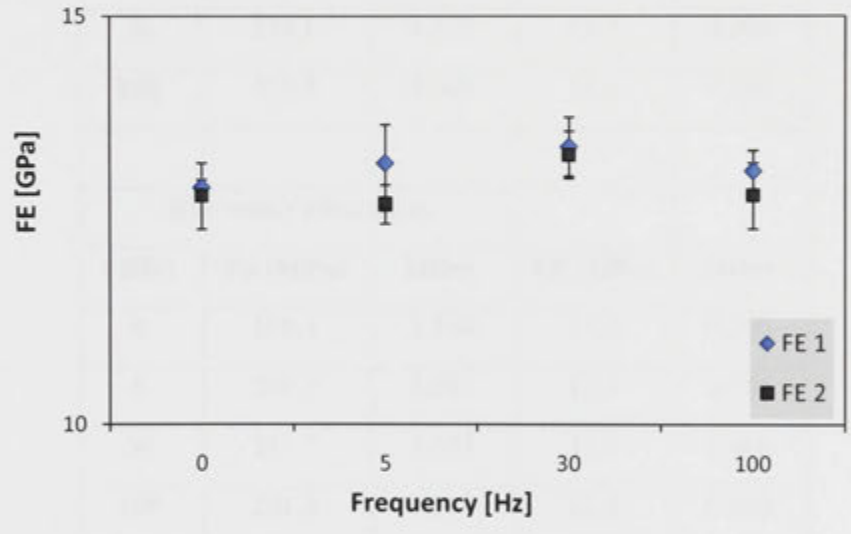

(b)

Figure 5.23: Comparison of flexural strength (a) and modulus (b) for glass/vinyl-ester laminates before (1) and after (2) water absorption; note the scale.

Figure 5.23 (a) shows higher values of flexural strength before water absorption, FS1 (blue rhombs), for 30 Hz than for laminates that used no vibrations (0Hz). The same trend is noted for flexural moduli in Figure 23 (b). This applies equally to after water testing, for both flexural strength and moduli, though some differences are small.

Glass/epoxy laminates that were previously in water (section 5.4.5.) were subjected to flexural testing. Flexural strength (FS) and modulus (FE) for glass/epoxy laminates (cured with 10min of vibrations), were determined before (denoted as 1) and after (denoted as 2) water absorption. Standard deviations were also calculated and are all shown in Table 5.17.

Table 5.17: Flexural properties of glass/epoxy laminates subjected to water.

Before water absorption				
f (Hz)	**FS (MPa)**	**StDev**	**FE (GPa)**	**StDev**
0	217.5	10.844	13.1	0.200
5	231.8	5.408	13.4	0.208
30	234.1	4.272	13.4	0.300
100	225.3	6.689	13.1	0.252
After water absorption				
f (Hz)	**FS (MPa)**	**StDev**	**FE (GPa)**	**StDev**
0	186.3	3.564	12.0	0.200
5	209.7	3.501	12.7	0.153
30	211.7	2.143	13.3	0.400
100	201.3	1.711	12.0	0.100

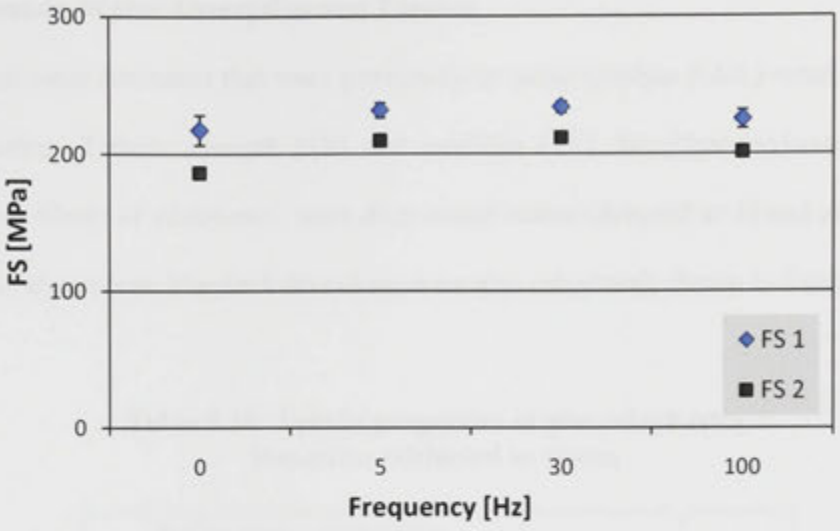

(a)

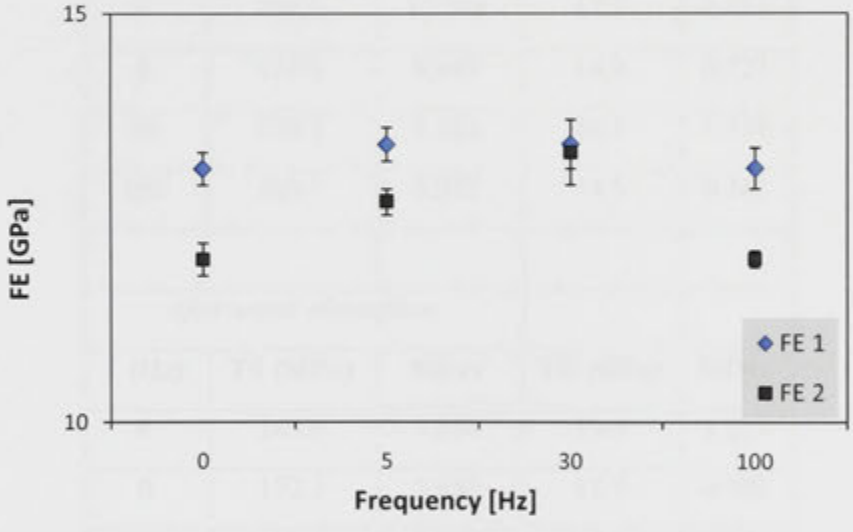

(b)

Figure 5.24: Comparison of flexural strength (a) and modulus (b) for glass/epoxy laminates before (1) and after (2) water absorption; note the scale.

Figure 5.24 (a) shows higher values of flexural strength before water absorption, FS1 (blue rhombs), for samples subject to vibration at 5 Hz and 30 Hz than for no vibrations, 0 Hz. The same trend is noted for flexural moduli, FE1, in Figure 5.24 (b). This applies equally to after water testing, for both flexural strength and moduli, with clear differences.

5.4.7. Speaker, Water Absorption and Tension

Glass/vinyl-ester laminates that were previously in water (section 5.4.5.) were subjected to tensile testing. Tensile strength (TS) and modulus (TE) for glass/vinyl-ester laminates (cured with 10min of vibrations), were determined before (denoted as 1) and after (denoted as 2) water absorption. Standard deviations were also calculated, shown in Table 5.18.

Table 5.18: Tensile properties of glass/vinyl-ester laminates subjected to water.

Before water absorption				
f (Hz)	**TS (MPa)**	**StDev**	**TE (GPa)**	**StDev**
0	163.3	12.946	13.8	0.794
5	175.0	9.849	14.9	0.723
30	173.3	1.262	16.1	1.739
100	165.7	8.275	14.5	0.361
After water absorption				
f (Hz)	**TS (MPa)**	**StDev**	**TE (GPa)**	**StDev**
0	145.0	7.638	13.4	1.217
5	152.3	3.687	12.9	0.808
30	174.0	2.000	14.8	1.150
100	156.3	6.752	13.7	0.058

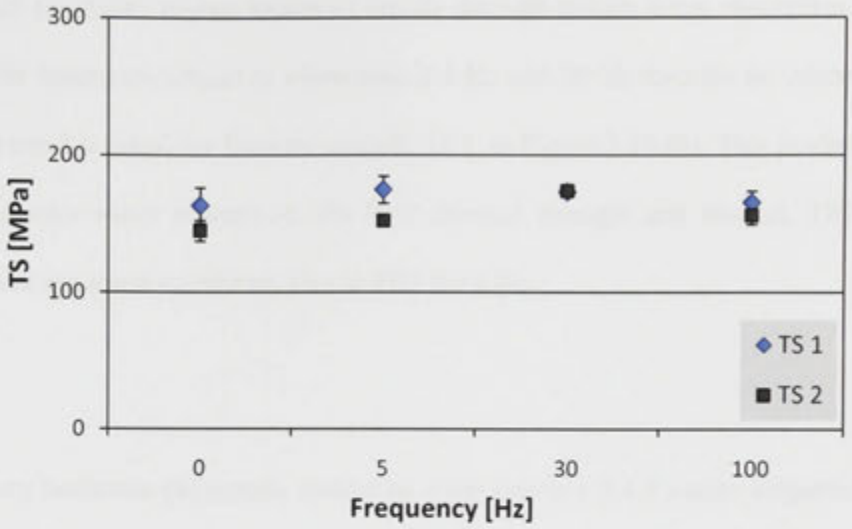

(a)

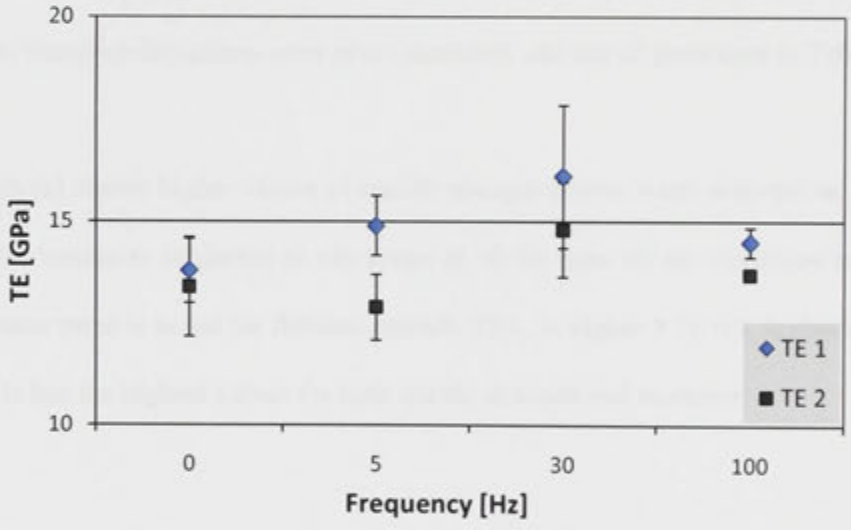

(b)

Figure 5.25: Comparison of tensile strength (a) and modulus (b) for glass/vinyl-ester laminates before (1) and after (2) water absorption; note the scale.

Figure 5.25 (a) shows higher values of tensile strength before water absorption, TS1 (blue rhombs) for laminates subject to vibrations at 5 Hz and 30 Hz than for no vibrations, 0 Hz. The same trend is noted for flexural moduli, TE1, in Figure 5.25 (b). This is also applicable for testing after water absorption, for both flexural strength and moduli, TS2 and TE2, though there are some variations, like in TE2 for 5 Hz.

Glass/epoxy laminates previously soaked in water (section 5.4.5.) were subjected to tensile testing. Tensile strength (TS) and modulus (TE) for glass/epoxy laminates (cured with 10min of vibrations), were determined before (denoted as 1) and after (denoted as 2) water absorption. Standard deviations were also calculated, and are all presented in Table 5.19.

Figure 5.26 (a) shows higher values of tensile strength before water absorption, TS1, (blue rhombs) for laminates subjected to vibrations at 30 Hz than for no vibrations laminates, 0 Hz. The same trend is noted for flexural moduli, TE1, in Figure 5.26 (b). It should be noted that 100 Hz has the highest values for both tensile strength and modulus.

Table 5.19: Tensile properties of glass/epoxy laminates subjected to water.

Before water absorption				
f (Hz)	**TS (MPa)**	**StDev**	**TE (GPa)**	**StDev**
0	165.3	3.006	13.7	0.208
5	152.0	7.024	13.5	0.551
30	170.3	4.671	13.8	0.503
100	171.7	6.049	13.9	0.513
After water absorption				
f (Hz)	**TS (MPa)**	**StDev**	**TE (GPa)**	**StDev**
0	152.3	2.143	12.8	1.258
5	156.0	6.557	12.5	0.462
30	156.3	1.540	12.8	0.300
100	156.7	4.005	13.1	1.210

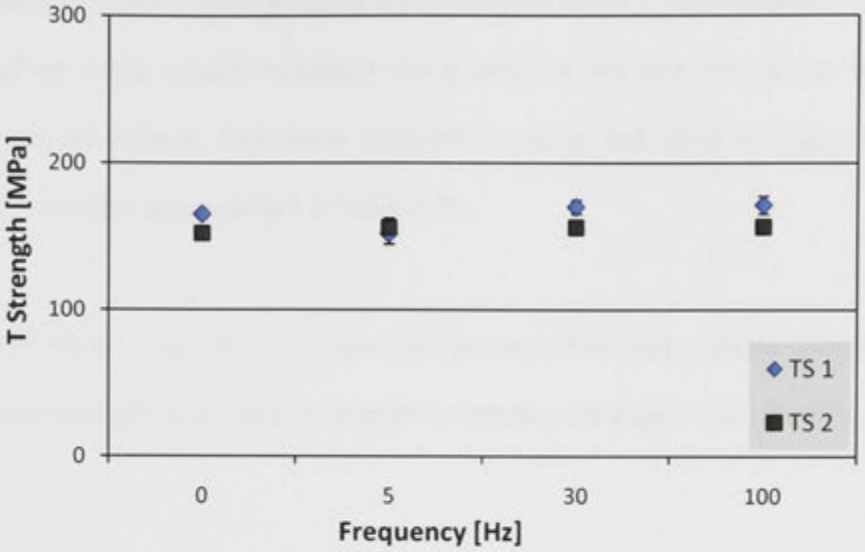

(a)

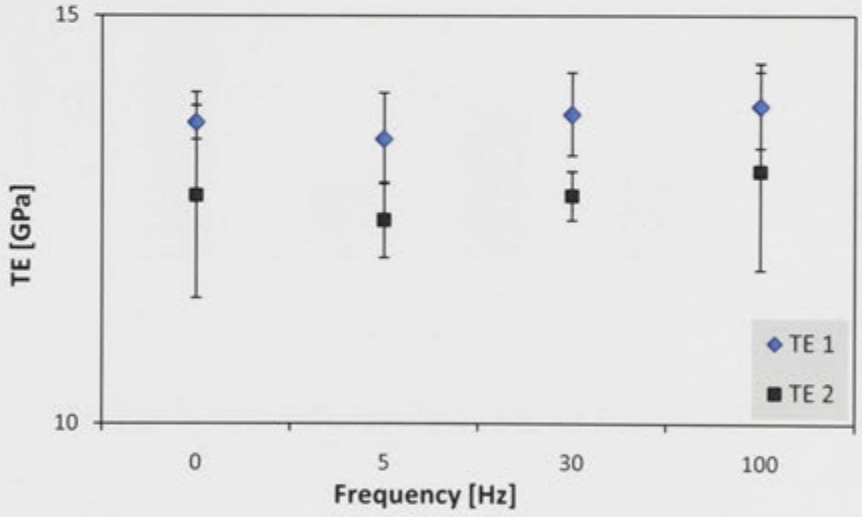

(b)

Figure 5.26: Comparison of tensile strength (a) and modulus (b) for glass/epoxy laminates before (1) and after (2) water absorption; note the scale.

5.4.8. Speaker, Shear Testing

Shear testing of unidirectional glass/epoxy composites cured with 10 min of vibrations was performed on seven sample laminates cut parallel to the direction of the fibres. Void content was determined. Calculated standard deviation and shear strength (ShS) mean values of 5 samples are presented in Table 5.20.

Figure 5.27 shows 5 Hz and 30 Hz laminates having lower void contents (purple bars) and higher shear strength (gold squares) than those samples not exposed to vibration, 0 Hz.

Table 5.20: Void content and shear strength of unidirectional glass/epoxy laminates cut along fibres.

f (Hz)	Void %	StDev	ShS (MPa)	StDev
0	6.102	2.822	27.14	1.256
5	1.853	1.317	31.98	1.074
30	3.642	2.654	30.09	0.713
100	2.049	0.839	30.95	0.410

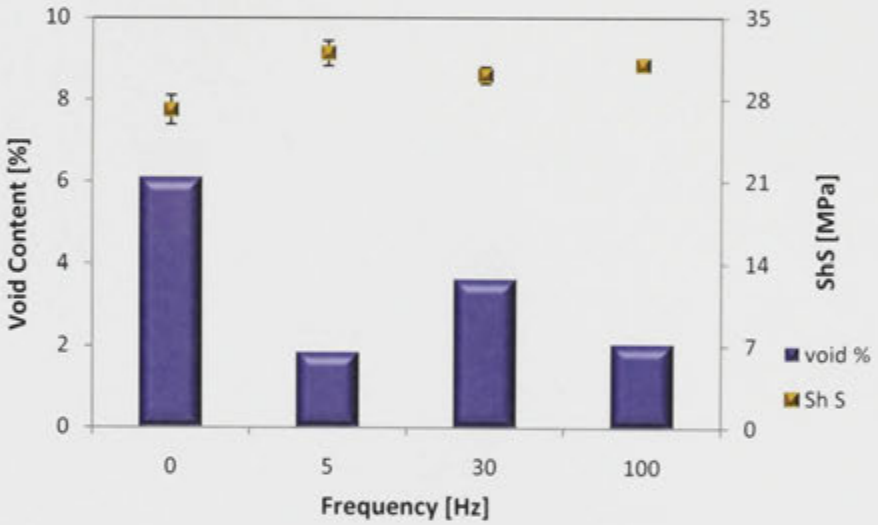

Figure 5.27: Comparison of void content and shear strength of unidirectional samples cut along fibres.

Shear testing of unidirectional glass/epoxy composites cured with 10 min of vibrations was performed on samples cut perpendicular to the direction fibres. Void content was determined. Standard deviation and mean values of four samples are presented in Table 5.21.

Shear strength values (ShS) in Figure 5.28 are lower than in Figure 5.27 (and at a different scale). It can also be noted that 5 Hz and 30 Hz laminates have lower void content (purple bars) and higher shear strength (gold squares) values than 0 Hz.

Table 5.21: Void content and shear strength of unidirectional glass/epoxy laminates cut perpendicular to fibres.

f (Hz)	Void %	StDev	ShS (MPa)	StDev
0	6.102	2.822	2.35	0.550
5	1.853	1.317	4.45	0.256
30	3.642	2.654	4.06	0.161
100	2.049	0.839	3.64	0.117

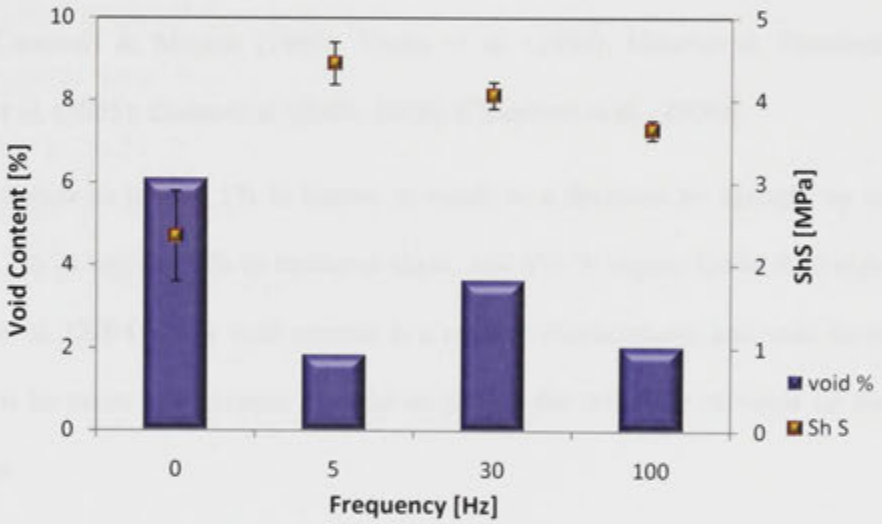

Figure 5.28: Comparison of void content and shear strength of unidirectional samples cut perpendicular to fibres.

Chapter 6 DISCUSSION

The property degradation of composite materials due to voids, inclusions, delamination, fiber-matrix debonding, fiber misalignment and fiber breakage has been well researched as these effects are the classic reasons for composites failure [Hancox (1977), Judd & Wright (1978), Cantwell & Morton (1992), Varna et al. (1995), Mouritz & Thomson (1999), Hamidi et al. (2005), Costa et al. (2005, 2006), Chambers et al. (2006)].

A void content as low as 1% is known to result in a decrease in strength up to 30% in bending, 3% in tension, 9% in torsional shear, and 8% in impact [Judd & Wright (1978), Barraza et al. (2004)]. The void content is a volume characteristic and void locations and sizes must be taken into account in order to predict the influence of voids on mechanical properties.

In this study, the level of void content and its reduction is the main objective. Implementation of mechanical vibration during composite material processing may affect the level of porosity, as indicated in Chapter 3. The effect of vibration will be governed by its parameters, e.g. frequency, amplitude and vibrational energy input.

The term void, bubble and cavity will be treated as the same, to reflect the level of porosity, void content or a type of defects in composite materials. It is defined as a bubble with a diameter from 20 μm to 1 mm.

It is not an imperative to eliminate all the voids from the laminate. It is sufficient to keep the void content below a certain limit; typically, <1% for aerospace structures and around 5% for other applications [Barraza et al. (2004), Liu et al. (2006)]

It is believed that this is the first published study on the effects of vibrations on void content in laminated composites covering systematically a wide range of frequencies, from 0 Hz to 40,000 Hz. Covering such a wide spectrum allows us to observe the variation of void content with frequency of vibrations and in this case to notice a clear minimum occurring between 10 to 30 Hz. Speaking in broad terms, high frequencies (1 kHz to 40 kHz) appear to have minimal effect on void content [Muric-Nesic et al. (2008)]; see Chapter 5, Figures 5.2-5.4.

At first, it may be thought that high frequencies should be more instrumental in dispersion or reduction of bubbles. However, it is the low frequencies that appear to be the most effective. What is also remarkable is that the trend is not monotonic, but has a definite minimum. This has attracted my attention and analysis.

The presence of the minimum, see Figures 5.9 and 5.10, indicates a coupling mechanism between the movement of the fluid with bubbles, and some specific frequency of the system, which can be the gas bubble surrounded by the fluid resin, the laminated sample encased in the vacuum bag, or the whole curing chamber with the curing laminates. The minimum for the glass/vinyl-ester laminates results (Figure 5.10) is less pronounced.

6.1. Internal Structure of Laminates

Three methods for determining internal structure of laminates were used and they all show fibres, resin and defects. Those methods are scanning electron microscopy (SEM), optical microscopy and computed tomography (CT). While SEM and optical microscope images show presence of defects very well, acquired images are 2D and it is not quite certain if the defects are actually bubbles. With CT scan and the possibility of seeing in 3D, the existence of bubbles is confirmed. As CT scan images are slices of samples they show electron density of samples constituents, and that is shown on tomograms in Section 4.4.5. Lack of electrons found in certain areas (black areas) indicates absence of any substance and therefore it can be considered that those defects are voids or bubbles.

Another type of images, obtained with CT, are radiographs, similar to X-ray images. Typical radiographs show fibre tows from different angles as shown in Figure 6.1; note fibre tows in two projections. These images corroborate the above observations, and in addition, provide a macroscopic view of the internal structure.

In the experimental system studied here the laminated composite samples consist of resin and plies of fibres, which present serious obstacles to bubble movement. On a macro scale the reinforcement is often treated as a porous medium and the flow is presumed to follow Darcy's law [Kurematsu & Koishi (1985)]. Analysis of the flow through such a medium indicates that the flow time will be increased by at least an order of magnitude [Song (2006)]. Nevertheless, increasing the size of the bubbles is very effective in removing the bubbles from the composite. Indeed, degassing of resin by the application of vacuum is a standard procedure in industry.

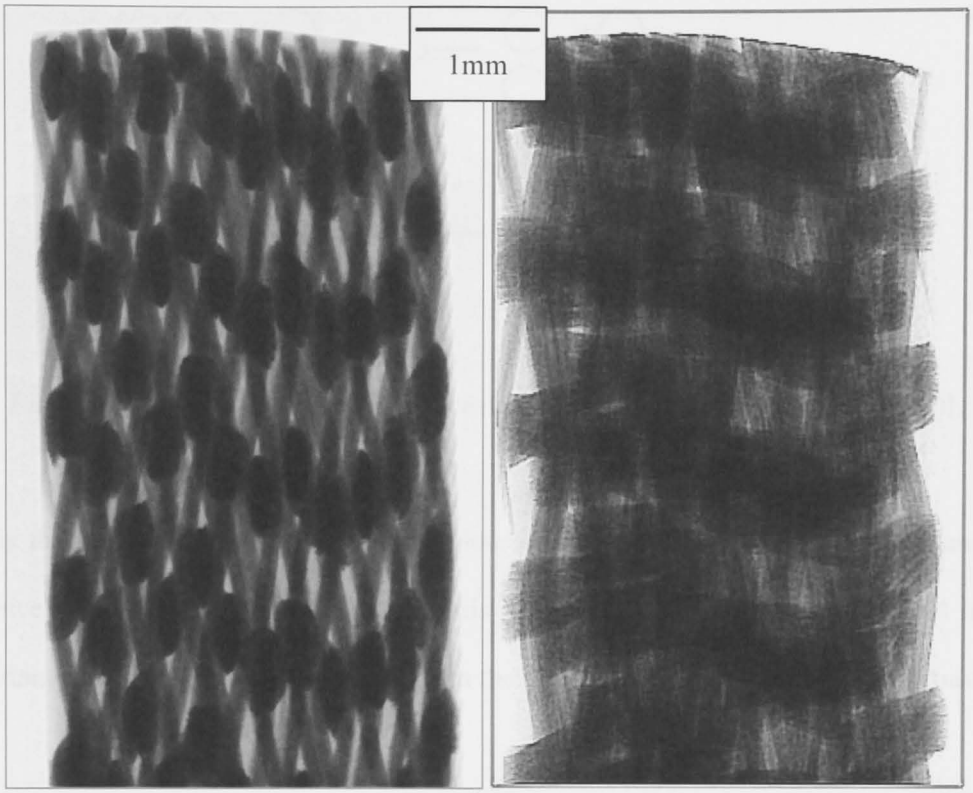

Figure 6.1: Typical radiographs of CT scanned samples.

6.2. Behavior of Bubbles in Laminates

Vibrations and buoyancy push bubbles through fibres (bundles and layers) or/and move them left/right to the edges of the laminate, and bubbles can disintegrate, break up into smaller bubbles, but it will not greatly affect the laminate's structure. Possible mechanism of bubbles movement through fibres as suggested by Kang & Koelling (2004) is depicted in Figure 6.2. It is assumed here that if small bubbles, with diameter less than 10 μm, stay in fibre tows they are not affecting laminate's properties.

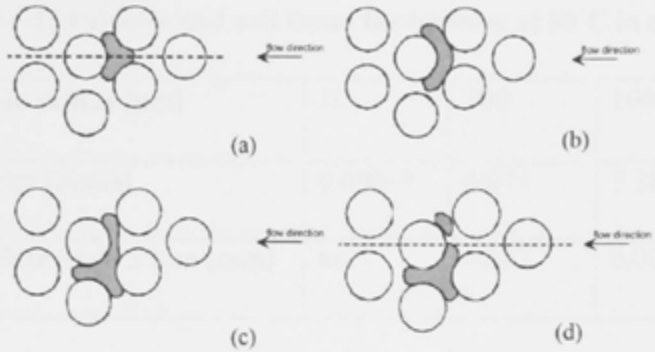

Figure 6.2: Demonstration of the breakup process [Kang&Koelling (2004)].

In this thesis the emphasis is on the behaviour of the bubbles in the liquid resin, and the presence of the fibres has been ignored. This is a simplification of the system, but it was important in allowing progress to be made in the understanding of bubble escape behavior.

A free spherical gas bubble in a viscous liquid will float to the liquid surface due to buoyancy. The velocity for a bubble moving upwards can be calculated as described in Section 3.4.

The results of calculations for the velocity and time to exit from depth of 3 mm (approximate laminate thickness) for different sized bubbles in epoxy/hardener mixture at 50°C, with viscosity of approximately 334 mPa.s, are shown in Table 6.1. Details for vinyl-ester mixture at 25°C, with viscosity of approximately 370 mPa.s, are shown in Table 6.2. The gelation time is approximately 30 minutes which is longer for most bubbles (in 3mm depth) except for the smallest ones.

Table 6.1: Velocity and exit times for bubbles at 50°C in epoxy.

bubble radius [μm]	10	100	1000
velocity [mm/s]	0.00073	0.073	7.28
exit time from 3 mm [min]	68.7	0.687	0.00687

Table 6.2: Velocity and exit times for bubbles at 25°C in vinyl-ester.

bubble radius [μm]	10	100	1000
velocity [mm/s]	0.00062	0.062	6.16
exit time from 3 mm [min]	81.2	0.812	0.00812

The exit times for the 1 mm bubble, shown in Table 1, are unrealistic since Stokes law applies to low Reynolds numbers only (laminar flow). Furthermore, the velocities will be decreased by an order of magnitude in account of the presence of the reinforcing fibres. Nevertheless, the calculations show that increasing bubble size by reducing pressure is an effective way to reduce exit time for the bubbles since the velocity depends on the square of the radius (see equation 3.17).

Numerous papers in published literature show that application of high pressure to composite materials during curing enable manufacturing of almost defect-free laminates [Lundstrom & Gebart (1994), Eom et al. (2001), Barraza et al. (2004), Hamidi et al. (2005), Guo et al. (2006)].

However, low-pressure environment of the ANUQSM was in place in this study. The Quickstep plant operates with pressures of 10-28 kPa (1-4 psi). Consequently, there's no high pressure available to act upon bubbles.

On the other hand, low pressure is the characteristic of vacuum assistance. There is a substantial evidence of vacuum assistance in literature [Ghiorse & Jurta (1991), Lundstrom & Gebart (1994)]. The application of vacuum significantly aids fibre wetting through improved resin flow. Furthermore, the void content is strongly reduced by an applied vacuum and can be almost completely eliminated. The lowering of the void content with vacuum assistance can be interpreted as a result of compression of voids when the vacuum is released and a higher mobility of voids created at a lower pressure.

Decreasing the external pressure from 100 kPa to 10^{-1} kPa (typical vacuum used in experiments here) results in an increase of the bubble's size by a factor of approximately 10 (see section 3.1). Hence, vacuum applied during curing is affecting the bubble size and its escape velocity significantly.

By contrast, increasing temperature from 25°C (298K) to 50°C (323K) would result in an increase of the bubble size by approximately 3%, a small variation that can be neglected in comparison to pressure effect.

According to the Arrhenius equation (3.12), a rise in temperature will also cause a change in viscosity. The viscosity of epoxy resin mixture changes from approximately 540 mPa.s at 25°C, to 334 mPa.s at 50°C. Therefore, increasing the temperature from 25°C during

sample preparation to 50°C while curing, will have some effect on the bubble upward velocity, but significantly less than the application of negative pressure, i.e. vacuum.

Figure 5.9 shows that applying vibrations for 20 minutes does not alter significantly the pattern of void reduction compared to 10 minutes application. It is conjectured that this is due to increasing viscosity of the resin as a result of increasing molecular weight of the copolymer. The curing reaction begins with copolymerization of the two components prior to gelation, and this slows down diffusion and hence bubble reduction and bubble escape.

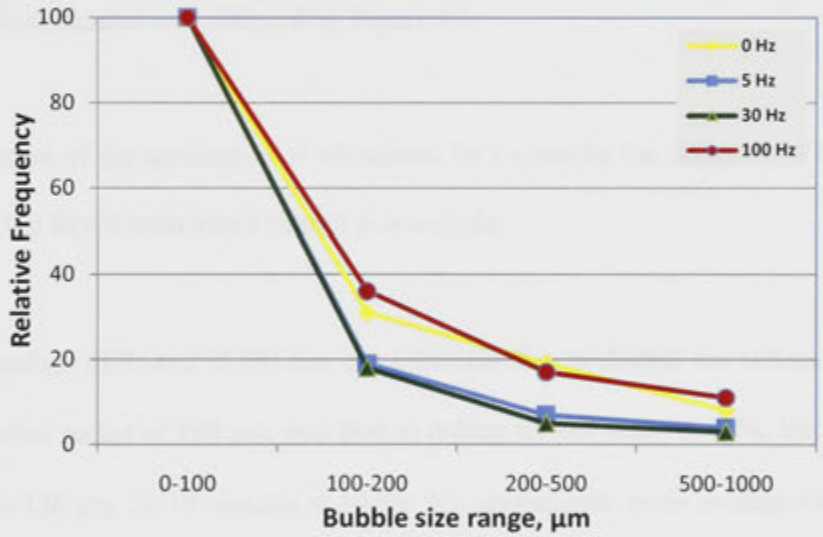

Figure 6.3: Summary statistics of the relative change in void content as a function of size and frequency.

Figure 6.3 shows summary statistics for bubble sizes measured in the cured experimental samples. The distributions are normalized to 100% for each bubble size range, and are presented together for the frequencies from 0 Hz to 100 Hz. The figure shows clearly a significant decrease in the larger size ranges (100-500 µm) relative to the small sized bubbles (20-100 µm). The decrease is most pronounced for 5-50 Hz frequencies,

corroborating the effect shown in Figure 5.9. I shall return later to the effect of frequency and the concept of resonance later in this Chapter.

6.3. Effect of Diffusion

From the Slyozov-Wagner equation (equation (3.11)) one can deduce that (at a constant temperature) the volume of the average bubble will increase in proportion to time. Furthermore, it also implies that the larger bubbles will grow faster than the smaller bubbles [Yin et al. (1996)]. At the same time, the larger sized bubbles will escape, thus reducing their number as evidenced by Figure 6.3.

In anticipation of the application of vibrations, let's consider the diffusion of dissolved gas (air) from the liquid resin into a bubble in one cycle.

Using equations (3.7) and (3.18) one can calculate that, to double the volume of a bubble with an initial radius of 100 μm, and thus to reduce its exit time by 60%, the radius has to increase to 126 μm. In 10 minutes at 10 Hz this corresponds to an average radius increase of approximately 0.005 μm (5 nm) per cycle. The growth of the bubble radius by 5 nm requires a transfer per cycle of approximately 698 μm^3 of air (dissolved in the resin) into the bubble. This volume of air weighs 449 x 10^{-15} g. When dissolved in the resin to the unenhanced level of solubility (i.e. 0.1 g/kg of resin), it will reside in a volume of approximately 18.6 x 10^3 μm^3 (assuming resin density of 1.2 x 10^3 kg/m^3). Alternatively, this can be expressed as concentration equal to 0.12 x 10^{-15} g air in 1 μm^3 of resin. The volume of resin containing 449 x 10^{-15} g of dissolved air, when spread over the surface of a

bubble of 100 μm radius, will extend to a depth of approximately 0.03 μm from the bubble/resin interface.

Let's now calculate the diffusion rate required to sustain the growth. In order for this volume of air to be transferred into the bubble, the flux, J, must be:

$$J = 449 \times 10^{-15} \text{ g} / 125.6 \times 10^{3} \text{ μm}^2 \, 0.1 \text{ s} = 35.7 \times 10^{-18} \text{ g/μm}^2\text{.s} \quad (6.1)$$

The diffusion coefficient for oxygen in liquid epoxy resin is taken as, $D = 2 \times 10^{-10}$ m^2/s [Chowdhury et al. (2007)]. Assuming that the diffusion coefficient for air is the same, then the concentration gradient required to drive this amount of diffusion can be calculated:

$$dc/dx = J/D = 0.178 \text{ (g/μm}^3\text{)(1/μm)} \quad (6.2)$$

A diagram depicting the bubble/resin interface with concentration gradient is shown in Figure 6.4.

The concentration gradient is expected to arise as a result of the Thomson-Freundlich effect described in Chapter 3 (see equation (3.10)).

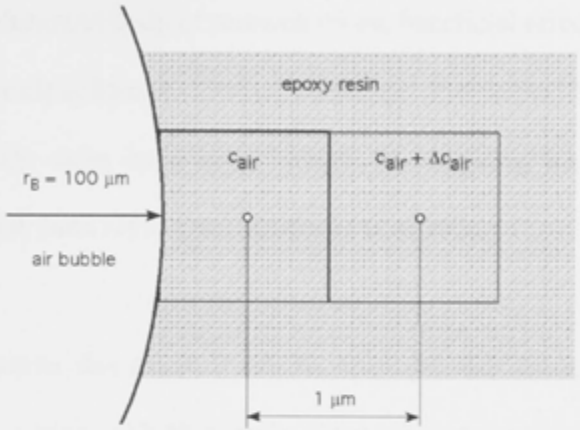

Figure 6.4: A schematic drawing of the bubble/resin interface, with concentration gradient between adjacent elemental volumes of resin.

The cube (square) of resin adjacent to the interface contains 0.12 x 10^{-15} g of dissolved air. The next cube adjacent to it will contain more dissolved air, thus providing the driving force for diffusion. This is based on calculations, where substitution of values mentioned in section 3.2 into equation (3.10) leads to a value of 0.75 µm for the term in the round brackets. Therefore, for a bubble of 10 µm radius, C_{rB}/C_e = 1.075, a small change, whereas for a bubble of 1 µm radius his ratio increases to 1.75, already a significant enhancement of solubility of 75%.

Therefore, one can expect that this process will contribute to the growth of the larger than average bubbles, thus reducing their exit time.

6.4. Effect of Vibrations

It is well documented that applying mechanical vibration to the mold during solidification of metallic melts has a profound effect on the microstructure and mechanical properties of castings [Pillai (1972), Shukla et al. (1980), Campbell (1981), Kocatepe (2007), Xu et al.

(2008)]. There is a substantial body of research on the beneficial effect of vibrations in gas–solids fluidization [Grinis & Monin (1999), Ellenberger & Krishna (2003)]. When it comes to composite materials there have been studies investigating the effect of vibrations published by Ghiorse & Jurta (1991) and Stabler et al. (1992).

From results presented in this thesis it can be observed that laminates cured with low-frequency vibration assistance (2-50 Hz) have lower void content when compared with high-frequency (100-8,000 Hz) or no frequency (0 Hz) vibration-assisted laminates (Figures 5.9 and 5.10). This is found for both time-intervals (10 and 20 min) and for both types of resin (epoxy and vinyl-ester), with little deviation for 30 Hz samples at 20 min. Furthermore, when laminates cured with low-frequency vibrations were subjected to flexural (Figures 5.11 – 5.16), tensile (Figures 5.17 – 5.20) and shear (Figures 5.27 and 5.28) testing they also exhibited better properties than high-frequency or no-frequency laminates. This is explained in more details in section 6.4.3.

Experiments with water absorption show less property-degradation, flexural (Figures 5.23 and 5.24) and tensile (Figures 5.25 and 5.26) for laminates cured with low-frequency vibrations. This is further explained in section 6.6.

Low frequency vibrations have longer period of time and bubbles have enough time to reach certain size (threshold) during pulsation that will enable them to:

a. leave the system faster (buoyancy) due to their big size;
b. diminish (collapse below 10 μm radius) due to their small size.

High frequency vibrations have very short period for bubble pulsation; they keep pulsating with majority of bubbles not leaving the system. Static laminates (cured with no vibrations,

frequency of 0Hz) have no pressure fluctuations, nor bubble pulsation, and the number and sizes of bubbles stay the same. Further explanations follow in section 6.4.2.

For a laminate made of 50% resin (density of 1150 kg/m^3, bulk modulus K=2.5 GPa) and 50% fibres (density of 2200 kg/m^3, elasticity modulus E=80 GPa) by weight, different observations can be made.

The speed of sound in the resin is calculated to be 2100 m/s, and 6000 m/s for glass fibres. Therefore, for a composite laminate the speed of sound (v) is assumed to be around 4000 m/s. Having in mind the laminate's thickness of 3 mm and taking it as the wavelength (λ) in following relationship:

$$\lambda = vT = \frac{v}{f} \tag{6.3}$$

one can find the frequency (f) to be 1.3 MHz.

When the size of a bubble is taken as the wavelength, determining the frequency is as following:

a. for a bubble of 50 μm radius the frequency is 80 MHz;
b. and for 500 μm radius the frequency is 8 MHz.

The highest frequency used in this study was 40 kHz (with piezoelectric crystal) and that experiment did not produce good results, suggesting that high-frequency vibrations are not the path to reducing void content.

In addition, current technology has not yielded vibration sources in adequate MHz ranges.

The measurement of the amplitude, p_A, of the pressure wave (equation (3.20)) was found to be unachievable. However, one can observe that at a constant input power (see Chapter 4) it

can be said that the amplitude will decrease with increasing frequency. This, in itself, means that the effectiveness of vibrations should decrease with increasing frequency. But the greatest effect will be when the frequency of vibrations approaches the resonance frequency of the system. As a result, the amplitude of the pressure wave, p_A, will be increased significantly, thus contributing to the pressure variation in the fluid and in the bubbles. This will magnify the bubble surface variation between expansion and contraction as predicted by equation (3.22). Further discussion is presented in the next section.

In the system studied here the wavelength of the pressure oscillations, even at the highest frequency, was always at least an order of magnitude longer than the thickness dimension of the curing chamber, therefore, the pressure at any instant of time can be considered as constant throughout the curing chamber. The vibrations were applied at a constant power, therefore the amplitude of the pressure oscillations depended inversely on frequency. In view of this relationship, the result of oscillating pressure should be most effective at low frequency, and decreasing with increasing frequency. This is not entirely the observed pattern as seen in 5.9 where a clear minimum is seen around 5-50 Hz.

6.4.1. Resonance Frequency Analysis

Resonance frequency analysis of simply supported plate and bubbles is described in section 3.5. Some components of ANUQSM are presented in Figure 6.5 (please note that it is shown not to scale).

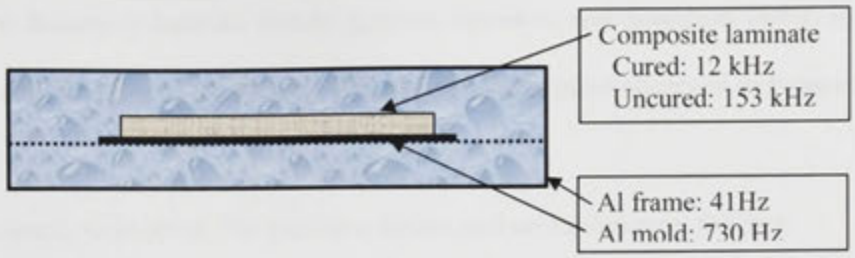

Figure 6.5: Scheme of ANUQSM components and their resonance frequencies.

Let's consider the resonance frequencies of every component involved in the curing process with widely ranging rigidity and masses, as shown in Table 6.3. Calculation is based on equations 3.24 and 3.25.

Table 6.3: Resonance frequencies, f_{11}, of ANUQSM components.

System	f_{11} [Hz]	size [mm]
Bubbles	2k - 100k	0.5-0.01
Resins	2,700	100x100x3
Glass fibres	10,640	100x100x3
Uncured laminate	153	100x100x3
Cured laminate	12,300	100x100x3
Al mold	730	300x300x2
Al frame	41	1200x1000x1.5
Curing chamber	8	1200x1000x40

The natural, resonance frequency of the whole curing chamber corresponds closely to the minimum in void content observed in Figure 5.9. As the applied frequency becomes close to the resonance frequency, the amplitude of oscillations increases, but the presence of fluid in the system causes dissipation and dictates a broad resonance peak. At and near the

resonance frequency bubbles should grow or dissolve, and disappear faster. It is proposed that this effect results in the broad minimum in void content observed in Figure 5.9.

When it comes to bubbles, the situation differs and an explanation follows.

Table 6.4 shows the resonance frequencies (in kHz) of bubbles of various radii. Since pressure during curing was not monitored, calculation is based on QS method parameters (10-28 kPa), atmospheric (101 kPa) and autoclave (600 kPa) pressures.

Table 6.4: Resonance frequency, f_{11} (kHz), of bubbles of various sizes at different pressure.

P (kPa)	500μm	100μm	50μm	25μm
10	1.64	8.36	17.22	36.23
28	2.73	13.70	27.80	56.73
101	5.17	25.88	52.06	104.62
600	12.60	62.94	123.13	252.52

Obviously, resonance frequencies of bubbles range from a few kHz to hundreds of kHz, and the higher the pressure the higher is the resonance frequency. Large bubbles (500 μm radii) with lower f_{11} were not present in laminates of this study in any significant number. Bubbles of 25-100 μm radii were mainly scattered in the studied laminates, and their resonance frequency is of tens of kHz.

If the composite plates of different sizes were made then uncured laminates would have following resonance frequencies (with negligible differences regarding type of the resin, and assuming squared plates):

Table 6.5: Resonance frequency of uncured laminates of different sizes.

size [mm]	f_{11} [Hz]
100x100x3	153
200x200x3	39
300x300x3	17
500x500x3	6

As a result, larger laminates have lower resonance frequencies.

Therefore, laminates cured in ANUQSM of 200 mm x 200 mm dimensions have resonance frequencies of around 40 Hz. That corroborates with results of having best void content and mechanical properties for laminates cured with vibrations assistance, especially with low frequencies of 2-50 Hz. Other factors are affecting certainly, not only what has just been described.

6.4.2. Effect of Time-durations

One of very important questions in composite production is how long the curing cycle should be. Quickstep with its shorter-than-autoclave cycles is more economically viable, and keeping it that way is desirable. I have tried to determine for how long do vibrations need to be implemented to ANUQSM curing system, in order to have a positive effect on the void content reduction. Besides, once gelation starts vibrations are no longer effective to the void content.

Based on experiments with EM shaker at room temperature it was found that 30 min of vibrations produced better results than 10 min, in terms of having lower void content (Figure 5.5). That is because no gelation occurred during that time.

Later with ANUQSM experiments, when higher temperatures were in use (like 50°C) the curing was faster, the gelation occurred earlier, and then shorter period, i.e. 10 min, was more effective than 20 min (Figures 5.9 and 5.10).

Therefore, 10 min of vibrations was established as a constant parameter, and it was considered as period long enough for void content reduction, yet short for industrial standard.

One of possible explanations is that when bubbles are exposed to low frequencies (<50 Hz) they have longer period of time to change their volume than when exposed to higher frequencies (>100 Hz).

a. for the frequency of 10 Hz the period T is 0.1 s,
b. for the frequency of 1 kHz the period T is 0.001 s,
c. while for MHz ranges the period is in μs and less.

When low frequency (<50 Hz) is employed a bubble has enough time to reach certain threshold during vibration cycle, i.e. to grow to certain size, after which it is not going to be greatly affected by high pressure region and will not contract to initial size because of diffusion. Repeating cycles enforce the bubble to constantly grow and leave the system by escape to the surface. Or bubble can become trapped inside fiber tows, not affecting laminates properties due to its tiny size.

6.4.3. Mechanical Properties

To understand and explain the size of the bubble influencing the mechanical properties of composite materials critical crack size in laminate structures needs to be addressed. Combining fracture mechanics with micro-mechanics level, one can express the critical crack size a_c as:

$$a_c = \frac{K_{Ic}^2}{\sigma_c^2 \pi} \tag{6.4}$$

From this equation the critical crack size, with values of 10 MPa $m^{1/2}$ for fracture toughness, K_{Ic}, [Zulkifli et al. (2009)] and 100 MPa for applied stress, σ_c, is 0.014 m; that is 14 mm. It is well beyond the bubble size analyzed in this study (up to 1 mm), and above radius of break-up bubbles (10 μm) that can be found in fibre tows.

Ten-micrometer radius is chosen as the limit because of the constraints of optical microscope with camera; it was not possible to determine bubbles with diameters less than 20 μm.

Three groups of composite laminates were identified when comparing their mechanical properties: no-frequency or static laminates (0 Hz), low-frequency laminates (2-50 Hz) and high-frequency vibrations laminates (100-8,000 Hz). As described earlier, lower void content should be reflected in higher values of mechanical properties.

Tensile properties of glass/vinyl-ester laminates cured with low-frequency vibrations are generally of higher values (up to 20 %) than static cured laminate (0 Hz) as shown in Table 5.13 and Figures 5.19 ad 5.20. Results are not showing consistent trend of higher property values, but are giving indication of 20 min low-frequency cured laminates as of improved

laminates. That can be observed for 5 Hz, 30 Hz and 50 Hz 20 min laminates in Figure 5.19, and for all low-frequency (2-50 Hz) 20 min laminates in Figure 5.20.

Glass/epoxy laminates cured with low-frequency vibrations exhibit enhanced tensile properties over static (0 Hz) and high-frequency laminates, but there is no clear indication if 10 min or 20 min curing is more suitable for producing better quality laminates; see Figures 5.17 and 5.18.

Flexural properties of low-frequency glass/vinyl-ester composite laminates are superior to static and high-frequency laminates, up to 15 %, for both flexural strength and modulus as shown in Figures 5.15 and 5.16.

Flexural strength values of glass/epoxy laminates are scattered but laminates cured with low-frequency (5-50 Hz) have higher values than static and high-frequency vibration laminates (up to 10%); see Figures 5.11 and 5.12. It can be noted that 10 min laminates are not consistently better than 20min, while looking at flexural modulus it is clear that 10 min samples are showing higher values than 20 min laminates, with exception for 2 Hz laminate (see Figures 5.13 and 5.14).

Unidirectional glass/vinyl-ester laminates experimental results are illustrated in Figures 5.27 and 5.28. The interlaminar shear strength is approximately 25% higher for the laminates cured with vibrations, particularly for 5 Hz and 30 Hz.

Results of mechanical properties of laminates exposed to water absorption indicate low-frequency vibration-assisted laminates (5 Hz and 30 Hz) as superior to static laminates for both conditions, dry and wet. Figures 5.23 and 5.24 depicts improved flexural properties of

up to 25%, while Figures 5.25 and 5.26 show higher values of tensile properties (up to 20%) for 30 Hz laminates, when compared with static laminates.

Mechanical properties trend inversely follows the trend in void content, with many exceptions noted; some within experimental error, and for some no explanation can be offered at this stage.

Results presented in Chapter 5 demonstrate low-frequency vibration-assisted laminates as improved when compared to static laminates, but there is no significant difference between the results for these laminates. Slight variations of properties are not highly significant.

6.4.4. Wrapping up on Vibrational Effect

In summary, the effect of the vibrations can be depicted schematically as shown in Figure 6.6. It shows the observed variation of void content as a function of frequency of the applied vibrations. With no vibrations (0 Hz) the initial 10% void content, resulting from hand lay-up, is reduced to approximately 5% by the application of vacuum. Further reduction in void content is realised with the application of vibrations. The effectiveness of this reduction is aided by the resonance of the curing system which increases the amplitude of vibrations that help the growth of bubbles by diffusion.

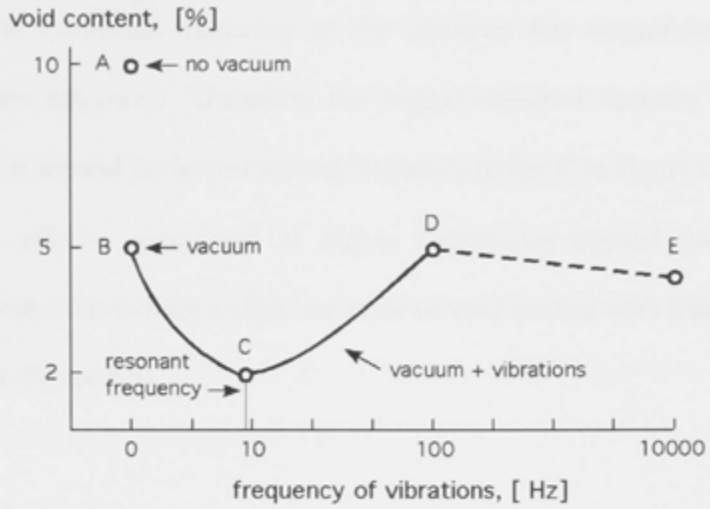

Figure 6.6: A schematic diagram of the relationship between void content, vacuum and applied frequency of vibrations for the studied system.

It appears that the void reduction mechanisms operating in the system are as follows:

1. After sample preparation, the laminate is likely to have approximately 10% voids (point A in Figure 6.6). Application of vacuum (a usual practice) reduces the void content to approximately a half of that (5%) (point B in Figure 6.6).
2. A further reduction of void content is achieved by application of vibrations to the system prior to resin viscosity increase and gelation. The observed relationship between frequency and void content involves:
    - Bubble dissolution, growth and escape by vibration assisted diffusion between points B through D.
    - The vibrations applied at constant power give amplitude varying with frequency as $1/\omega^2$. Consequently, the greatest effect should be observed at the lowest frequency used.

- Natural resonance frequency of the chamber has magnifying effect on the pressure amplitude. Therefore, the largest observed decrease in void content happens around the lowest natural frequency (point C in Figure 6.6).
- Other effects, operational at higher frequencies beyond point D, may be involved, contributing a slight decrease of void content with frequency (points D to E in Figure 6.6).

6.5. Effect of Temperature

Previous research showed that higher temperature brings lowering in viscosity and that helps flow of resin and better fibre wetting, leaving no dry spots or voids [Lundstrom & Gebart (1994), Olivier et al. (1995), Guo et al. (2006), Costa et al. (2006), Liu et al.(2006), Davies et al. (2007)]. Viscosity decreases with the increase of the temperature up until the gelation point is reached and the cure process begins. Even in the best case scenario (lowest viscosity possible) there is still certain probability of not having complete wet-out, due to other reasons (interface, fibre misalignment, inclusions, resin vapors etc).

The Quickstep plant achieves temperatures of up to 200°C. In this study the temperature of 50°C was not enough to lower the viscosity significantly.

Viscosity relationship at different temperatures (equation 3.13) shows that viscosity can be halved if resin is heated from 20°C to 50°C.

On the other hand higher temperatures brings bubble expansion, and it is not certain if bubble size is large enough for it to leave the system by buoyancy, or the bubble just expands and stays in the system, due to the constraints of fibres.

The distortion of fibers can occurs due to the shrinkage of the matrix material during the curing of the composite. In the curing process the fibers are subjected to thermal strains caused by the heating and cooling of the part.

6.6. Effect of Water Absorption

Higher fiber volume content results in higher flexural and tensile strength and modulus of GFRP composite. Higher void content resulted in higher weight gain and higher water saturated level, and therefore water absorption decreased the flexural and tensile strength and modulus of composite laminates.

As expected, the flexural and tensile strength and modulus decreased with moisture absorption. Tensile strength declined less than flexural for both resins, as is presented in Table 6.6.

The flexural strength of all samples decreases by ≈ 7–28%, and tensile strength by ≈ 6–13%. It is to be noted that some samples have negative decrease, which means that they have higher values of tensile strength after water absorption. That can be explained by different samples tested from the same laminate, therefore different void content in those samples. The flexural modulus of all samples decreases by ≈ 0.7–9% after the exposure,

and tensile modulus by ≈ 3–13%. Flexural modulus is a fiber-dominated property. Unlike the flexural strengths, the flexural modulus is strongly dominated by the fibre fraction of the sample.

Tensile strength of all glass/epoxy samples decreased by ≈ 8%, except 5 Hz laminate that has negative decrease, and modulus by ≈ 6-7%, after water exposure. The same trend goes for glass/vinyl-ester samples where tensile strength decreased more, by ≈ 6-13%, except 30 Hz that has negative decrease, and modulus by ≈ 3-14%, after water exposure.

Table 6.6: Mechanical properties degradation (%) with water absorption.

FLEXURAL					
Epoxy			**Vinyl-ester**		
Hz	**FS%**	**FE%**	**Hz**	**FS%**	**FE%**
0	14.3	8.4	**0**	17.9	0.8
5	9.5	5.2	**5**	27.7	3.8
30	9.6	0.7	**30**	9.9	0.7
100	10.7	8.4	**100**	6.9	2.3
TENSILE					
Epoxy			**Vinyl-ester**		
Hz	**TS%**	**TE%**	**Hz**	**TS%**	**TE%**
0	7.9	6.6	**0**	11.0	2.9
5	-2.6	7.4	**5**	12.9	13.4
30	8.2	7.2	**30**	-0.4	8.1
100	8.7	5.8	**100**	5.7	5.5

Results are not consistent and there is no unique frequency showing the best possible results for both strength and modulus, but overall trend indicates 30 Hz as the best. Tensile strength is more sensitive than the modulus in most experiments, but there is a considerable scatter in the results.

As expected, the performance values decrease with the porosity of laminates and/or with the absorption of water in this case.

6.7. Effect of Materials and Manufacturing

Two types of matrices (vinyl-ester and epoxy resin) and one type of reinforcement (glass fibres) were used in this study.

While pure epoxy resin has viscosity of 800 mPa s, when mixed with hardener at room temperature (25°C) the mixture's viscosity is 540 mPa s. Based on equation 3.13, the viscosity of the mixture at 50°C is 334 mPa s.

Vinyl-ester resin has lower viscosity than epoxy and flows easier. Pure vinyl-ester resin has viscosity of 370 mPa s, and remains much the same when mixed with photoinitiator Irgacure.

A high-viscosity resin will not properly penetrate the fibre and wet-out the fibres.

From the experiments with pure resin Lundstrom (1996) has found that air dissolves much faster in the vinyl-ester resin tested than in the epoxy at the evaluated conditions.

Results of this study corroborate their findings and reveal that laminates cured with epoxy resin have higher void content than those with vinyl-ester (Figures 5.9 and 5.10).

Nonetheless, if there are cracks in the matrix, the laminate can still sustain loads. Fibres are the main load-bearing component, but break mostly in the final stage. There is a possibility when shaking the laminate the bubbles will come off of the fibres that are the main carrier of the load. And yet, when there are bubbles in the resin, the structure can still sustain the load. The voids will move with the resin if they are not hindered by the reinforcement.

It can be concluded that, on micro-level, vibrations successfully remove bubbles from matrix (liquid resin), but not from reinforcement (solid fabrics of fibres). Remaining of the bubbles in the laminate is due to the fabric architecture (inside tows).

Equipment used in this study had certain imperfections that limited the possibility of fully investigating all project aims.

The most important was the air inside the ANUQSM chambers. It was not possible to eliminate the air completely, especially in the lower chamber. That is why experiments with the speaker attached to the lower chamber from below did not produce good results. And project's aim of investigating the most appropriate position of applying vibrations to the system has not been completely investigated. Albeit previous Quickstep research indicates applying vibrations from the top as the best method.

I was also not able to measure or regulate amplitude and pressure, and their changes, during curing process.

One of the constraints of equipment was no higher than 55ºC temperature curing. As mentioned earlier QS plant operates at temperatures up to 200ºC that enables low viscosity and other parameters' changes.

Limited by the time allocated for this study I was not able to explore and test other vibration sources that could have probably created many other possibilities in handling vibration-assisted curing.

And lastly reproducibility of samples was affected by human error i.e. myself.

6.8. Statistical Significance of the Findings

It may be noted that the variation of void content with frequency of vibrations follows a clear trend as summarised in Figure 6.6. This trend is well above any uncertainties due to experimental errors and other influences. It does not depend on any nuances of interpretation or unique behaviour. This trend is well reflected and corroborated in the variation of mechanical properties measured in the short beam shear experiments and the results from water soaked samples. One can accept this correlation as reasonable because these material properties measured in these mechanical tests are directly sensitive to the void content.

One can also notice that the mechanical test results for the tensile and flexural measurements show only a slight correlation with the general void content trend. In fact, the variations are almost within the range of experimental and other errors, and cannot be used alone as an argument supporting the main observation with regard to the void content.

The general trend of void content with frequency of vibrations is corroborated by independent results (for example, Quickstep). The novel hypothesis presented in this thesis is that the observed minimum is related to a resonant frequency of the vibrating system, and the proposed mechanism of void reduction through the diffusion assisted growth and eventual escape of bubbles.

Chapter 7 CONCLUSIONS

7.1. Thesis Conclusions

Composite materials have complex and variable geometrical and component-material morphology and it can be concluded that exact analyses are virtually impossible to obtain. As an alternative, approximate solutions are often sought in order to model and capture the most important features of the system.

The numerous combinations of parameters are complicated making it impossible to include all relevant factors in one discussion. Nevertheless, with parameters involved in this study it can be concluded that:

- Elevated temperature processing, accompanied by vacuum aid, is beneficial for improving composite laminates' quality,
- Vibration-assisted vacuum curing process produces composite laminates with void content lower than static vacuum curing,
- Low-frequency vibration-assisted vacuum curing generates composite laminates with mechanical properties superior to static and high-frequency vibration-assisted curing,

- Mechanical properties deteriorate when exposed to water, with low-frequency vibration-assisted cured composite laminates deteriorating less than static cured composite laminates.
- Suitably designed and tuned vibration system appears to be effective in reducing void content in such a short cycle curing method as described here.

Curing cycle of the vibration-assisted vacuum curing depends on the system components, materials to be processed, and they determine the optimum processing temperature as well as the time-duration of vibrations utilised.

Failure mechanisms of composite laminates and environmental condition experiments used to describe vibration and vacuum assisted curing, are in the agreement with outcome of known manufacturing systems. Quality of the composite laminates decline to less extent

7.2. Future Work

Further experiments and analyses are required to understand and resolve the vibration-assisted curing process completely.

This work may provide guidelines to suitable frequency range and position of vibrations sources. The actual vibration source still needs to be investigated for the optimum performance sought. Another aspect worth of trying would be a combination of different frequencies during vibration-assisted curing and establishing time-periods for each of the segments.

APPENDIX A

Publications

The conference papers listed below have been presented during the course of the work described in this thesis. Additional journal papers have been published and submitted for publishing.

Papers

- Muric-Nesic J, Stachurski Z, Compston P, Noble N, *Effect of vibrations on void content in composites*, Advanced Materials Research Vol. 32, 2008.
- Muric-Nesic J, Compston P, Noble N, Stachurski Z.H, *Effect of low frequency vibrations on void content in composite materials*, Composites: Part A 40 (4), 2009.
- Muric-Nesic J, Compston P, Stachurski Z.H, *Effect of vibration-assisted consolidation on void content and shear properties of a glass-fiber composite*, submitted to Journal of Materials Science Letters.
- Muric-Nesic J, Stachurski Z.H, Compston P, *On the void reduction mechanisms in vibration assisted consolidation of fibre reinforced polymer composites*, submitted to Composites Part A: Applied Science and Manufacturing.

Conferences

- Muric-Nesic J, Compston P, Noble N, Stachurski Z.H, *Composite materials-how to improve mechanical properties*, ARNAM Workshop, Brisbane, Australia, 2007.
- Muric-Nesic J, Compston P, Noble N, Stachurski Z.H, *ANU-QS project*, Quickstep Global Technology Exchange, Perth, Australia, 2007.

- Muric-Nesic J, Compston P, Noble N, Stachurski Z.H, *Minimizing void content in composites*, Materiais 2007, Porto, Portugal, 2007.
- Muric-Nesic J, Compston P, Noble N, Stachurski Z.H, *Minimizing void content in composites*, Deformation and Fracture of Composites 9, Sheffield, UK, 2007.
- Muric-Nesic J, Compston P, Noble N, Stachurski Z.H, *Vibration project*, Quickstep Global Technology Exchange, Perth, Australia, 2008.
- Muric-Nesic J, Stachurski Z.H, *Effect of vibrations on void content in composite materials,* Polymer Processing Society 24, Salerno, Italy, 2008.
- Muric-Nesic J, Compston P, Noble N, Stachurski Z.H, *Effect of vibrations on void content in composite materials*, ARNAM Workshop, Geelong, Australia, 2008.
- Muric-Nesic J, Compston P, Noble N, Stachurski Z.H, *Vibrations in composite materials production*, Research Fest, ANU, Canberra, Australia, 2009.
- Muric-Nesic J, Stachurski Z.H, Compston P, *Quality improvement by vibrations in composite materials production*, CECS Poster Day, ANU, Canberra, Australia, 2009.

APPENDIX B

ANU-QS MACHINE Instructions

ANUQSM experiments have to be performed with safety on mind, and specific steps involved while operating are presented here.

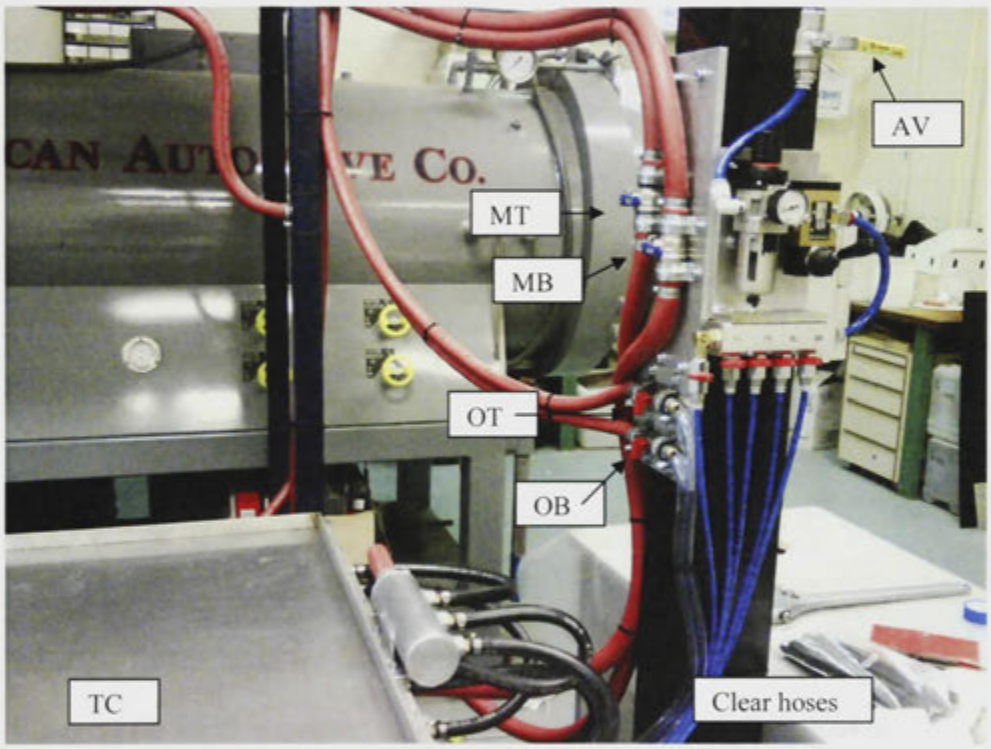

Fig A: Water- and air-flow control valves of ANUQSM.

Some of the following abbreviations are shown in the Figure A.

TC- Top Chamber

BC- Bottom Chamber

LT- Lower water Tank (heater) connected with TC

HT- Higher water Tank (heater) connected with BC

MT- Main valve for Top chamber

MB- Main valve for Bottom chamber

OT- Overflow valve for Top chamber

OB- Overflow valve for Bottom chamber

EB- Exit valve for Bottom chamber

PV- Pressure Valve for the pump

DV- Drain Valve for top chamber (on MT hose)

AV- Air Valve

ST- Storage Tank (reservoir)

ES- Electric Switches on the heaters

PS- Pump Switch

Instructions:

1. Check if all valves are closed.
2. Check if water tanks are full by opening OT and OB.
    a) the water is running through clear hoses –tanks are full, go to 6;
    b) the water is not running, go to 4.;
    c) if the water runs through one of the hoses and not the other one go to 3.
3. Close the valve where water is running, wait for water to appear in the second hose.
4. Check the water level in the storage tank:
    a) there is no water, go to 14;
    b) there is water more than 1/3, go to 5.

5. Open PV, start the pump.

6. When water starts running through clear hoses tanks are full:

    a) to stop the machine go to 13;

    b) to continue the process go to 7.

7. To fill BC (always fill Bottom Chamber first!): while OT and OB are open, open EB, open MB, open PV, start the pump.

8. Make sure BC is not overfilled, that is it is not ballooning.

9. When BC is filled enough, lift TC and insert mold with a laminate, vacuum etc.

10. Close chambers, open MT to fill TC.

11. When chambers are full, and hot water is running start vibrations.

12. To stop all: stop the pump, close PV, MT, MB, OT, OB, EV.

13. To drain chambers:

    a) first drain TC by keeping EV closed and opening DV, go to 15;

    b) to drain BC open EV.

14. Be sure not to overflow ST.

15. When TC is drained, lift it up and take the laminate out.

16. Close all valves.

Warnings:

1. Do not run the pump if OB and OT are not opened!
2. Do not open DV while the machine is running. ONLY when TC is to be drained.
3. The gap between TC and BC should be around 2cm, when filled.
4. Find suitable positions for MT and MB, or EV for good pace flow.

APPENDIX C

Examples of laminates' manufacturing and mechanical testing.

1. Laminates manufacturing details of stage 4 with ANUQSM, where m_f is the weight of the fibres, m_m is the weight of the matrix, and V_f is the fibre fraction by weight.

Table C1: Details of laminates manufacturing.

Epoxy @20min					Epoxy @10min			
f, Hz	m_f (g)	m_m (g)	Vf (%)		f, Hz	m_f (g)	m_m (g)	Vf (%)
0	88.0	96.4	47.7		0	82.0	95.4	46.2
2	83.5	87.3	48.9		2	92.4	106.0	46.6
5	88.0	98.0	47.3		5	87.0	89.3	49.3
10	89.6	99.3	47.4		10	88.9	91.7	49.5
30	87.3	90.4	50.3		30	90.9	100.0	47.6
50	86.1	94.0	47.8		50	85.8	93.5	47.8
100	81.0	79.4	50.5		100	87.0	100.0	46.5
1000	87.6	100.3	46.6		1000	91.0	98.0	48.2
8000	84.1	94.0	47.2		8000	87.2	102.0	46.1
Vinyl @20min					Vinyl @10min			
f, Hz	m_f (g)	m_m (g)	Vf (%)		f, Hz	m_f (g)	m_m (g)	Vf (%)
0	87.2	87.0	50.1		0	83.9	88.2	48.8
2	83.4	95.0	46.8		2	79.7	84.0	48.7
5	81.2	85.0	48.9		5	86.5	93.5	48.1
10	84.4	90.0	48.4		10	85.0	93.0	47.8
30	83.0	89.5	48.2		30	91.4	101.0	47.5
50	87.2	87.0	50.1		50	87.5	95.3	47.9
100	86.4	90.0	49.0		100	82.8	90.0	47.9
1000	86.4	91.0	48.7		1000	85.8	84.5	50.5
8000	81.7	85.6	48.8		8000	81.6	88.0	48.1

Table C2: Details of laminates manufacturing.

Epoxy			
f, Hz	**m_f (g)**	**m_m (g)**	**Vf (%)**
0	101.5	107.5	48.6
5	101.5	111.0	47.8
30	103.5	114.0	47.6
100	104.2	106.4	49.5
Vinylester			
0	99.2	107.2	48.1
5	98.8	106.0	48.2
30	102.0	110.6	48.0
100	98.4	105.0	48.4

2. Example of void content calculation for vinyl-ester laminates cured with 10min of vibrations, with 4 samples per laminate. Presented below are void areas and percentage within the sample. M% is the mean value of all four.

Table C3: Void content calculation of 4 samples per laminate.

Hz	**μm^2**	**μm^2**	**μm^2**	**μm^2**	**%**	**%**	**%**	**%**	**M%**
0	461100	108100	19100	129800	0.070	0.474	1.683	0.395	0.707
2	9400	54300	18600	16700	0.068	0.061	0.034	0.198	0.073
5	13300	39300	4600	16600	0.016	0.061	0.048	0.143	0.054
10	100500	19800	26500	23200	0.097	0.085	0.367	0.072	0.141
30	6700	11000	11800	10500	0.043	0.038	0.024	0.040	0.008
50	145200	86100	17000	7700	0.062	0.028	0.523	0.314	0.232
100	117400	160300	360800	44600	1.317	0.163	0.428	0.585	0.494
1000	236700	592000	89900	279000	0.328	1.018	0.864	2.161	0.771
8000	78900	180700	118800	278400	0.434	1.014	0.288	0.660	0.317

3. Example of flexural testing, that is modulus, FE, for vinyl-ester laminates cured with 10min of vibrations, with 3 samples per laminate. ME is the mean value of all three, and StDev is standard deviation.

Table C4: Flexural properties results.

Hz	FE, GPa	FE, GPa	FE, GPa	ME, GPa	StDev
0	13.7	12.8	14.0	13.5	0.624
2	14.3	15.2	14.7	14.7	0.451
5	13.5	13.5	13.9	13.6	0.231
10	13.1	13.4	13.6	13.4	0.252
30	13.6	14.7	14.8	14.4	0.666
50	13.8	13.6	14.4	13.9	0.416
100	13.5	11.8	12.5	12.6	0.854
1k	13.5	13.7	14.2	13.8	0.361
8k	12.9	12.8	12.7	12.8	0.100

4. Example of tensile testing, that is strength, TS, for vinyl-ester at 10min of vibrations, with three samples per laminate. TSm is the mean value of all three, and StDev is standard deviation.

Table C5: Tensile properties results.

Hz	TS (MPa)	TS (MPa)	TS (MPa)	TSm (MPa)	StDev
0	175	170	145	163.3	12.946
5	166	189	170	175.0	9.849
30	176	171	173	173.3	1.262
100	173	154	170	165.7	8.275

5. Example of water intake (tap water at 45°C for 7 days) of epoxy laminates cured with 10min of vibrations, with 6 samples per laminate. MI is the mean value of all 6.

Table C6: Total water intake (%) of all samples after 7 days.

Hz	1	2	3	4	5	6	MI
0	0.741	0.830	0.743	0.746	0.660	0.741	0.744
5	0.546	0.726	0.762	0.640	0.637	0.737	0.675
30	0.642	0.728	0.727	0.640	0.551	0.734	0.670
100	0.757	0.842	0.757	0.749	0.753	0.844	0.784

Table C7: Water absorption of one sample per laminate over 7 days.

Hz	0	1	2	3	4	5	6	7
0	10.80	10.83	10.84	10.86	10.88	10.87	10.87	10.88
5	10.98	11.00	11.01	11.02	11.04	11.04	11.04	11.04
30	10.90	10.95	10.95	10.96	10.98	10.97	10.97	10.97
100	10.57	10.61	10.62	10.63	10.65	10.67	10.65	10.65

6. Example of shear testing for epoxy laminates cured with 10min of vibrations, with 5 samples per laminate. MS is the mean value of all 5, and StDev is standard deviation.

Table C8: Shear testing results

Hz	ShS (MPa)	MS (MPa)	StDev
0	28.74		
0	28.15		
0	28.04		
0	26.02		
0	26.12	**27.14**	**1.256**
5	31.50		
5	32.61		
5	33.26		
5	30.45		
5	32.06	**31.98**	**1.074**
30	29.01		
30	29.85		
30	30.84		
30	30.58		
30	30.17	**30.09**	**0.713**
100	30.84		
100	30.69		
100	31.68		
100	30.78		
100	30.77	**30.95**	**0.410**

REFERENCES

Alonso Rasgado M.T, Davey K, *The effect of vibration on surface finish for semisolid and cast components*, Journal of materials processing technology 125-126:543-548, 2002.

Baley C, Davies P, Grohens Y, Dolto G, *Application of interlaminar tests to marine composites. A literature review*, Applied composite materials 11 (2): 99-126, 2004.

Barraza H.J, Hamidi Y.K, Aktas L, O'Rear E.A, Altan M.C, *Porosity reduction in the high-speed processing of glass-fiber composites by RTM*, Journal of composite materials 38 (3): 195-226, 2004.

Campbell F.C, Mallow A.R, Browning C.E, *Porosity in carbon fiber composites –an overview of causes*, Journal of advanced materials 26 (4): 18-33, 1995.

Campbell J, *Effects of vibration during solidification*, International Metals Reviews 26 (2): 71-108, 1981.

Campbell J, Compston P, Stachurski Z.H, *Analysis of thermoforming techniques for laminated structures*, Innovation: The path for growth in composites – Composites Australia and the Composites CRC Annual Conference, Melbourne, 2005.

Cantwell W.J, Morton J, *Significance of damage and defects and their detection in composite materials: a review*, Journal of Strain Analysis 27 (1): 29-42, 1992.

Cantwell W.J, Scudamore R, Ratcliffe J, Davies P, *Interfacial fracture in sandwich laminates*, Composite science and technology 59 (14): 2079-2085, 1999.

Chambers A.R, Earl J.S, Squires C.A, Suhot M.A, *The effect of voids on the flexural fatigue performance of unidirectional carbon fibre composites developed for wind turbine applications*, International journal of fatigue 28: 1389-1398, 2006.

Chen P, Lu C, Yu Q, Gao Y, Li J, Li X, *Influence of fiber wettability on the interfacial adhesion of continuous fiber-reinforced PPESK composite*, Journal of applied polymer science 102 (3): 2544-2551, 2006.

Chen Y-T, Davies H.T, Macosko C.W, *Wetting of fiber mats for composites manufacturing: I. Visualization experiments*, AIChE Journal 41 (10): 2261-2273, 1995.

Chowdhury S, Bhethanabolta V.R, Sen R, Measurement of diffusion coefficient of oxygen in FRP Using luminescence quenching, Composite and Polycon 2007.

Compston P, Jar P.-Y.B, *Comparison of interlaminar fracture toughness in unidirectional and woven roving marine composites*, Applied composite materials 5 (3): 189-206, 1998.

Compston P, Jar P.-Y.B, *The influence of fibre volume fraction on the mode I interlaminar fracture toughness of a glass-fibre/vinyl ester composite*, Applied composite materials 6 (6): 353-368, 1999.

Comte E, Merhi D, Michaud V, Manson J.A.E, *Void formation and transport during SMC manufacturing: effect of the glass fibre sizing*, Polymer composites 27 (3): 289-298, 2006.

Costa M.L, de Almeida S.F.M, Rezende M.C, *The influence of porosity on the interlaminar shear strength of carbon/epoxy and carbon/bismaleimide fabric laminates*, Composites science and technology 61 (14): 2101-2108, 2001.

Costa M.L, de Almeida S.F.M, Rezende M.C, *Critical void content for polymer composite laminates*, AIAA Journal 43 (6): 1336-1341, 2005.

Costa M.L, Rezende M.C, de Almeida S.F.M, *Strength of hygrothermally conditions polymer composites with voids*, Journal of composite materials 39 (21): 1943-1961, 2005.

Costa M.L, Rezende M.C, de Almeida S.F.M, *Effect of void content on the moisture absorption in polymeric composites*, Polymer-plastics technology and engineering 45 (6): 691-698, 2006.

Davies L.W, Day R.J, Bond D, Nesbitt A, Ellis J, Gardon E, *Effect o cure cycle heat transfer rates on the physical and mechanical properties of an epoxy matrix composite*, Composites science and technology 67 (9): 1892-1899, 2007.

Davies P, Pomies F, Carlssom L.A, *Influence of water and accelerated aging on the shear fracture properties of glass/epoxy composite*, Applied composite materials 3 (2): 71-87, 1996.

De Hoff R.T, Rhines F.N, *Quantitative Microscopy*, McGraw-Hill, 1968.

Dirand X, Hilaire B, Soulier J.P, Nardin M, *Interfacial shear strength in glass-fiber/vinylester-resin composites*, Composites science and technology 56 (5): 533-539, 1996.

Doinikov A.A, Zavrtak S.T, *Interaction of gas bubble in a compressible fluid*, Fluid dynamics 23 (6): 883-887, 1987.

Doinikov A.A, *Acoustic radiation pressure on a compressible sphere in a viscous liquid*, Journal of fluid mechanics 267: 1-21, 1994.

Doinikov A.A, *Acoustic radiation pressure on a rigid sphere in a viscous liquid*, Proceedings Royal Society of London A 447: 447-466, 1994.

Doinikov A.A, *Acoustic radiation pressure exerted by a spherical wave on a bubble in a viscous liquid*, Wave motion 24 (3): 275-279, 1996.

Doinikov A.A, Zavrtak S.T, *Interaction force between a bubble and a solid particle in a sound field*, Ultrasonic 34 (8): 807-815, 1996.

Doinikov A.A, *Bubble and particle dynamics in acoustics fields: modern trends and applications, Bjerknes forces and translational bubble dynamics*, Research Singpost: 95-143, 2005.

Ellenberger J, Krishna R, *Shaken, not stirred, bubble column reactors: enhancement of mass transfer by vibration excitement*, Chemical Engineering Science 58 (3-6): 705-710, 2003.

Eom Y, Boogh L, Michaud V, Manson J.-A, *A structure and property based process window for void free thermoset composites*, Polymer composites, 22 (1): 22-31, 2001.

Frishfelds V, Lundstrom T.S, Jakovics A, *Bubble motion through non-crimp fabrics during composite manufacturing*, Composites: Part A 39 (2): 243-251, 2008.

Ghiorse S.R, Jurta R.M, *Effects of low frequency vibration processing on carbon/epoxy laminates*, Composites 22 (1): 3-8, 1991.

Ghiorse S.R, *Effect of void content on the mechanical properties of carbon/epoxy laminates*, Sampe Quarterly 24 (2): 54-59, 1993.

Glickman M.E, Wang K.G, Crawford P, *Stochastic Effects in Microstructure*, Materials Research, 5 (3), 2002.

Graham D.B, *The role of vibration in fibre consolidation and void reduction*, private communication, QS, 2002.

Grinis L, Monin Y, *Influence of vibrations on gas bubble formation in liquids*, Chemical Engineering Technology 22 (5): 439-442, 1999.

Guo Z.S, Liu L, Zhang B.M, Du S, *Critical void content for thermoset composite laminates*, Journal of composite materials Vol. 00 No. 00, 2006.

Hagstrand P.-O, Bonjour F, Manson J.-A.E, *The influence of void content on the structural flexural performance of unidirectional glass fibre reinforced polypropylene composites*, Composites: Part A 36 (5): 705-714, 2005.

Hamidi Y.K, Altan M.C, *Spatial variation of void morphology in resin transfer molded E-glass/epoxy composites*, Journal of materials science letters 22 (24): 1813-1816, 2003.

Hamidi Y.K, Aktas L, Altan M.C, *Three-dimensional features of void morphology in resin transfer molded composites*, Composites science and technology 65 (7-8): 1306-1320, 2005.

Hamidi Y.K, Aktas L, Altan M.C, *Effect of packing on void morphology in resin transfer molded E-glass/Epoxy composites*, Polymer composites 26 (5): 614-627, 2005.

Hancox N.L, *The effects of flaws and voids on the shear properties of CFRP*, Journal of materials science 12 (5): 884-892, 1977.

Hancox N.L, *The influence of voids on the hydrothermal response of carbon fibre reinforced plastics*, Journal of Material science 16 (3): 627-632, 1981.

Hao Y, Prosperetti A, *The collapse of vapor bubbles in a spatially non-uniform flow*, International journal of heat and mass transfer 43 (19): 3539-3550, 2000.

Hodzic A, Kalyanasundaram S, Kim J.K, Lowe A.E, Stachurski Z.H, *Application of nano-indentation, nano-scratch and single fibre tests in investigation of interphase in composite materials*, Micron 32 :765-775, 2001.

Hodzic A, Stahurski Z.H, *Droplet on a fibre: surface tension and geometry*, Composite interfaces 8 (6): 415-425, 2001.

Hodzic A, Kim J.K, Lowe A.E, Stachurski Z.H, *The effects of water aging on the interphase region and interlaminar fracture toughness in polymer-glass composites*, Composites science and technology 64 (13-14): 2185-2195, 2004.

Huang H, Talreja R, *Effect of void geometry on elastic properties of unidirectional fibre reinforced composites*, Composites science and technology 65 (13): 1964-1981, 2005.

Iglesias J.G, Gonzales-Benito J, Aznar A.J, Bravo J, Baselga J, *Effect of Glass Fiber Surface Treatments on Mechanical Strength of Epoxy Based Composite Materials*, Journal of colloid and interface science 250 (1): 251-260, 2002.

Jimenez-Fernandez J, Crespo A, *The collapse of gas bubbles and cavities in a viscoelastic fluid*, International journal of multiphase flow 32 (10-11): 1294-1299, 2006.

Jinlian H, Yi L, Xueming S, *Study on void formation in multi-layer woven fabrics*, Composites: Part A 35 (5): 595-603, 2004.

Judd N.C.W, Wright W.W, *Voids and their effects on the mechanical properties of composites-an appraisal*, Sampe Journal 14 (1): 10-14, 1978.

Kang K, Koelling K, *Void transport in resin transfer molding*, Polymer Composites, 25 (4): 417-432, 2004.

Kang M.K, Lee W.I, Hahn H.T, *Formation of microvoids during resin-transfer molding process*, Composites science and technology 60 (12-13): 2427-2434, 2000.

Keusch S, Queck H, Gliesche K, *Influence of glass fibre/epoxy resin interface on static mechanical properties of unidirectional composites and on fatigue performance of cross ply composites*, Composites Part A 29 (5-6): 701-705, 1997.

Keusch S, Haessler R, *Influence of surface treatment of glass fibres on the dynamic mechanical properties of epoxy resin composites*, Composites: Part A 30 (8): 997-1002, 1999.

Krishna R, Ellenberger J, *Influence of low-frequency vibrations on bubble and drop sizes formed at a single orifice*, Chemical engineering and processing 42 (1): 15-21, 2003.

Kocatepe K, *Effect of low frequency vibration on porosity of LM25 and LM6 alloys*, Materials and design 28 (6): 1767-1775, 2007.

Kousourakis A, Mouritz A.P, Bannister M.K, *Interlaminar properties of polymer laminate containing internal sensor cavities*, Composite structures 75 (1-4): 610-618, 2006.

Kousourakis A, Bannister M.K, Mouritz A.P, *Tensile and compressive properties of polymer laminates containing internal sensor cavities*, Composites: Part A 39 (9): 1394-1403, 2008.

Kurematsu K, Koishi M, *Kinetic Studies on void formation during liquid epoxy resin impregnation through polyester non-woven fabric*, Colloid and Polymer Science 263: 454-461, 1985.

Lauterborn W, Kurz T, Mettin R, Ohl C.D, *Experimental and theoretical bubble dynamics*, Advances in Chemical Physics 110: 295-380, 1999.

Leighton T.G, *The acoustic bubble*, Academic, London, 1994.

Leterrier Y, G'Sell C, *Formation and elimination of voids during the processing of thermoplastic matrix composites*, Polymer composites 15 (2): 101-105, 1994.

Liu L, Zhang B-M, Wang D-F, Wu Z-J, *Effects of cure cycles on void content and mechanical properties of composite laminates*, Composite structures 73 (3): 303-309, 2006.

Logvinyuk V.P, Makarenov V.V, Malyshev V.V, Pauchenkov G.M, *Solubility of gases in petroleum products*, Translated from Khimiya i Tekhnologiya Topliv i Masel, 5: 27-29, 1970.

Lundstrom T.S, Gebart B.R, *Influence from process parameters on void formation in resin transfer molding*, Polymer composites 15 (1): 25-33, 1994.

Lundstrom T.S, *Bubble transport through constricted capillary tubes with application to resin transfer molding*, Polymer composites 17 (6): 770-779, 1996.

Lundstrom T.S, *Measurement of void collapse during resin transfer moulding*, Composites Part A 28 (3): 201-214, 1997.

Mariatti M, Chum P.K, *Effect of resin:fiber ratio on the properties of glass fiber reinforced plastic composites*, International Journal of Polymeric Materials 54 (10): 975-984, 2005.

Mariatti M, Chum P.K, *Effect of laminates configuration on the properties of glass fiber-reinforced plastics (GFRPs) mixed composites*, Journal of reinforced plastics and composites 24 (16): 1713-1721, 2005.

Michaelides E.E, *Particles, bubbles & drops. Their motion, heat and mass transfer*, World Scientific Publishing, 2006.

Mitrovic J, *Upon equilibrium of gas bubble in infinite liquid*, Chemical engineering science 55 (12): 2265-2270, 2000.

Mouritz A.P, Thomson R.S, *Compression, flexure and shear properties of a sandwich composite containing defects*, Composite structures 44 (4): 263-278, 1999.

Mouritz A.P, *Ultrasonic and interlaminar properties of highly porous composites*, Journal of composite materials 34 (3): 218-239, 2000.

Nightingale C, Day R.J, *Flexural and interlaminar shear strength properties of carbon fibre/epoxy composites cured thermally and with microwave radiation*, Composites: Part A 33 (7): 1021-1030, 2002.

Olivier P, Cottu J.P, Ferret B, *Effects of cure cycle pressure and voids on some mechanical properties of carbon/epoxy laminates*, Composites 26 (7): 509-515, 1995.

Pantano V, Compston P, Stachurski Z.H, *Effect of matrix toughness on the shear strength of brittle and rubber-modified glass-fiber/vinyl ester composites*, Journal of materials science letters 21 (10): 771-773, 2002.

Pantelelis N.G, *Evaluation of the vibration assisted RTM technique in the production of real parts*, 7th FPCM, 2004.

Patel N, Rohatgi V, Lee J, *Influence of processing and material variables on resin-fiber interface on liquid composite molding*, Polymer composites 14 (2): 161-172, 1993.

Patel N, Lee L.J, *Effects of fiber mat architecture on void formation and removal in liquid composite molding*, Polymer composites 16 (5): 386-399, 1995.

Patel N, Lee L.J, *Modeling of void formation and removal in liquid composite molding. Part I: wettability analysis*, Polymer composites 17 (1): 96-103, 1996.

Paul A, *Chemistry of glasses*, Chapman and Hall, 1990.

Pillai N.R, *Effect of low frequency mechanical vibration on structure of modified Aluminum-Silicon Eutectic*, Metallurgical transactions 3, 1972.

Plonka R, Mader E, Gao S.L, Bellmann C, Dutschk V, Zhandarov S, *Adhesion of epoxy/glass fibre composites influenced by aging effects on sizings*, Composite: Part A 35 (10): 1207-1216, 2004.

Prosperetti A, *Bubble dynamics: a review and some recent results*, Applied scientific research 38 (1): 145-164, 1982.

Prosperetti A, *Bubble phenomena in sound fields: part one*, Ultrasonics 22 (2): 69-77, 1984.

Prosperetti A, *Bubble phenomena in sound fields: part two*, Ultrasonics 22 (3): 115-124, 1984.

Quickstep web site www.quickstep.com.au

Ranganathan S, Advani S.G, Lamontia M.A, *Non-Isothermal Process Model for Consolidation and Void Reduction during In-Situ Tow Placement of Thermoplastic Composites*, Journal of composite materials 29 (8): 1040-1062, 1995.

Rohatgi V, Patel N, Lee L.J, *Experimental investigation of flow-induced microvoids during impregnation of unidirectional stitched fiberglass mat*, Polymer composites 17 (2): 161-170, 1996.

Rubin A.M, Jerina K.L, *Evaluation of porosity in composite aircraft*, Mechanics of composite materials 30 (6): 587-600, 1994.

Saidpour S.H, Richardson M.O.W, *Glass fibre coating for optimum mechanical properties of vinyl ester composites*, Composites Part A 28 (11): 971-975, 1997.

Santulli C, Drezet D, Brooks R, Rudd C.D, *Relation between void content and mechanical and impact properties in commingled E-glass/Polypropylene thermoplastic composites*, Euromat conference, Rimini, 2001.

Santulli C, Garcia Gil R, Long A.C, Clifford M.J, *Void content measurements in commingled E-glass/polypropylene composites using image analysis from optical microgrpahs*, Science and engineering of composite materials 10 (2): 77-90, 2002.

Scudamore R.J, Cantwell W.J, *The effect of moisture and loading rate of the interfacial fracture properties of sandwich structures*, Polymer composites 23 (3): 406-417, 2002.

Shukla D.P, Goel D.B, Pandey P.C, *Effect of vibration on the formation of porosity in aluminum alloy ingots*, Metallurgical transactions B 11 (1): 166-168, 1980.

Silcock M.D, Garschke C, Hall W, Fox B.L, *Rapid composite tube manufacture utilizing the Quickstep™ Process*, Journal of composite materials 41 (8): 965-978, 2007.

Song Y.S, *Mathematical analysis of resin flow through fibrous porous media*, Applied composite materials 13: 335-343, 2006.

Stabler W.R, Tatterson G.B, Sadler R.L, El-Shiekh A.H.M, *Void minimization in the manufacturing of carbon fiber composites by RTM*, Sampe Quarterly 23 (2): 38-42, 1992.

Suri C, Hamada H, Fujihara K, *Influence of aging and surface treatment on the mode II fracture behaviour in a glass/vinylester composite*, Composite interfaces 8 (2): 135-149, 2001.

Thomas M.M, Joseph B, Kardos J.L, *Experimental characterization of autoclave-cured glass-epoxy composite laminates: cure cycle effects upon thickness, void content, and related phenomena*, Polymer composites 18 (3): 283-299, 1997.

Thomason J.L, *The interface region in glass fibre-reinforced epoxy resin composites: 1. Sample preparation, void content and interfacial strength*, Composites 26 (7): 467-475, 1995.

Thomason J.L, *The interface region in glass fibre-reinforced epoxy resin composites: 2. Water absorption, voids and the interface*, Composites 26 (7): 477-485, 1995.

Thomason J.L, *The interface region in glass fibre-reinforced epoxy resin composites: 3. Characterization of fibre surface coatings and the interphase*, Composites 26 (7): 487-498, 1995.

Varna J, Joffe R, Berglund L.A, Lundstrom T.S, *Effect of voids on failure mechanism in RTM laminates*, Composites science and technology 53 (2): 241-249, 1995.

Ventsel E, Krauthammer T, *Thin Plates and Shells: theory, analysis and applications*, M Dekker, New York 2001.

Xu Z, Yan J, Chen W, Yang S, *Effects of ultrasonic vibration on the grain refinement and SiC particle distribution in Zn-based composite filler metal*, Materials letters 62 (17-18): 2615-2618, 2008.

Ye L, Friedrich K, Kastel J, *Consolidation of GF/PP commingled yarn composites*, Applied composite materials 1: 415-429, 1995.

Yin M, Long Y, Edward G.H, Stachurski Z.H, *Particle Coarsening in Polyethylene/Polypropylene Blends*, Macromolecules 29: 2131-2137, 1996.

Young F.R, *Cavitation*, Imperial College Press, 1999.

Yuan H, Oguz H.N, Prosperetti A, *Growth and collapse of a vapor bubble in a small tube*, International journal of heat and mass transfer 42 (19): 3643-3657, 1999.

Zhang B, Liu L, Wu Z, Wang D, *Experimental investigation of porosity in carbon/epoxy composite laminates*, Composites technologies for 2020, ACCM4, 2004.

Zhang J, Fox, B.L, *Characterization and analysis of delamination fracture and nanocreep properties in carbon epoxy composites manufactured by different processes*, Journal of composite materials 40 (14): 1287-1299, 2006.

Zulkifli R, Azhari C.H, Ghazali M.J, Ismail A.R, Sulong A.B, *Interlaminar fracture toughness of multi-layer woven silk/epoxy composites treated with coupling agent*, European journal of scientific research 27 (3):454-462, 2009.

BIBLIOGRAPHY

Abraham D, McIlhager R, *Investigations into various methods of liquid injection to achieve mouldings with minimum void contents and full wet out*, Polymer and polymer composites 4 (6): 437-443, 1996.

Afendi Md, Banks W.M, Kirkwood D, *Bubble free resin for infusion process*, Composites Part A 36 (6): 739-746, 2005.

Alonso Rasgado M.T, Davey K, *The effect of vibration on surface finish for semisolid and cast components*, Journal of materials processing technology 125-126:543-548, 2002.

Baley C, Davies P, Grohens Y, Dolto G, *Application of interlaminar tests to marine composites. A literature review*, Applied composite materials 11 (2): 99-126, 2004.

Barakhov V.I, Dimitrienko I.P, Goncharov V.I, Stepanov A.P, Nikolaev V.A, *Internal structure of composite materials by using computer tomography*, Journal of engineering physics 51 (6): 1476-1481, 1986.

Barraza H.J, Hamidi Y.K, Aktas L, O'Rear E.A, Altan M.C, *Porosity reduction in the high-speed processing of glass-fiber composites by RTM*, Journal of composite materials 38 (3): 195-226, 2004.

Callister W.D, *Materials Science and Engineering: an introduction*, New York: Wiley, 1997.

Campbell F.C, Mallow A.R, Browning C.E, *Porosity in carbon fiber composites –an overview of causes*, Journal of advanced materials 26 (4): 18-33, 1995.

Campbell J, *Effects of vibration during solidification*, International Metals Reviews 26 (2): 71-108, 1981.

Campbell J, *Rapid Manufacture of a High Quality Composite Sandwich Structures Using a Novel Thermoforming Technique*, M Phil Thesis, ANU, 2004.

Cantwell W.J, Morton J, *Significance of damage and defects and their detection in composite materials: a review*, Journal of Strain Analysis 27 (1): 29-42, 1992.

Cantwell W.J, Scudamore R, Ratcliffe J, Davies P, *Interfacial fracture in sandwich laminates*, Composite science and technology 59 (14): 2079-2085, 1999.

Carruthers J, *Crashworthy capability of composite material structures*, Composite structures 37 (2):109-134, 1997.

Chambers A.R, Earl J.S, Squires C.A, Suhot M.A, *The effect of voids on the flexural fatigue performance of unidirectional carbon fibre composites developed for wind turbine applications*, International journal of fatigue 28: 1389-1398, 2006.

Chen C-S, *Investigation on the vibration and stability of hybrid composite plates*, Journal of reinforced plastics and composites 24 (16): 1747-1758, 2005.

Chen P, Lu C, Yu Q, Gao Y, Li J, Li X, *Influence of fiber wettability on the interfacial adhesion of continuous fiber-reinforced PPESK composite*, Journal of applied polymer science 102 (3): 2544-2551, 2006.

Chen Y-T, Davies H.T, Macosko C.W, *Wetting of fiber mats for composites manufacturing: I. Visualization experiments*, AIChE Journal 41 (10): 2261-2273, 1995.

Chowdhury S, Bhethanabolta V.R, Sen R, Measurement of diffusion coefficient of oxygen in FRP Using luminescence quenching, Composite and Polycon 2007.

Comte E, Merhi D, Michaud V, Manson J.A.E, *Void formation and transport during SMC manufacturing: effect of the glass fibre sizing*, Polymer composites 27 (3): 289-298, 2006.

Compston P, Jar P.-Y.B, *Comparison of interlaminar fracture toughness in unidirectional and woven roving marine composites*, Applied composite materials 5 (3): 189-206, 1998.

Compston P, Jar P.-Y.B, *The influence of fibre volume fraction on the mode I interlaminar fracture toughness of a glass-fibre/vinyl ester composite*, Applied composite materials 6 (6): 353-368, 1999.

Compston P, Jar P.-Y.B, Burchill P.J, Takahashi K, *The transfer of matrix toughness to composite mode I interlaminar fracture toughness in glass-fibre/vinyl ester composites*, Applied composite materials 9 (5): 291-314, 2002.

Costa M.L, de Almeida S.F.M, Rezende M.C, *The influence of porosity on the interlaminar shear strength of carbon/epoxy and carbon/bismaleimide fabric laminates*, Composites science and technology 61 (14): 2101-2108, 2001.

Costa M.L, de Almeida S.F.M, Rezende M.C, *Critical void content for polymer composite laminates*, AIAA Journal 43 (6): 1336-1341, 2005.

Costa M.L, Rezende M.C, de Almeida S.F.M, *Strength of hygrothermally conditions polymer composites with voids*, Journal of composite materials 39 (21): 1943-1961, 2005.

Costa M.L, Rezende M.C, de Almeida S.F.M, *Effect of void content on the moisture absorption in polymeric composites*, Polymer-plastics technology and engineering 45 (6): 691-698, 2006.

Cvetanovska A, Compston P, *Degree of cure and tensile properties of vinylester resin cured with ultraviolet light*, Journal of materials science 39 (5): 1791-1793, 2004.

Davies L.W, Day R.J, Bond D, Nesbitt A, Ellis J, Gardon E, *Effect of cure cycle heat transfer rates on the physical and mechanical properties of an epoxy matrix composite*, Composites science and technology 67 (9): 1892-1899, 2007.

Davies P, Pomies F, Carlssom L.A, *Influence of water and accelerated aging on the shear fracture properties of glass/epoxy composite*, Applied composite materials 3 (2): 71-87, 1996.

Davis J.L, *Wave Propagation in Solids and Fluids*, Springer, 1988.

De Hoff R.T, Rhines F.N, Quantitative Microscopy, McGraw-Hill, 1968.

Dirand X, Hilaire B, Soulier J.P, Nardin M, *Interfacial shear strength in glass-fiber/vinylester-resin composites*, Composites science and technology 56 (5): 533-539, 1996.

Doinikov A.A, Zavrtak S.T, *Interaction of gas bubble in a compressible fluid*, Fluid dynamics 23 (6): 883-887, 1987.

Doinikov A.A, *Acoustic radiation pressure on a compressible sphere in a viscous liquid*, Journal of fluid mechanics 267: 1-21, 1994.

Doinikov A.A, *Acoustic radiation pressure on a rigid sphere in a viscous liquid*, Proceedings Royal Society of London A 447: 447-466, 1994.

Doinikov A.A, *Acoustic radiation pressure exerted by a spherical wave on a bubble in a viscous liquid*, Wave motion 24 (3): 275-279, 1996.

Doinikov A.A, *Theory of acoustic radiation pressure for actual fluids*, physical review E 54 (6): 6297-6303, 1996.

Doinikov A.A, Zavrtak S.T, *Interaction force between a bubble and a solid particle in a sound field*, Ultrasonic 34 (8): 807-815, 1996.

Doinikov A.A, Bubble and particle dynamics in acoustics fields: modern trends and applications, Bjerknes forces and translational bubble dynamics, Research Singpost: 95-143, 2005.

Ellenberger J, Krishna R, *Shaken, not stirred, bubble column reactors: enhancement of mass transfer by vibration excitement*, Chemical Engineering Science 58 (3-6): 705-710, 2003.

Endruweit A, Ruijter W, Johnson M.S, Long A.C, *Transmission of ultraviolet light through reinforcement fabrics and its effect on ultraviolet curing of composite laminates*, Polymer composites 29 (7): 818-829, 2008.

Eom Y, Boogh L, Michaud V, Manson J.-A, *A structure and property based process window for void free thermoset composites*, Polymer composites, 22 (1): 22-31, 2001.

Fox B, Lowe A, Hodgkin J, *Investigation of failure mechanisms in aged aerospace composites*, Engineering Failure Analysis 11 (2): 235-241, 2004.

Frishfelds V, Lundstrom T.S, Jakovics A, *Bubble motion through non-crimp fabrics during composite manufacturing*, Composites: Part A 39 (2): 243-251, 2008.

Gay D, Hao S.V, Tsai S.W, *Composite materials design and applications*, CRC Press, 2003.

Ghiorse S.R, Jurta R.M, *Effects of low frequency vibration processing on carbon/epoxy laminates*, Composites 22 (1): 3-8, 1991.

Ghiorse S.R, *Effect of void content on the mechanical properties of carbon/epoxy laminates*, Sampe Quarterly 24 (2): 54-59, 1993.

Glickman M.E, Wang K.G, Crawford P, *Stochastic Effects in Microstructure*, Materials Research, 5 (3), 2002.

Gough W, Richards J.P.G, Williams R.P, Vibrations and waves, Prentice Hall, 1995.

Graham D.B, *The role of vibration in fibre consolidation and void reduction*, private communication, QS, 2002.

Grant P.V, Cantwell W.J, McKenzie H, Corkhill P, *The damage threshold of laminated glass structures*, International Journal of Impact Engineering 21 (9): 737-746, 1998.

Grinis L, Monin Y, *Influence of vibrations on gas bubble formation in liquids*, Chemical Engineering Technology 22 (5): 439-442, 1999.

Guo Z.S, Liu L, Zhing B.M, Du S, *Critical void content for thermoset composite laminates*, Journal of composite materials 5, 2006.

Gutowski T.G, Advanced Composites Manufacturing, Wiley-Interscience, 1997.

Hagstrand P.-O, Bonjour F, Manson J.-A.E, *The influence of void content on the structural flexural performance of unidirectional glass fibre reinforced polypropylene composites*, Composites: Part A 36 (5): 705-714, 2005.

Hamidi Y.K, Altan M.C, *Spatial variation of void morphology in resin transfer molded E-glass/epoxy composites*, Journal of materials science letters 22 (24): 1813-1816, 2003.

Hamidi Y.K, Aktas L, Altan M.C, *Three-dimensional features of void morphology in resin transfer molded composites*, Composites science and technology 65 (7-8): 1306-1320, 2005.

Hamidi Y.K, Aktas L, Altan M.C, *Effect of packing on void morphology in resin transfer molded E-glass/Epoxy composites*, Polymer composites 26 (5): 614-627, 2005.

Hancox N.L, *The effects of flaws and voids on the shear properties of CFRP*, Journal of materials science 12 (5): 884-892, 1977.

Hancox N.L, *The influence of voids on the hydrothermal response of carbon fibre reinforced plastics*, Journal of Material science 16 (3): 627-632, 1981.

Hao Y, Prosperetti A, *The effect of viscosity on the spherical stability of oscillating gas bubbles*, Physics of fluids 11 (6): 1309-1317, 1999.

Hao Y, Prosperetti A, *The dynamics of vapor bubbles in acoustic pressure fields*, Physics of fluids 11 (8): 2008-2019, 1999.

Hao Y, Prosperetti A, *The collapse of vapor bubbles in a spatially non-uniform flow*, International journal of heat and mass transfer 43 (19): 3539-3550, 2000.

Hearle J, *High performance fibers*, Cambridge: Woodhead, 2001.

Hitt D.L, Prosperetti A, *Viscous forces on acoustically levitated gas bubbles*, Nonlinear analysis 63 (5-7): e1517-e1527, 2005.

Hodzic A, Stahurski Z.H, *Droplet on a fibre: surface tension and geometry*, Composite interfaces 8 (6): 415-425, 2001.

Hodzic A, Kalyanasundaram S, Kim J.K, Lowe A.E, Stachurski Z.H, *Application of nano-indentation, nano-scratch and single fibre tests in investigation of interphase in composite materials*, Micron 32 :765-775, 2001.

Hodzic A, Kim J.K, Lowe A.E, Stachurski Z.H, *The effects of water aging on the interphase region and interlaminar fracture toughness in polymer-glass composites*, Composites science and technology 64 (13-14): 2185-2195, 2004.

Houshyar S, Shanks R.A, Hodzic A, *The effect of fiber concentration on mechanical and thermal properties of fiber-reinforced polypropylene composites*, Journal of applied polymer science 96 (6): 2260-2272, 2005.

Huang H, Talreja R, *Effect of void geometry on elastic properties of unidirectional fibre reinforced composites*, Composites science and technology 65 (13): 1964-1981, 2005.

Iglesias J.G, Gonzales-Benito J, Aznar A.J, Bravo J, Baselga J, *Effect of Glass Fiber Surface Treatments on Mechanical Strength of Epoxy Based Composite Materials*, Journal of colloid and interface science 250 (1): 251-260, 2002.

Ijaz M, Robinson M, Wright P.N.H, Gibson A.G, *Vacuum consolidation of commingled thermoplastic matrix composites*, Journal of composite materials 41 (2): 243-262, 2007.

Jimenez-Fernandez J, Crespo A, *The collapse of gas bubbles and cavities in a viscoelastic fluid*, International journal of multiphase flow 32 (10-11): 1294-1299, 2006.

Jinlian H, Yi L, Xueming S, *Study on void formation in multi-layer woven fabrics*, Composites: Part A 35 (5): 595-603, 2004.

Johnson W, Ghosh S.K, *Some physical defects arising in composite material fabrication*, Journal of materials science 16 (2): 285-301, 1981.

Judd N.C.W, Wright W.W, *Voids and their effects on the mechanical properties of composites-an appraisal*, Sampe Journal 14 (1): 10-14, 1978.

Kang K, Koelling K, *Void transport in resin transfer molding*, Polymer Composites, 25 (4): 417-432, 2004.

Kang M.K, Lee W.I, Hahn H.T, *Formation of microvoids during resin-transfer molding process*, Composites science and technology 60 (12-13): 2427-2434, 2000.

Kelly A, Cahn R.W, Bever M.B, *Concise encyclopedia of composite materials*, Oxford: Pergamon Press, 1989.

Keusch S, Queck H, Gliesche K, *Influence of glass fibre/epoxy resin interface on static mechanical properties of unidirectional composites and on fatigue performance of cross ply composites*, Composites Part A 29 (5-6): 701-705, 1997.

Keusch S, Haessler R, *Influence of surface treatment of glass fibres on the dynamic mechanical properties of epoxy resin composites*, Composites: Part A 30 (8): 997-1002, 1999.

Krishna R, Ellenberger J, *Influence of low-frequency vibrations on bubble and drop sizes formed at a single orifice*, Chemical engineering and processing 42 (1): 15-21, 2003.

Kocatepe K, *Effect of low frequency vibration on porosity of LM25 and LM6 alloys*, Materials and design 28 (6): 1767-1775, 2007.

Kootsookos A, Mouritz A.P, *Seawater durability of glass- and carbon-polymer composites*, Composites science and technology 64 (10-11): 1503-1511, 2004.

Kousourakis A, Mouritz A.P, Bannister M.K, *Interlaminar properties of polymer laminate containing internal sensor cavities*, Composite structures 75 (1-4): 610-618, 2006.

Kousourakis A, Bannister M.K, Mouritz A.P, *Tensile and compressive properties of polymer laminates containing internal sensor cavities*, Composites: Part A 39 (9): 1394-1403, 2008.

Kuentzer N, Simacek P, Advani S.G, Walsh S, *Correlation of void distribution to VARTM manufacturing techniques*, Composites Part A 38 (3): 802-813, 2007.

Kurematsu K, Koishi M, *Kinetic Studies on void formation during liquid epoxy resin impregnation through polyester non-woven fabric*, Colloid and Polymer Science 263: 454-461, 1985.

Lauterborn W, Kurz T, Mettin R, Ohl C.D, *Experimental and theoretical bubble dynamics*, Advances in Chemical Physics 110: 295-380, 1999.

Leterrier Y, G'Sell C, *Formation and elimination of voids during the processing of thermoplastic matrix composites*, Polymer composites 15 (2): 101-105, 1994.

Liu L, Zhang B-M, Wang D-F, Wu Z-J, Effects of cure cycles on void content and mechanical properties of composite laminates, Composite structures 73 (3): 303-309, 2006.

Logvinyuk V.P, Makarenov V.V, Malyshev V.V, Pauchenkov G.M, *Solubility of gases in petroleum products*, Translated from Khimiya i Tekhnologiya Topliv i Masel, 5: 27-29, 1970.

Lu F, Cantwell W.J, Kausch h.H, *The role of cavitation and debonding in the toughening of core-shell rubber modified epoxy systems*, Journal of materials science 32 (11): 3055-3059, 1997.

Lundstrom T.S, Gebart B.R, *Influence from process parameters on void formation in resin transfer molding*, Polymer composites 15 (1): 25-33, 1994.

Lundstrom T.S, *Bubble transport through constricted capillary tubes with application to resin transfer molding*, Polymer composites 17 (6): 770-779, 1996.

Lundstrom T.S, *Measurement of void collapse during resin transfer moulding*, Composites Part A 28 (3): 201-214, 1997.

Mamalis A.G, Robinson M, Manolakos D.E, Demosthenous G.A, Ioannidis M.B, Shih C-H, Lee L.J, *Effect of fiber architecture permeability in liquid composite molding*, Polymer composites 19 (5): 626-639, 1998.

Mariatti M, Chum P.K, *Effect of resin:fiber ratio on the properties of glass fiber reinforced plastic composites*, International Journal of Polymeric Materials 54 (10) 2005.

Mariatti M, Chum P.K, *Effect of laminates configuration on the properties of glass fiber-reinforced plastics (GFRPs) mixed composites*, Journal of reinforced plastics and composites 24 (16): 1713-1721, 2005.

Michaelides E.E, *Particles, bubbles & drops. Their motion, heat and mass transfer*, World Scientific Publishing, 2006.

Mitrovic J, *Upon equilibrium of gas bubble in infinite liquid*, Chemical engineering science 55 (12): 2265-2270, 2000.

Mouritz A.P, Thomson R.S, *Compression, flexure and shear properties of a sandwich composite containing defects*, Composite structures 44 (4): 263-278, 1999.

Mouritz A.P, *Ultrasonic and interlaminar properties of highly porous composites*, Journal of composite materials 34 (3): 218-239, 2000.

Mouritz A.P, *Fire resistance of aircraft composite laminates*, Journal of materials science letters 22 (21): 1507-1509, 2003.

Mouritz A.P, Kootsookos A, Mathys G, *Stability of polyester- and vinyl ester-based composites in seawater*, Journal of materials science 39 (19): 6073-6077, 2004.

Nightingale C, Day R.J, *Flexural and interlaminar shear strength properties of carbon fibre/epoxy composites cured thermally and with microwave radiation*, Composites: Part A 33 (7): 1021-1030, 2002.

Nilsson G, Fernberg S.P, Berglund L.A, *Strain field inhomogeneities and stiffness changes in GMT containing voids*, Composites Part A 33 (1): 75-85, 2002.

Ohl C.D, Tijink A, Prosperetti A, The *added mass of an expanding bubble*, Journal of fluid mechanics (482): 271-290, 2003.

Olivier P, Cottu J.P, Ferret B, *Effects of cure cycle pressure and voids on some mechanical properties of carbon/epoxy laminates*, Composites 26 (7): 509-515, 1995.

Ory E, Yuan H, Prosperetti A, Popinet S, Zaleski S, *Growth and collapse of a vapor bubble in a narrow tube*, Physics of fluid 12 (6); 1268-1277, 2000.

Pantano V, Compston P, Stachurski Z.H, *Effect of matrix toughness on the shear strength of brittle and rubber-modified glass-fiber/vinyl ester composites*, Journal of materials science letters 21 (10): 771-773, 2002.

Pantelelis N.G, *Evaluation of the vibration assisted RTM technique in the production of real parts*, 7th FPCM, 2004.

Patel N, Rohatgi V, Lee J, *Influence of processing and material variables on resin-fiber interface on liquid composite molding*, Polymer composites 14 (2): 161-172, 1993.

Patel N, Lee L.J, *Effects of fiber mat architecture on void formation and removal in liquid composite molding*, Polymer composites 16 (5): 386-399, 1995.

Patel N, Lee L.J, *Modeling of void formation and removal in liquid composite molding. Part I: wettability analysis*, Polymer composites 17 (1): 96-103, 1996.

Pelekasis N.A, Gaki A, Doinikov A, Tsamopoulos J.A, *Secondary Bjerknes forces between two bubbles and the phenomenon of acoustic streamers*, Journal of fluid mechanics (500): 313-347, 2004.

Pillai N.R, *Effect of low frequency mechanical vibration on structure of modified Aluminum-Silicon Eutectic*, Metallurgical transactions 3, 1972.

Plonka R, Mader E, Gao S.L, Bellmann C, Dutschk V, Zhandarov S, *Adhesion of epoxy/glass fibre composites influenced by aging effects on sizings*, Composite: Part A 35 (10): 1207-1216, 2004.

Potter M.C, Wiggert D.C, *Mechanics of fluids*, Prentice-Hall, 1991.

Prosperetti A, *Bubble dynamics: a review and some recent results*, Applied scientific research 38 (1): 145-164, 1982.

Prosperetti A, *Bubble phenomena in sound fields: part one*, Ultrasonics 22 (2) 1984.

Prosperetti A, *Bubble phenomena in sound fields: part two*, Ultrasonics 22 (3) 1984.

Ranganathan S, Advani S.G, Lamontia M.A, *Non-Isothermal Process Model for Consolidation and Void Reduction during In-Situ Tow Placement of Thermoplastic Composites*, Journal of composite materials 29 (8): 1040-1062, 1995.

Rao S.S, *Vibration of continuous system*, John Wiley and Sons, 2007.

Rohatgi V, Patel N, Lee L.J, *Experimental investigation of flow-induced microvoids during impregnation of unidirectional stitched fiberglass mat*, Polymer composites 17 (2): 161-170, 1996.

Roylance D, *Mechanics of Materials*, New York: Wiley, 1996.

Rubin A.M, Jerina K.L, *Evaluation of porosity in composite aircraft*, Mechanics of composite materials 30 (6): 587-600, 1994.

Saidpour S.H, Richardson M.O.W, *Glass fibre coating for optimum mechanical properties of vinyl ester composites*, Composites Part A 28 (11): 971-975, 1997.

Santulli C, Drezet D, Brooks R, Rudd C.D, *Relation between void content and mechanical and impact properties in commingled E-glass/Polypropylene thermoplastic composites*, Euromat conference, Rimini, 2001.

Santulli C, Garcia Gil R, Long A.C, Clifford M.J, *Void content measurements in commingled E-glass/polypropylene composites using image analysis from optical microgrpahs*, Science and engineering of composite materials 10 (2): 77-90, 2002.

Schell J.S.U, Renggli M, van Lenthe G.H, Muller R, Ermanni P, *Micro-computed tomography determination of glass fibre reinforced polymer meso-structure*, Composites Science and Technology 66 (13): 2016-2022, 2006.

Scudamore R.J, Cantwell W.J, *The effect of moisture and loading rate of the interfacial fracture properties of sandwich structures*, Polymer composites 23 (3): 406-417, 2002.

Shukla D.P, Goel D.B, Pandey P.C, *Effect of vibration on the formation of porosity in aluminum alloy ingots*, Metallurgical transactions B 11 (1): 166-168, 1980.

Silcock M.D, Garschke C, Hall W, Fox B.L, *Rapid composite tube manufacture utilizing the Quickstep™ Process*, Journal of composite materials 41 (8): 965-978, 2007.

Stabler W.R, Tatterson G.B, Sadler R.L, El-Shiekh A.H.M, *Void minimization in the manufacturing of carbon fiber composites by RTM*, Sampe Quarterly 23 (2): 38-42, 1992.

Suri C, Hamada H, Fujihara K, *Influence of aging and surface treatment on the mode II fracture behaviour in a glass/vinylester composite*, Composite interfaces 8 (2): 135-149, 2001.

Tang J.-M, Lee W.I, Springer G.S, *Effects of cure pressure on resin flow, voids, and mechanical properties,* Journal of composite materials 21 (5): 421-440, 1987.

Thomas M.M, Joseph B, Kardos J.L, *Experimental characterization of autoclave-cured glass-epoxy composite laminates: cure cycle effects upon thickness, void content, and related phenomena*, Polymer composites 18 (3): 283-299, 1997.

Thomason J.L, *The interface region in glass fibre-reinforced epoxy resin composites: 1. Sample preparation, void content and interfacial strength*, Composites 26 (7): 467-475, 1995.

Thomason J.L, *The interface region in glass fibre-reinforced epoxy resin composites: 2. Water absorption, voids and the interface*, Composites 26 (7): 477-485, 1995.

Thomason J.L, *The interface region in glass fibre-reinforced epoxy resin composites: 3. Characterization of fibre surface coatings and the interphase*, Composites 26 (7): 487-498, 1995.

Tierney J, Gillespie Jr.J.W, *Modeling of heat transfer and void dynamics for the thermoplastic composite tow-placement process*, Journal of composite materials 37 (19): 1745-1768, 2003.

Tse F.S, Morse I.E, Hinkle R.T, Mechanical vibrations, Allyn and Bacon, 1964.

Varna J, Joffe R, Berglund L.A, Lundstrom T.S, *Effect of voids on failure mechanism in RTM laminates*, Composites science and technology 53 (2): 241-249, 1995.

Ventsel E, Krauthammer T, *Thin Plates and Shells: theory, analysis and applications*, M Dekker, New York 2001.

Wolfrum B, Kurz T, Mettin R, Lauterborn W, *Shock wave induced interaction of microbubbles and boundaries*, Physics of fluid 15 (10): 2916-2922, 2003.

Xu Z, Yan J, Chen W, Yang S, *Effects of ultrasonic vibration on the grain refinement and SiC particle distribution in Zn-based composite filler metal*, Materials letters 62 (17-18): 2615-2618, 2008.

Yang B, Prosperetti A, *The transient rise of a bubble subject to shape or volume changes*, Physics of fluids 15 (9): 2640-2648, 2003.

Ye L, Friedrich K, Kastel J, *Consolidation of GF/PP commingled yarn composites*, Applied composite materials 1: 415-429, 1995.

Yin M, Long Y, Edward G.H, Stachurski Z.H, *Particle Coarsening in Polyethylene/Polypropylene Blends*, Macromolecules 29: 2131-2137, 1996.

Young F.R, *Cavitation*, Imperial College Press, 1999.

Yuan H, Prosperetti A, *Gas-liquid heat transfer in a bubble collapsing near a wall*, Physics of fluids, 9 (1): 127-142, 1997.

Yuan H, Oguz H.N, Prosperetti A, *Growth and collapse of a vapor bubble in a small tube*, International journal of heat and mass transfer 42 (19): 3643-3657, 1999.

Zhang B, Liu L, Wu Z, Wang D, *Experimental investigation of porosity in carbon/epoxy composite laminates*, Composites technologies for 2020, ACCM4, 2004.

Zhang J, Fox, B.L, *Characterization and analysis of delamination fracture and nanocreep properties in carbon epoxy composites manufactured by different processes,* Journal of composite materials 40 (14): 1287-1299, 2006.

Zinchenko V.F, *Predicting the porosity of glass-reinforced plastics from their thermal conductivity*, Polymer mechanics 7 (3): 457-460, 1973.

Zulkifli R, Azhari C.H, Ghazali M.J, Ismail A.R, Sulong A.B, *Interlaminar fracture toughness of multi-layer woven silk/epoxy composites treated with coupling agent*, European journal of scientific research 27 (3):454-462, 2009.